THE ELUSIVE ROLE OF MIR-182 AND CLUSTERED PARALOGS IN ADAPTIVE IMMUNITY

by

Joseph Nicholas Pucella

A Dissertation

Presented to the Faculty of the Louis V. Gerstner Jr.

Graduate School of Biomedical Sciences,

in Partial Fulfillment of the Requirements for the Degree of

Doctor of Philosophy

New York, NY

November 2017

_____ _____

Jayanta Chaudhuri, PhD — Date

Dissertation Mentor

ABSTRACT

While primary humoral responses are vital to durable protection against pathogenic insult, fine-tuned regulation of these responses is critical to preventing catastrophic outcomes such as autoimmunity, chronic inflammation and lymphomagenesis. MicroRNA-mediated regulation is particularly well-suited for fine-tuning roles in physiology. The well-studied miR-182 has previously been implicated in many aspects of T cell function, DNA repair and cancer. In B cells, expression of miR-182, miR-96 and miR-183 (together the 183c microRNA cluster) are robustly induced upon activation, entry into the germinal center and plasmablast differentiation. miR-182 is also highly induced in $CD4^+$ and $CD8^+$ T cells. To elucidate the requirement of miR-182 in lymphocyte function, I extensively characterized adaptive immunity in mice with a targeted deletion of *Mir182*. I show that despite its dramatic induction, loss of miR-182 has minimal impact on B cell development, the ability of B cells to undergo class switch recombination *ex vivo* and to undergo antigen-driven affinity maturation *in vivo*. Furthermore, in striking contrast to knockdown studies that demonstrated the requirement of miR-182 in T cell function, *Mir182*$^{-/-}$ mice display no defect in T cell development and activation. Finally, I show that T cell dependent immune response to experimental *Listeria monocytogenes* infection is intact in *Mir182*$^{-/-}$ mice. I conclude that, contrary to previous studies, miR-182 does not play a significant role in all measured aspects of mouse adaptive immunity. In a follow-up study, I utilized 183c$^{GT/GT}$ mice that lack any detectable 183c microRNA expression to investigate the role of these miRs in humoral immunity and assess compensatory mechanisms. 183c$^{GT/GT}$ mice exhibit largely normal primary humoral responses, encompassing class switch recombination, affinity

maturation and the germinal center reaction, as well as plasmablast differentiation. My rigorous analysis included *ex vivo* class switch recombination and plasmablast differentiation models, as well as *in vivo* immunization with several thymus-dependent and thymus-independent antigens. My work sways the debate concerning the role of miR-182 in plasmablast differentiation programs, strongly suggesting 183c microRNAs are dispensable for this process. In the process, I have assembled a valuable framework for systematically evaluation of primary humoral responses. Lastly, this work bolsters the notion of robustness and malleability in microRNA:target interaction networks that may distinguish them from traditional genetic networks.

ACKNOWLEDGMENTS

I would like to thank the entire Chaudhuri Lab past and present, especially Wei-Feng Yen, Montserrat Cols, William T. Yewdell, Laura Nicolas and Bharat Vaidyanathan, for support, experimental assistance, and insightful discussion. I would also like to thank Davide Angeletti (NIAID) for assistance with ELISpot, Pragati Nigam (NYU Langone) for use of and assistance with their CTL Immunospot S6 Entry ELISpot analyzer, and Alejandra Mendoza (MSKCC) for assistance with CXCR5 staining for flow cytometry. I would also like to thank members of the Ventura, Rudensky and Li laboratories for technical and conceptual advice, and especially Gaspare La Rocca (MSKCC) for insightful discussion. I would also like to thank Naoharu Iwai and Yukiko Naito (UMIN Center, Japan) for use of their *Mir182*$^{-/-}$ mouse model and Shunbin Xu (Wayne State University) for use of his 183c$^{GT/GT}$ mouse model. I would like to thank the MSKCC Integrated Genomics Operation and Bioinformatics core facilities, especially Nicholas Socci, for collaboration on this work. I would sincerely like to thank my committee members, Joseph Sun, Andrew Koff, and Nina Papavasiliou, for incredible advice and support all along the way. In addition, I would like to acknowledge Andrea Ventura for volunteering to be my thesis examination chairperson. I would like to thank Thomas Magaldi (MSKCC), Ushma Neill (MSKCC), Theresa Lu (HSS), Andrea Schietinger (MSKCC), Sergei Koralov (NYU Langone), Mamta Tahiliani (NYU Langone), Katerina Hatzi (MSKCC), and Alexander Rudensky (MSKCC) for invaluable career advice. Lastly, and most of all, I would like to thank my mentor, Jayanta Chaudhuri, for his patience and unwavering support throughout my graduate career.

TABLE OF CONTENTS

LIST OF TABLES

LIST OF FIGURES

LIST OF ABBREVIATIONS

Ag = antigen

AID = activation-induced deaminase

BCR = B cell receptor

BSA = bovine serum albumin

C = constant gene segment

CD = cluster of differentiation

CGG = chicken γ-globulin

CLP = common lymphoid progenitor

CSR = class switch recombination

D = diversity gene segment

DN = double negative T cell

DP = double positive T cell

DSB = DNA double strand break

DZ = dark zone of GC

EAE = experimental autoimmune encephalomyelitis

ELISA = enzyme-linked immunosorbent assay

ELISpot = enzyme-linked immunospot assay

Fo = follicular B cell

GC = germinal center

HSC = hematopoietic stem cell

IFN = interferon

Ig = immunoglobulin

IgH = Ig heavy chain peptide

IgH = the Ig heavy chain locus

IgL = Ig light chain polypeptide

Igκ = Ig kappa light chain locus

Igλ = Ig lambda light chain locus

IL = interleukin

LLO = listeriolysin O

LPS = lipopolysaccharide

LZ = light zone of GC

J = joining gene segment

MHC = major histocompatibility complex

miR = microRNA

MZ = marginal zone B cell

NP = 4-hydroxy-3-nitrophenylacetyl

OVA = ovalbumin

PBS = phosphate-buffered saline

RBC = red blood cell

S = switch region of *IgH*

SHM = somatic hypermutation

SP = single positive T cell

SRBC = sheep red blood cell

T1 = B cell transitional stage 1

T2 = B cell transitional stage 2

T3 = B cell transitional stage 3

TD = thymus-dependent

Tfh = follicular helper T cell

TGF = transforming growth factor

Th = helper T cell

TI = thymus-independent

TLR = toll-like receptor

TNF = tumor necrosis factor

Treg = regulatory T cells

V = variable gene segment

WT = wild-type

CHAPTER 1

INTRODUCTION

The Adaptive Immune System

As proposed by Frank Burnet in 1957, adaptive immunity is governed by the principle of clonal selection. B and T lymphocytes, being the principal effectors of adaptive immunity, adhere to clonal specificity in that each clone expresses a distinctly-arranged antigen (Ag) recognition receptor (1). Thus, a specific response to a threat can be engendered by the selection, i.e. specific activation and expansion, of only those lymphocytes whose expressed antigen receptor gene recognizes an available Ag. The principle became engrained when Nossal and Lederberg first demonstrated that one B cell can produce only one antibody. With this foundation and the groundbreaking advances that have followed in molecular and cellular immunology, we now boast considerable understanding of the precise events that together manifest as adaptive immune protection to infectious agents.

A characteristic feature of the adaptive immune system is immunological memory, the feature that forms the basis of the efficacy of inoculation. Upon first encounter with Ag, the primary response of both B and T cells is relatively slow. Importantly, a successful primary response results in the generation of specific memory B and T cells, as well as long-lived antibody-secreting plasma cells, that enable a more robust and rapid secondary response upon reencountering the same Ag (1). It is precisely this specific accelerated recall response that is deemed immunological memory, and is a distinctive feature of adaptive immune systems in jawed vertebrates.

The Two Branches of Adaptive Immunity

The adaptive immune system is divided into two main branches: The cellular arm deploys T cells to enact immune defenses while the humoral arm utilizes B cells (Fig. 1).

In the cellular branch, immunity is cell-mediated. Effector T cells primarily exist in two groups that can be distinguished by coreceptor expression: One group expresses CD8 while the other expresses CD4. $CD8^+$ T cells become cytotoxic effector T cells when activated. $CD8^+$ T cells survey for the presence of intracellular pathogens via Ag presentation mediated by MHC class I. Upon recognition of Ag presented by an infected or otherwise compromised cell via MHC I, cytotoxic T cells can directly kill the cell by delivering lytic granules carrying cytotoxic payloads of perforin and granzymes that drive apoptosis of the target cell. Cytotoxic T cells can also secrete cytokines to help coordinate and further promote the response (1).

$CD4^+$ T cells comprise the other major group of effector T cells. They are also known as helper T cells (Th) due to their critical role in galvanizing cytotoxic T cell, macrophage and B cell responses. Depending on the type of threat and other contextual cues, Th cells can assume a variety of polarizations each with proficiency in secreting a certain milieu of effector cytokines, in turn activating particular downstream responses. For example, Th1 cells secrete interferon (IFN), interleukin-2 (IL-2) and tumor necrosis factor (TNF), and play a vital role in combatting intracellular pathogens including bacteria and viruses by stimulating macrophages and cytotoxic $CD8^+$ T cells. On the other hand, follicular helper T cells (Tfh) coordinate humoral responses by regulating B

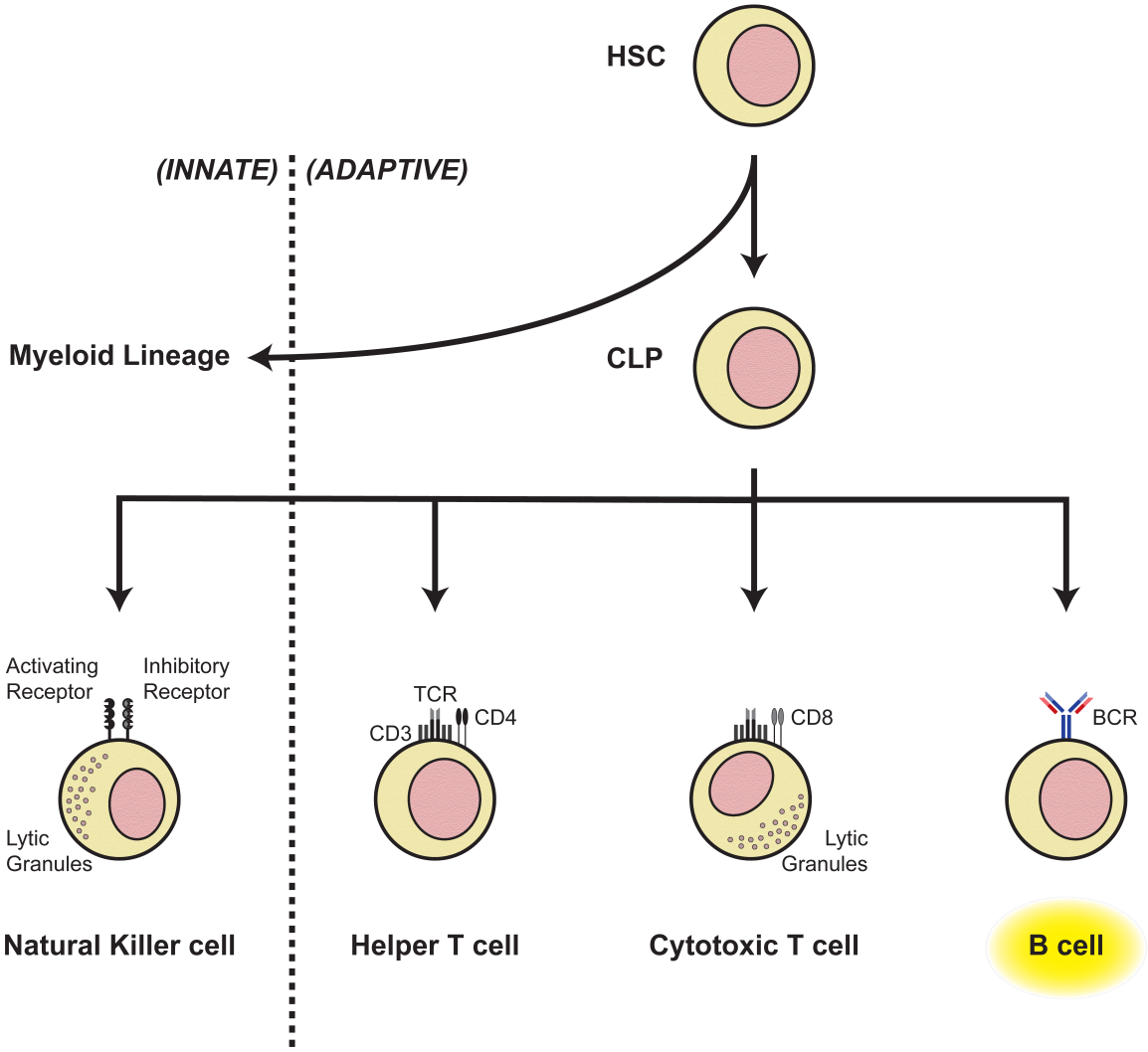

Figure 1. Lymphopoiesis in the mammalian primary lymphoid tissue, the bone marrow.
The pluripotent hematopoietic stem cell (HSC) gives rise to the common lymphoid progenitor (CLP) as well as the myelo-erythroid progenitor that generates the cells of the innate immune system. The CLP regenerates the entire adaptive immune branch, canonically comprised of B and T cells. Shown is the B cell receptor (BCR), the characteristic receptor of the B cell lineage. Natural killer cells, technically innate immune cells, are also derived from the CLP.

cells via secretion of IL-21 and IL-4, as well as cell-to-cell interaction via CD154-mediated activation of the B cell CD40 signaling pathway (2, 3).

The humoral branch of the adaptive immune system, also referred to as antibody-mediated immunity, will be the focus of this dissertation. This arm of adaptive immunity employs plasma cells as effector cells that secrete antibodies. All plasma cells descend from the B cell lineage, and it is the mature B cell that first detects and responds to cognate Ag. Given that plasma cells are terminally differentiated, have lost the ability to sense Ag, and claim antibody secretion as their chief duty, the humoral response is largely shaped by events that occur before terminal differentiation to the plasma fate. Of significant interest is the T cell-dependent germinal center (GC) response that drives Ag-specific B cell clonal expansion and the generation of antibodies with enhanced affinity (1, 3, 4).

The Antibody

The antibody, the aforementioned effector of humoral immunity, also constitutes the characteristic receptor of the B cell and is central throughout the lineage for development and function. The antibody is the founding member of the Immunoglobulin (Ig) superfamily and is comprised of four polypeptides, two identical Ig heavy chain (IgH) peptides encoded by the *IgH* locus (Fig. 2), and two identical Ig light chain (IgL) peptides encoded by either the *Igκ* or *Igλ* locus (Fig. 3) (1). These loci can be conceptually split by function of peptide domain, with the variable (V), diversity (D), and joining (J) gene segments encoding the variable region responsible for antigen

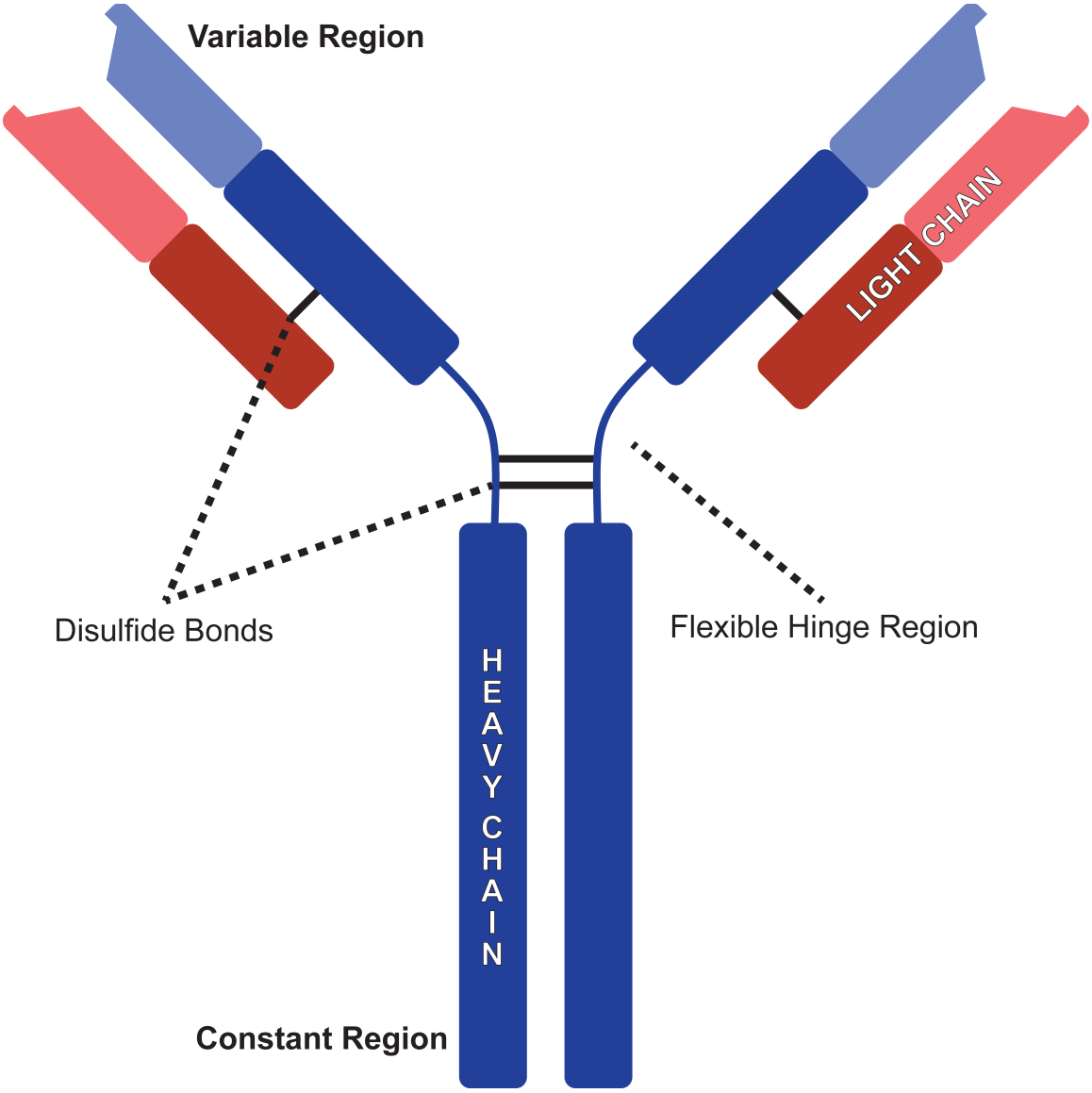

Figure 2. Schematic diagram of the antibody molecule.
The antibody molecule is composed of 2 identical heavy chain and 2 identical light chain polypeptides connected by disulfide bonds. The variable region, constructed by a combination of heavy and light chains, is responsible for epitope binding. The constant region, part of the heavy chain, is responsible for signal transduction through the BCR, as well as multimerization, localization, and Fc receptor binding of secreted antibodies. The middle sections of the heavy chains form a flexible hinge region.

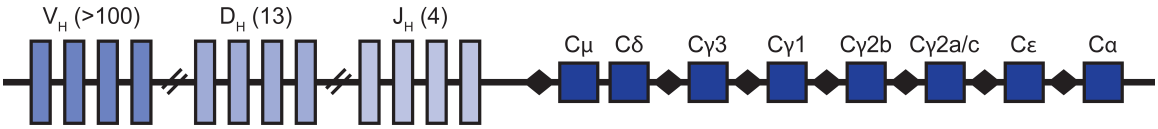

Figure 3. Schematic diagram of the *IgH* locus.
The *IgH* locus contains arrays of variable (V), diversity (D) and joining (J) gene segments that are variably utilized by individual B cells, conferring combinatorial diversity in the primary antibody repertoire. In the mouse genome, *IgH* contains at least 100 V, 13 D and 4 J gene segments. The constant (C) gene segments are downstream, with the capacity to encode for 8 different antibody isotypes. The intervening black diamonds represent switch (S) regions necessary for class switch recombination, and thus expression of non-default isotypes. Cγ2a and Cγ2c are paralogs, the identity of this segment depends on mouse strain.

recognition and the constant (C) gene segments encoding the constant region responsible for signal transduction (Fig. 4) (5).

Forming the central component of the B cell receptor (BCR), the antibody is critical for mediating how B cells respond to their environment. Secretion of antibody is the chief and most well-characterized ultimate objective of most B cells and so naturally, maturation of the antibody molecule is a pervasive force throughout the B cell lineage up through terminal differentiation.

Early B cell Development

The canonical B cell lineage originates from bone marrow-derived precursors, beginning with long-term hematopoietic stem cells (HSCs) that are the ultimate source of continuous repopulation of the pool of mature B cells in the periphery (6, 7). When prompted by a void in the niche, HSCs undergo asymmetric division with one daughter maintaining stemness and the other differentiating into a common lymphoid progenitor (CLP) (1). The CLP can then give rise to B cell, T cell and NK cell precursors (Fig. 1).

The next stage in the B cell lineage is the pro B cell. The centrality of the antibody can first be appreciated in the subsequent pro to pre B cell transition. Primary diversification of Ig occurs in the form of V(D)J recombination of *IgH* and VJ recombination of *Igκ* and/or *Igλ* alleles, therein generating the primary antibody repertoire (8). Pro B cells undergo *IgH* D to J rearrangement, followed by V to DJ rearrangement. Signaling through pre-BCR, composed of this newly rearranged heavy chain with surrogate light chain, indicates a functional IgH polypeptide has been formed. This is absolutely required for continued development to the pre B cell stage; B cells that

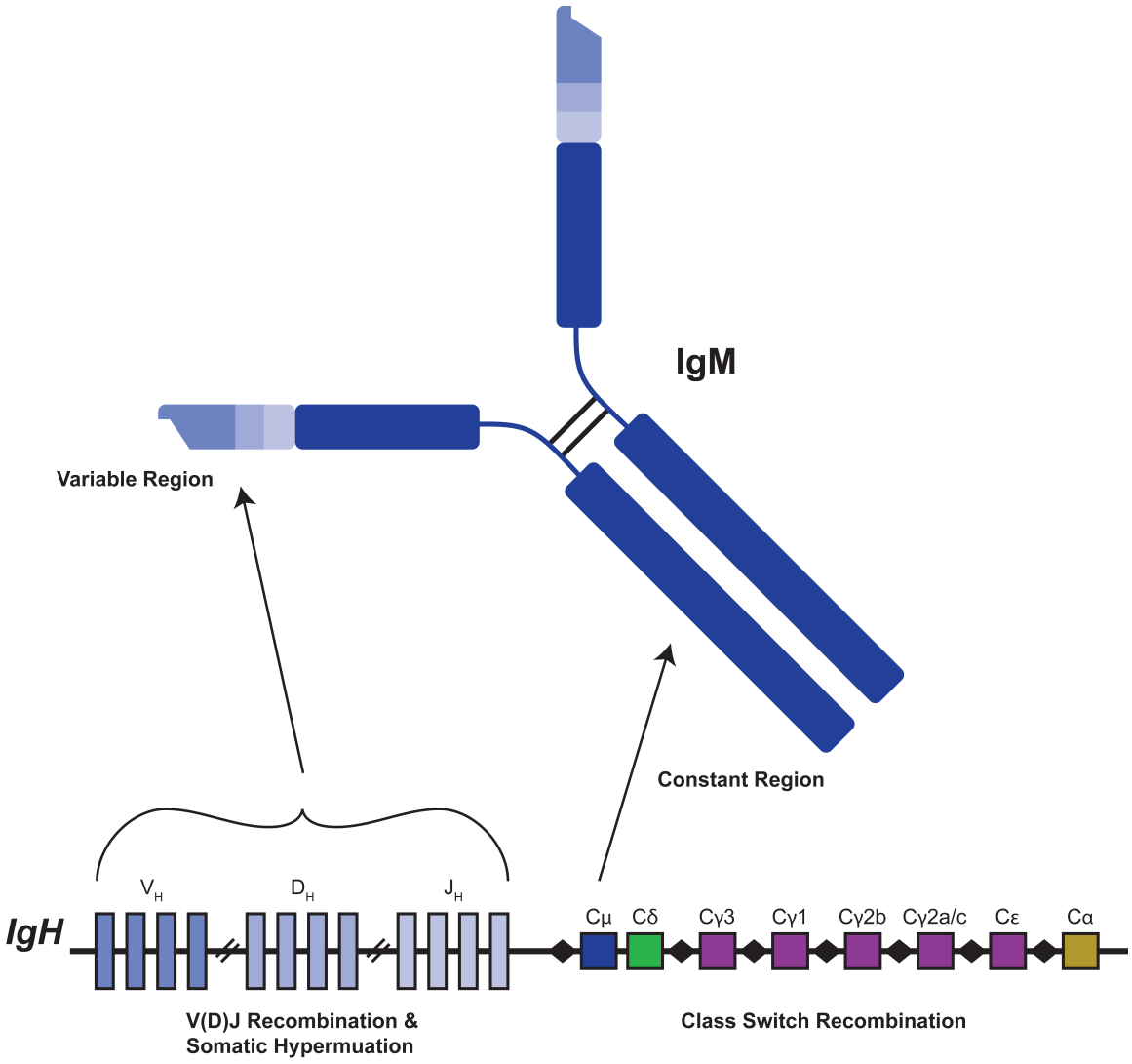

Figure 4. The *IgH* locus can be split based on encoded function.
The upstream V, D, and J gene segments together encode for the variable region that partakes in epitope binding. 3' to this are the C regions that encode for the constant region. the default configuration encodes for IgM. This split view is also informative for conceptualizing B cell maturation. V(D)J recombination and somatic hypermutation exclusively involve V, D, and J gene segments, while class switch recombination occurs exclusively at C gene segments.

fail this checkpoint are deleted by apoptosis. Subsequently, pre B cells undergo V to J rearrangement in *Igκ*, and if that fails then in *Igλ*. Productive rearrangement in at least 1 of 4 Ig light chain alleles is necessary to construct a functional mature BCR, and permit the cell to pass the checkpoint to become an immature B cell. Immature B cells can then exit the bone marrow and continue their development in the periphery (Fig. 5) (1, 8).

Upon entering circulation in the peripheral pool, immature B cells continue to develop through transitional (T)1, T2, T3 stages and finally become mature B cells capable of participating in *bona fide* humoral responses upon Ag encounter and/or other stimuli such as toll-like receptor (TLR) ligands. Mature B cells circulate via blood and lymphatics, and congregate in follicles of secondary lymphoid organs such as spleen and lymph nodes where they can survey for the presence of cognate Ag. In the spleen there exists a parallel subset termed marginal zone (MZ) B cells that branches off from the T2 stage. MZ B cells are specializers in rapid response to blood-borne bacterial and viral threats, and can participate in extrafollicular humoral responses but are excluded from GC responses (9).

Class Switch Recombination & Somatic Hypermutation

Upon activation, mature B cells in secondary lymphoid organs can undergo two molecular maturation processes: class switch recombination (CSR) and somatic hypermutation (SHM) (Fig. 4). During CSR, IgM^+ B cells exchange the default Cμ constant region exons for an alternate constant region gene segment (Cγ, Cε, Cα). The B cell thus shifts from expressing IgM to IgG, IgE or IgA, with each antibody isotype conferring a distinct effector function during an immune response (10). Mechanistically,

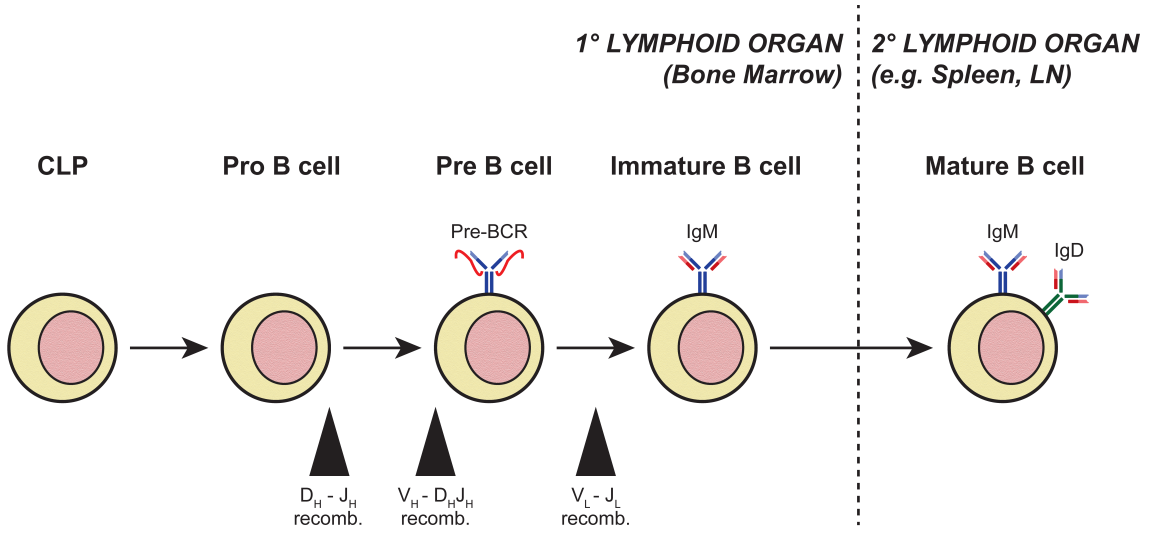

Figure 5. Early B cell developmental stages.
The first steps of B cell development occur in the bone marrow. The B cell lineage derives from the common lymphoid progenitor (CLP), giving rise to the pro B cell. V(D)J recombination at *IgH* occurs, with D - J coming first then V - DJ. Successful production of functional heavy chain polypeptides is necessary for achieving the pre B cell stage, confirmed by signaling through the membrane-bound pre-BCR complex composed of heavy chains and surrogate light chains (represented here as red squiggles). The pre B cell then undertakes light chain VJ recombination at *Igκ*, and if unproductive at *Igλ*. Productive light chain generation completes BCR assembly and signals attainment of the immature B cell stage. Immature B cells migrate from the bone marrow to peripheral secondary lymphoid organs to continue maturation.

CSR is a DNA deletional-recombination reaction occurring between repetitive switch (S) region DNA elements in *IgH*. The broadly-accepted model posits that the DNA deaminase AID (activation-induced cytidine deaminase) deaminates cytidines to uridines in S regions. Engagement of base excision and mismatch repair proteins at the deaminated residues generates DNA double strand breaks (DSBs) at acceptor and donor S regions. Synapsis of distal DNA ends, excision of intervening DNA and resolution by non-homologous end-joining complete CSR (Fig. 6) (10).

CSR proceeds through the deliberate introduction of DNA lesions and relies on subversion of faithful DNA repair so as to promote accumulations of DSBs and long-range (productive) versus intra-switch (abortive) recombination (11, 12). While obligatory intermediates for CSR, DSBs also constitute one of the most toxic lesions that can occur in a cell, causing either cell death or initiating oncogenic translocations (13, 14). Processes that regulate the activity of AID to generate DNA lesions have been extensively investigated, however the mechanisms that tip the delicate balance of DNA repair to mediate CSR while simultaneously suppressing genomic instability remain incompletely understood (12, 15).

AID also drives another Ig maturation process that instigates DNA damage. SHM involves the intentional introduction of point mutations into V gene segments of Ig genes, and is necessary for the secondary diversification of the antibody repertoire that occurs upon Ag encounter (3, 12). While both necessitate the activity of AID, SHM differs from CSR in that it does not seem to require the outright generation of DSBs.

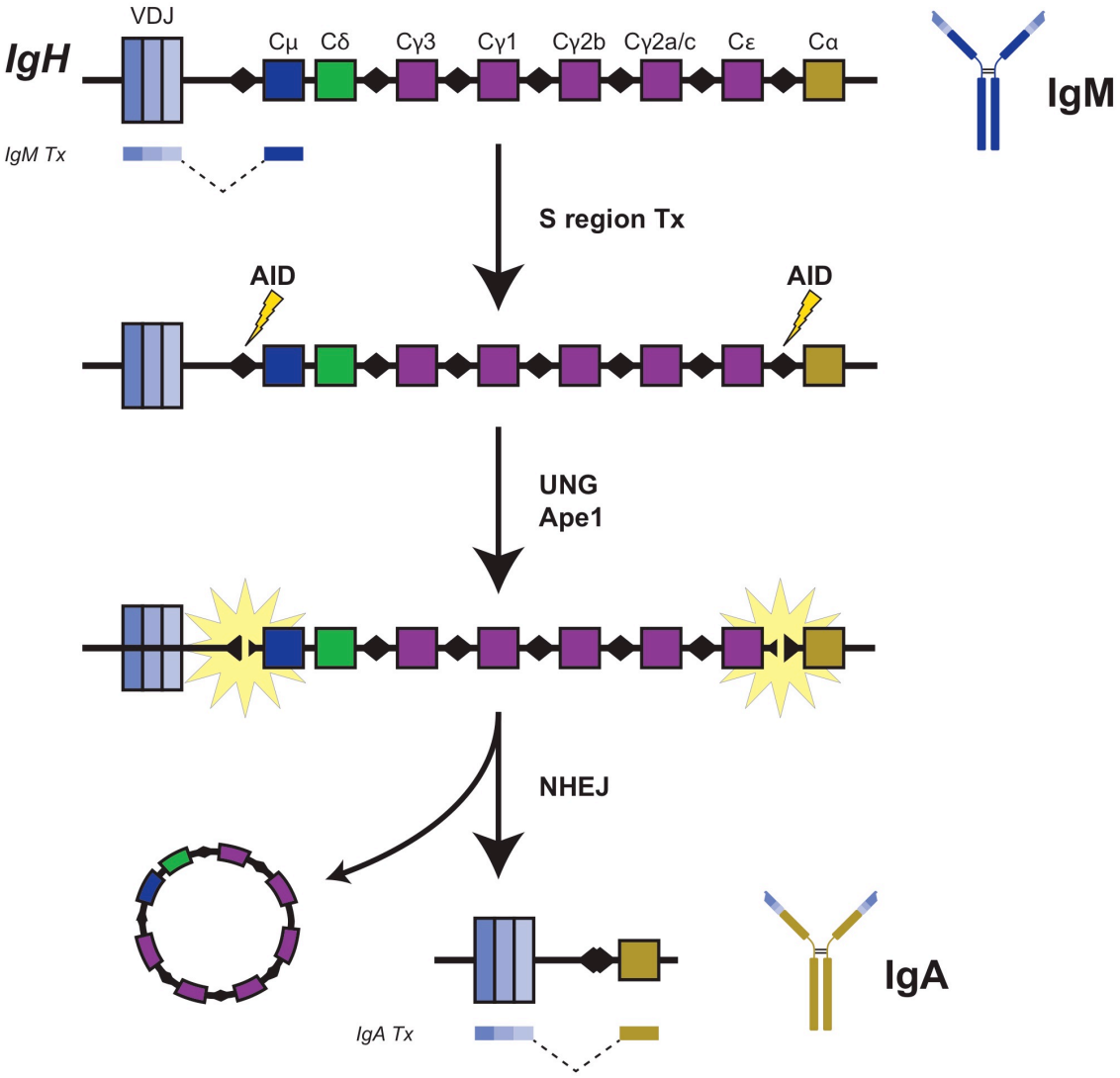

Figure 6. Class switch recombination at the *IgH* locus.
The default configuration of *IgH* encodes for the IgM isotype. Upon activation, non-coding transcription occurs at Sμ and a downstream S region depending on context. Black diamonds represent switch (S) regions. Transcription makes S region cytidines available for deamination by AID (depicted as lightning bolts). Uridines are processed by BER proteins UNG and APE1, resulting in S region DNA double strand breaks (highlighted by yellow stars). Ligation of distal incongruent DNA ends by NHEJ and excision of circularized intervening DNA completes CSR. Depicted here is CSR to produce an IgA-expressing B cell.

Fate Decisions upon Initial Antigen Encounter

Of course, these molecular processes do not occur in a vacuum, but rather in the context of complex maturation decisions in response to Ag encounter. Upon Ag encounter, a mature B cell will initiate proliferation and migrate to the T cell zone of secondary lymphoid organs. Here, the B cell is confronted with the choice to enter the follicular GC response, or the extrafollicular plasmablast response (Fig. 7). This branch point is navigated by B cells based on a number of factors, but most prominent among them is the type of Ag that is sensed as this also impacts the quality of available secondary signal (16, 17). This dynamic is reflected by categorization of Ag as thymus-independent (TI) and thymus-dependent (TD).

TI Ags invoke humoral responses dominated by early plasmablast differentiation in extrafollicular foci, without the need of T cell help. There is consequently very little if any GC response. TI Ags generally do not elicit appreciable levels of SHM, but CSR does occur to varying levels. For example, immunization with TI-2 Ag NP-Ficoll invokes considerable CSR to IgG3, with IgG3 secreted by nearly as many induced plasmablasts as is IgM (18). Instead, immunization with TI-1 Ag results in less frequent $IgG3^{+}$ plasmablasts, predominantly producing IgM-secreting cells (19).

Conversely, TD Ags are dominated by follicular GC reactions, though they tend to also induce delayed plasmablast differentiation in extrafollicular foci (16). Unlike extrafollicular responses, ample SHM occurs during GC reactions (3). GCs also generally support substantial CSR, with resultant isotype dependent on context.

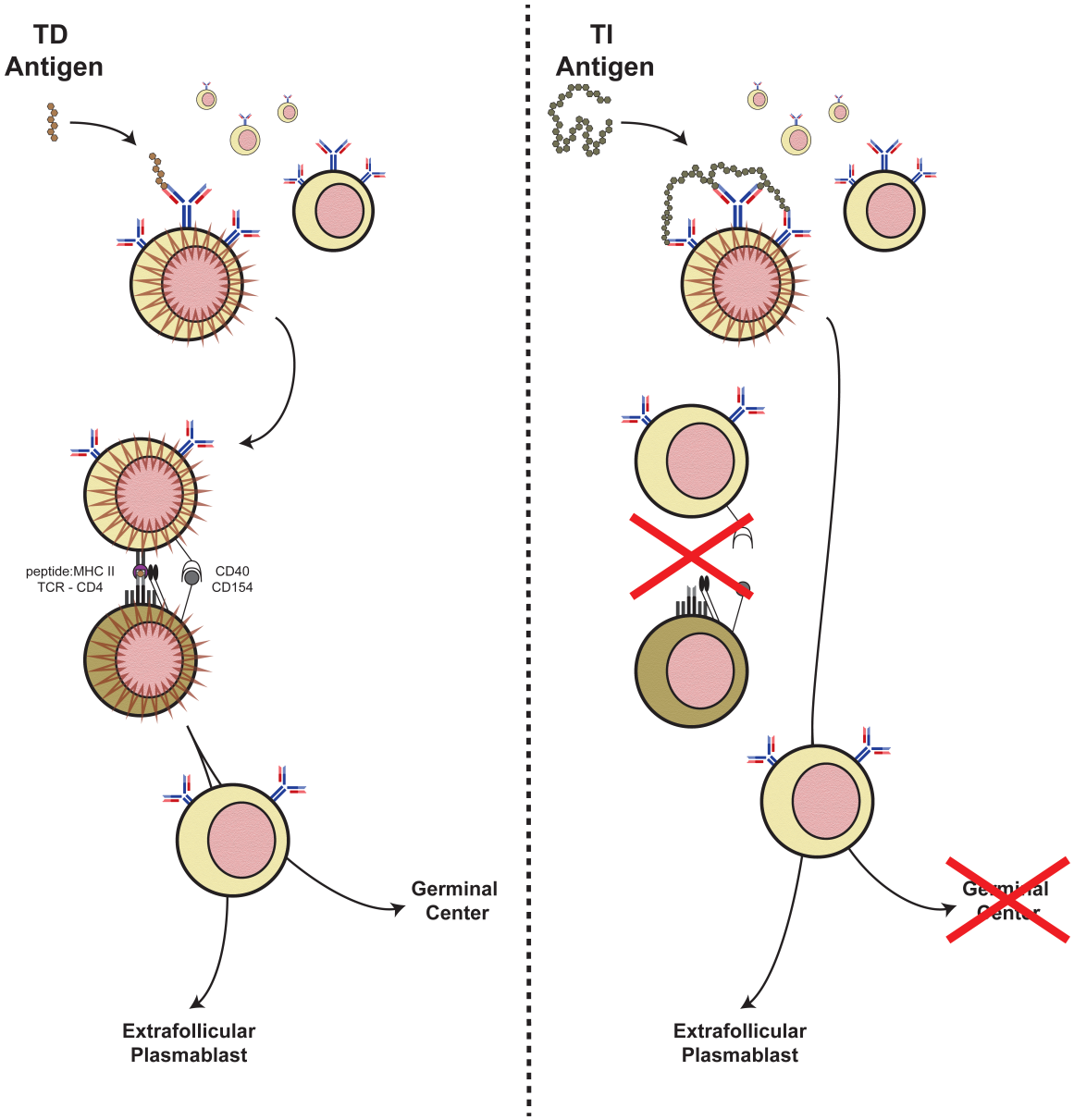

Figure 7. Mature B cell fate decisions depend on the quality of antigen.
Upon recognition of a thymus-dependent (TD) antigen (Ag) (represented as brown hexagon chains) via its BCR, B cell activation and migration to the follicle:T zone boundary occurs. In the process, the B cell internalizes the bound BCR, processes the antigen and presents peptide:MHCII in an attempt to interact with a $CD4^+$ T cell. $CD4^+$ T cells that have been activated by peptide:MHCII-presenting dendritic cells will also migrate to this area. Cognate B:T interaction via peptide:MHCII and the T cell receptor (TCR) leads to activation of B cell CD40 by T cell CD154. The quality of these B:T interactions is critical to determining B cell fate, choosing either the follicular germinal center (GC) or extrafollicular plasmablast response. Likewise, recognition of a thymus-independent (TI) Ag (TI-2 Ag represented as navy green hexagon chains) occurs via BCR. But, this Ag cannot be processed and presented on MHC so is invisible to T cells. Nonetheless, sufficient BCR crosslinking will drive the B cell down the extrafollicular plasmablast program independently of CD40 signaling, though no GCs will form.

For example IgG1 is the dominant isotype elicited by model Ags like sheep red blood cells (SRBCs) and 4-hydroxy-3-nitrophenylacetyl (NP) conjugated to chicken γ-globulin (CGG), though GCs responding to gut Ags in Peyer's patches are predominantly IgA^+ and GCs responding to viral Ags are often $IgG2a/c^+$ (3, 20). Because TD Ags typically elicit both follicular and extrafollicular responses, this context is valuable for probing regulatory mechanisms determining B cell fate. Though much remains to be learned about this fate decision, strength and duration of signaling via BCR and CD40 have been shown to correlate with plasmablast differentiation (21, 22).

Extrafollicular Plasmablast Responses Prompted by Various Ag Classes

The extrafollicular humoral response is characterized by the clonal expansion and differentiation of Ag-specific plasmablasts, observable as extrafollicular foci in the splenic red pulp (16). The majority of cells that acquire plasma-like properties are short-lived, unlike the GC-derived long-lived plasma cells that sustain antibody secretion from specialized niches in bone marrow (4). As mentioned, there is an extrafollicular component to each of the categories of Ag described (TI-1, TI-2, and TD), indicating there are various paths leading to this fate (18, 23, 24).

The most commonly used TI-1 model Ag is gram-negative bacterial lipopolysaccharide (LPS), but other TLR ligands can also suffice. The key to this type of response is engagement of TLR signaling in the B cell. In fact, TLR signaling without BCR signaling is likely to be sufficient for a low rate of plasmablast differentiation. However, the synergy endowed when both signals are present maintains the defining

feature of adaptive immunity, clonal expansion via specific engagement of Ag receptor (16, 23).

A TI Ag is classified as TI-2 if the ensuing response depends on extensive BCR crosslinking, and transducing BCR signal via Bruton's tyrosine kinase (Btk) activity (16). TI-2 Ags tend to be multivalent to enhance BCR crosslinking. Thus, molecules such as bacterial capsular polysaccharides that are inert to TLRs tend to invoke this type of response. 4-Hydroxy-3-nitrophenylacetyl (NP) hapten, a highly immunogenic Ag, conjugated in high ratio to Ficoll, a branched high molecular weight polysaccharide, can extensively crosslink reactive BCRs, making it an excellent TI-2 model Ag (18, 25, 26).

TI-1 and 2 Ags share some similarities that set them apart from TD Ags. Besides lacking a requirement for T cell help, they both induce early extrafollicular responses, as opposed to the delay observed with TD Ags (16). In the case of TI Ags, the extrafollicular component dominates, while the follicular GC reaction dominates the response to TD Ags. Another commonality is that TI Ags engage a significant cohort of MZ B cells, whereas TD Ags are generally more restricted to follicular B cells (16).

TD Ags are those in which $CD4^+$ T cells are engaged in addition to B cells, and contribute to the quality of the humoral response. TD Ags are by necessity protein Ags, as $CD4^+$ T cells must be activated via Ag peptide:MHC class II complexes. Unlike TI Ags, TD Ags incite a response branded by GC reactions taking place in B cell follicles (3). Though the majority of cells participate in GCs, there is also a substantial but delayed extrafollicular response to be observed (16).

Germinal Center Reaction and Affinity Maturation Prompted by Thymus-Dependent Antigen

GCs are highly specialized and transient microanatomical structures that develop in follicles of secondary lymphoid organs upon B cell encounter of cognate Ag. This microenvironment is necessary for efficient antibody affinity maturation, the process that enhances an antibody's ability to bind an epitope and leads to more effective pathogen neutralization. As discussed, CSR occurs during the GC reaction (3). The GC is also the principal source of the Ag-specific memory B cells and long-lived plasma cells that confer long-term protection against recurrent infection, and are fundamental to the humoral arm of adaptive immune memory (27).

The GC reaction is a multi-stage progression involving a complex interplay of numerous cell types (Fig. 8), including GC B cells, Tfh cells, follicular dendritic cells (FDCs) of stromal origin, and myeloid cells like conventional dendritic cells and tingible body macrophages. In the first step, Ag encounter activates mature follicular B cells to proliferate, upregulate chemokine receptor CCR7, and migrate from the follicle to the interfollicular T cell zone boundary where there is potential for cognate interaction with an activated $CD4^+$ T cell. $CD4^+$ T cells that have been stimulated in the T cell zone by dendritic cells presenting peptide:MHC II complex derived from the same Ag are incited to upregulate chemokine receptor CXCR5 and migrate to the interfollicular T cell zone boundary. During this time, B cells have internalized Ag sensed by BCR-binding and processed it for presentation via peptide:MHC class II complexes. It is in the follicle:T cell zone border area that the first B:T cell cognate interaction can occur, requiring Ag presentation by B cells to signal through a cognate T cell's TCR. The T cell in turn

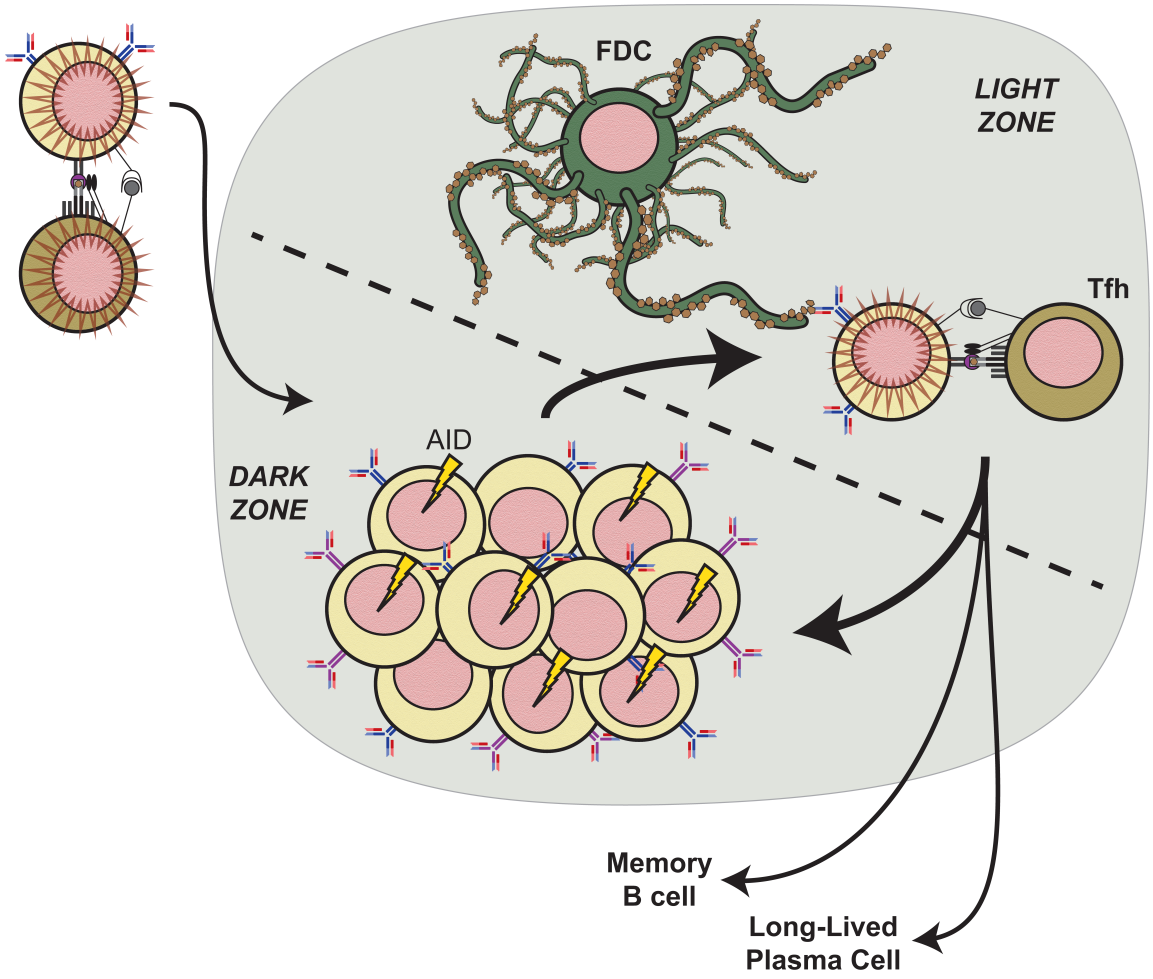

Figure 8. The germinal center reaction.
The response to thymus-dependent (TD) antigens (Ags) is dominated by the follicular germinal center (GC) response. Upon Ag recognition and successful cognate B:T interaction, an activated B cell can initiate or enter a GC reaction. The B cell follicle is represented by the light green box. In the dark zone (DZ), B cells undergo intense proliferation and AID-mediated somatic hypermutation (SHM) of *IgH* and *IgL* alleles. Substantial AID-mediated class switching also occurs (appearance of purple surface antibodies in the DZ represents switching to IgG1). The time spent by B cells and number of divisions that occur in the DZ is determined in part by the strength of B:T interaction that activates CD40 signaling in the light zone (LZ). Subsequently, GC B cells migrate into the LZ where interaction with follicular dendritic cells (FDCs) is critical to picking up Ag to present via MHCII to Tfh cells. Interaction with Tfh cells is necessary for continued survival, and impacts the fate decision of re-cycling to the DZ or differentiating to memory B cell or long-lived plasma cell. Limited Tfh cells drives competition among GC B cells, whereby the cells expressing higher affinity BCRs are more successful in picking up Ag and thus interacting with Tfh cells. Clonal expansion of B cells with higher affinity BCR by this mechanism manifests as antibody affinity maturation.

signals to the B cell via CD154-mediated activation of the B cell CD40 signaling, in addition to T cell secreted cytokines like IL-21 (3). This interaction is unique to TD Ag responses and as discussed, plays a major part in determining whether the B cell will reenter the follicle to initiate the GC reaction, or divert into the extrafollicular plasmablast response (17). In any case, successful T:B cognate interaction leads to further activation and proliferation of both the B cell and the T cell. Interaction promotes the B cell to acquire the GC phenotypic state (characterized as $GL7^{+}$ Fas^{+} $CD38^{-}$ IgD^{-}) and the T cell to acquire the Tfh polarization (characterized as $CD4^{+}$ $CXCR5^{+}$ $PD\text{-}1^{+}$), both driven by master transcriptional regulator Bcl6 (28-31). The B and T cell are inextricably linked during this response, as each is necessary for the other's ability to differentiate (3, 32). On the molecular level, reciprocal antagonism between Bcl6 and Blimp1 (the master regulator of the plasma fate) roots a bistable positive feedback loop reinforcing the GC or plasmablast cell state (in B cells) (31, 33-35). This serves as molecular validation that this stage represents a pivotal juncture in B cell fate.

Once the GC reaction has initiated, GC B cells undergo iterative cycles of proliferation and SHM, followed by Tfh-mediated selection. The GC can be spatially divided into a dark zone (DZ) and light zone (LZ). The DZ is the space characterized by intense B cell proliferation and AID-mediated somatic hypermutation of *IgH* and *IgL* alleles. DZ GC B cells are marked by high CXCR4 and low CD86 surface expression. Instead, the LZ is comprised of $CD86^{hi}$ $CXCR4^{lo}$ GC B cells, FDCs and Tfh cells. In this space, GC B cells compete for help from limited Tfh cells by presenting peptide:MHC II complexes derived from Ag that is held by FDCs. B cells with higher affinity antibodies are more successful in binding antigen and subsequently interacting with Tfh cells. This

interaction, mediated again by stimulation of the B cell CD40 pathway, is necessary for continued survival of GC B cells that are inherently programmed to undergo apoptosis without it (36). In addition, Tfh interaction in LZ authorizes B cell proliferation (37, 38). Thus, SHM in the DZ provides the raw material for Tfh-mediated expansion in the LZ of the B cell clones carrying the highest affinity Ag-specific antibody (3). This Darwinian mechanism is known as affinity maturation, a consummate illustration of the principle of clonal selection fundamental to adaptive immunity.

GC B cells confront frequent fate decisions while in the GC, every time they enter the LZ to be exact. In the LZ, a GC B cell may reenter the DZ to continue cycling and feeding affinity maturation, or exit the GC. If exiting the GC, the secondary decision arises between becoming a memory B cell and terminally differentiating to a plasma cell. These decisions are not well-understood, though it has become clear that BCR affinity and the consequent quality of Tfh interaction are certainly embedded in these choices (39, 40). Surface Ig isotype appears to impact post-GC fate, as $IgG1^+$ B cells appear to favor plasma fate in lieu of memory B cell differentiation (41). In addition, Myc signaling has been demonstrated to promote DZ reentry (42).

Fine-Tuning Humoral Adaptive Immunity

Despite their value, humoral responses must be tightly regulated for several reasons. For one, aberrant antibody activity is often at the center of autoimmune pathology, for example in systemic lupus erythematosus, where autoantibodies specific for nucleic acid direct host tissue damage (43, 44). Another impetus for meticulous regulation hinges on the intense proliferative bursts and genomic instability that are

typical of humoral responses. The recently described example of the GC response immediately comes to mind, wherein antigen-specific GC B cells are coerced into rounds of clonal proliferation and intentional DNA damage for Ig secondary diversification (45). Lymphomagenic transformation of B cells is an inherent hazard accompanying humoral responses, evidenced by the correlation of persistent GCs, and inflammation in general, with cancer (46, 47). Thus, a nuanced understanding of the mechanisms regulating humoral response quality and magnitude is a vital goal, with immediate translatable implications in fine-tuning vaccine potency as well.

Of particular interest is the DNA mutator AID, specifically expressed in activated B cells to promote antibody diversity via CSR and SHM (5, 12, 15). I was initially drawn to the conundrum faced by activated B cells in balancing DNA damage repair responses: Subtle subversion of faithful repair to allow efficient CSR and SHM, while simultaneously averting catastrophic genome instability and chromosomal translocation, is a delicate undertaking. The requisite fine-tuning for such a precarious balance prompted my interest in microRNA.

MicroRNAs as Fine-Tuning Regulators

MicroRNAs (miRs) comprise a class of short ~21 nucleotide RNA that employ RNA-induced silencing complexes (RISC) containing Argonaute proteins to achieve regulation of gene expression via mRNA transcript degradation and/or translational inhibition (48, 49). In the brief time since their discovery, the prevalence and sway of miR-mediated regulation has become increasingly apparent; Well-accepted roles for miRs seemingly pervade all disciplines, including embryonic development, immunology, and oncology (50-55).

miRs are generated through a unique biogenesis pathway. First, primary microRNA (pri-miR) rich in secondary structure is transcribed, typically by RNA polymerase II. This transcript contains one or more hairpins embedded with mature miR sequences, as well as a varying amount of flanking sequences. The Drosha nuclease complex cleaves hairpins from the pri-miR to generate ~60 - 120nt precursor microRNA (pre-miR). Pre-miRs are exported from the nucleus via Exportin-5 to undergo further processing in the cytoplasm. Here, Dicer complex cleaves a ~21nt RNA duplex from a pre-miR to generate the mature double-stranded miR. This double-stranded miR is then loaded into RISC complex containing Argonaute and other proteins. One strand from the duplex is removed and degraded, while the other strand is selected to guide silencing of messenger RNA transcripts via sequence complementarity typically targeting mRNA 3' untranslated regions (UTRs) (56).

Due to the authority of the short ~6 nucleotide seed sequence in directing target interactions and the relatively non-stringent criteria the seed sequence imposes, it is not uncommon for a single miR species to bind and repress hundreds of transcripts, typically via target sites located in transcript 3' untranslated regions. For each individual target, repression need not be absolute, but may in fact be quite modest. Consequently, miR-mediated regulation is capable of subtle manipulation of entire gene networks, such as signaling pathways, a desirable feature for precise fine-tuning (54, 57-59). Taken together with the fact that repression via translational inhibition permits rapid and reversible modulation, miR-mediated regulation of humoral responses is an intriguing prospect, for example during the transient subversion of DNA repair mechanisms during CSR (11, 12).

Documented Roles of 183c MicroRNAs

In this study, I have identified miR-182 as a promising candidate for regulating humoral responses. miR-182 is a member of a cluster encoded from an intronic locus on murine chromosome 6. As part of this highly-conserved cluster (herein referred to as 183c) (60), paralogous family members miR-183, miR-182 and miR-96 may be synchronously expressed as part of a polycistronic transcript (61). miR-182, along with the 183c family, was originally identified as being highly expressed in mouse retina (62, 63). Later, it was also shown to be expressed in other sensory tissues including the inner ear, tongue epithelia, olfactory epithelia, olfactory bulbs, vomeronasal organ, pineal body and dorsal root ganglions (61). Though genetic knockout of miR-182 does not appear to have a sensory phenotype (64), a mouse model in which miR expression from 183c is abrogated exhibits progressive retinal degeneration as well as vestibular dysfunction resulting in circling behavior and unstable gait (61). Another report has demonstrated that loss of miR-96 results in progressive hearing loss (65, 66).

Expression of miR-182 has been associated with a wide variety of tumors including those originating in breast, lungs, thyroid, ovary, and others (60, 67-70). In fact, PubMed search returns over 100 papers suggesting a link between 183c miRs and cancer. Of these studies, the most intriguing implicates miR-182 as a driver of metastasis in a mouse model of *p53*-inactivated *Kras*-driven soft tissue sarcoma (71). They found miR-182 to be consistently amplified in metastases, but unlike most other reports that rely solely on correlation and/or miR knockdown studies, they went on to generate genetic mouse models to conditionally ablate and overexpress miR-182 in tumor cells. When miR-182 was deleted, the rate of metastasis dropped. Conversely, when miR-182 overexpression was forced, they observed enhanced metastatic rate. They implicated joint

derepression of miR-182 targets *Rsu1*, *Mtss1*, *Pai1*, and *Timp1* in mediating the enhanced metastatic rate seen when miR-182 expression was ablated in tumor cells (71).

Besides roles in sensory organs and cancer, miR-182 has been implicated in many aspects of lymphocyte function and DNA repair. AntagomiR-mediated depletion experiments demonstrated a central role of miR-182 in IL-2 driven helper T cell-dependent immune response through the ability of the miR to regulate expression of the transcriptional factor *Foxo1* (72). The work presented herein conflicts with this study; The basis and implications of this discordance will be a point of discussion in this dissertation. Separately, miR-182 was shown to be a key modulator of regulatory T cell (Treg) differentiation and function. Firstly, in Tregs recruited to inflammation during a Th2-biased helminth infection model, miR-182 and miR-183 were found to be highly induced, necessary for regulating IL-2 production, and required for suppression of activated Th2 cells (73). Secondly, in an experimental autoimmune encephalomyelitis (EAE) model, miR-182 knockdown promoted Treg differentiation, purportedly mediated by *FoxO1* derepression (74). Interestingly, 183c miRs have also been reported to promote Th17 pathogenicity in an EAE mouse model via suppression of *FoxO1* (75), suggesting a miR-182 – *FoxO1* regulatory axis acting across different immune cell types during autoimmune inflammation. In line with this, miR-182-mediated repression of *FoxO1* has also been reported in a myocyte negative feedback loop regulating glucose utilization (76).

In an interesting sensory organ and immunity crossover study, loss of 183c miRs was shown to diminish corneal inflammation and severity of keratitis during *Pseudomonas aeruginosa* infection. 183c miRs were found to play a dual role in this

context: On the one hand, 183c miRs augment corneal innervation and proinflammatory neuropeptide production, while also regulating innate immunity by reining in phagocytic capacity and intracellular killing efficiency of macrophages and neutrophils (77).

While the work presented here was ongoing, a role for miR-182 was reported in the extrafollicular plasmablast response (78). Li et al. measured Ag-specific serum antibodies by ELISA upon TD Ag immunization (NP-CGG) and found reduced serum antibodies in *Mir182*$^{-/-}$ mice versus WT at an early timepoint, but not at peak or late timepoints. In addition, they quantified significantly fewer Ag-specific antibody-secreting cells upon TI-2 Ag immunization (NP-Ficoll) (78). The work presented herein conflicts with this study; The basis and implications of this discordance will be a point of discussion in this dissertation.

Lastly, and also directly relevant to regulation of humoral responses, miR-182 has been implicated in regulating expression of BRCA1 and over 30 gene products that participate in BRCA1-dependent homologous recombination DNA repair (79, 80). This positions miR-182 as a mediator of fine-tuning regulation of the DNA DSB response. One very enticing miR-182 target reported by Krishnan et al. is 53BP1, a protein with a well-established role in the synapsis and ligation phase of CSR (81-84).

CHAPTER 2

MATERIALS & METHODS

Mice. The generation of *Aicda*$^{-/-}$, *Mir182*$^{-/-}$ and 183c$^{GT/GT}$ mice has been described (61, 64, 85). WT BALB/c mice and C57BL/6 were obtained from The Jackson Laboratories. For all experiments, we strived to use 6-10 week old healthy mice of both genders, with sex-matched littermate WT controls. Due to unexpected non-Mendelian rate of homozygous 183c$^{GT/GT}$ births, and inconsistent vitality and viability of mice through early life, this was not always possible. However, age never exceeded 26 weeks, and if littermate controls were unavailable, then care was taken to use closely age- and sex-matched mice from different litters. Mouse colonies were maintained according to IACUC policies.

Purified B cell cultures. Naïve mature B cells were purified by negative selection from RBC-lysed splenocyte cell suspensions using MACS α-mouse CD43 microbeads (#130-049-801; Miltenyi Biotec) on a MidiMACS magnetic separation apparatus (Miltenyi Biotec). Purified cells were cultured in sterile-filtered RPMI 1640 (#22400-089; Gibco) + 15% fetal bovine serum (#35-010-CV; Corning) + 1% additional L-glutamine (200mM stock) + 1% penicillin/streptomycin cocktail (#400-109; Gemini) + 0.0005% β-mercaptoethanol (#BP176-100; Fisher Scientific) and stimulated with various conditions: LPS {(20μg/mL; #L4130; Sigma-Aldrich)}, LI {LPS (20μg/mL) + IL-4 (12.5ng/mL; #404-ML-010; R&D Systems)}, LII {LPS (20μg/mL) + IL-2 (100U/mL; recombinant human; NIH) + IL-5 (5ng/mL; #215-15; PeproTech)}, LTD {LPS (10μg/mL) + TGFβ (2ng/mL; #240-B-010; R&D Systems) + αIgD-dextran (0.33μg/mL; FinaBio#0001; Fina

BioSolutions)}, aCI {αCD40 (0.5μg/mL; clone HM40-3; #16-0402-86; eBioscience) + IL-4 (12.5ng/mL)}, and aCII {αCD40 (0.5μg/mL) + IL-4 (12.5ng/mL) + IL-5 (2ng/mL)}. Cell cultures were initiated at 0.5 x 10^6 cells/mL and split 1:2 at 48 hrs and 72 hrs. IL-5 was used at a concentration of 6μg/mL in plasmablast differentiation experiments with *Mir182*$^{-/-}$ B cells.

Small RNA sequencing. Small RNA library preparation and subsequent sequencing was performed by the MSKCC Genomics Core Laboratory using standard Illumina HiSeq protocol. Raw data was processed by the MSKCC Bioinformatics Core Laboratory.

Real-time qPCR. All RNA was prepared from cell samples using standard TRIzol (#15596026; Invitrogen/Thermo Fisher Scientific) protocol. All qPCR experiments were performed in 96-well format on a Bio-Rad CFX96 instrument (*Mir182*$^{-/-}$ experiments) or in 384-well format on an Applied Biosystems Quantstudio 6 Flex instrument (183c$^{GT/GT}$ experiments) using the following components from Applied Biosystems (Life Technologies): TaqMan miRNA Reverse Transcription Kit (#4366596), TaqMan Universal Master Mix II, no UNG (#4427788), TaqMan miRNA Assays (#4427975: miR-182 ID 002599; miR-96 ID 000186; miR-183 ID 00269; snoRNA251 ID 001236). Data was normalized to snoRNA251. Data analysis was performed using the Comparative Ct method (86). Standard curve interpolation was used to determine the copy number of miR-182 in different cell types. A standard curve was generated by spiking 5'-phosphorylated miR-182 RNA oligonucleotide (miRBase.org) over a range of concentrations into *Mir182*$^{-/-}$ RNA samples.

Bone marrow harvest. Bone marrow was flushed out of femurs with PBS+0.5% FBS.

NP-CGG immunization. NP(>30)-CGG (#N-5055D-5; Biosearch Technologies) was precipitated with 10% alum. Mice were immunized intraperitoneally in 200μL doses with 50 or 100 μg on day 0 and boosted with 50μg on day 10 (as indicated in figure legend). Mice were sacrificed on day 14, or serum was collected by standard submandibular bleeding procedure on days 0, 7, 14, 21, and 28 (as indicated in figure legend). To analyze expression of miR-182 in B cells *in vivo*, mice were immunized intraperitoneally on day 0 with 100 mg alum-precipitated NP(20-29)-CGG and sacrificed on day 10.

ELISA. Assays were done in Thermo Fisher Scientific MaxiSorp clear flat-bottom 96-well plates (#439454). Coating antibodies for binding IgM, IgG1, IgG2b, IgG2c, IgG3, and IgA were purchased from Southern Biotech (#1020-01, 1070-01, 1090-01, 1079-01, 1100-01, and 1040-01, respectively). The following isotype standards were used to calculate absolute concentration values: IgM (#14-4752-81; eBioscience), IgG1 (#0102-01; Southern Biotech), IgG2b (#14-4732-81; eBioscience), IgG2c (#0122-01; Southern Biotech), IgG3 (#553486, BD Pharmingen), IgA (#553478; BD Pharmingen). Secondary antibodies for detecting IgM, IgG1, IgG2b, IgG2c, IgG3, IgA were purchased from Southern Biotech (#1020-05, 1070-05, 1090-05, 1079-05, 1100-05, 1040-05 respectively). eBioscience ELISA diluent (#00-4202-56) was used as blocking buffer, eBioscience TMB substrate (#00-4201-56) to develop, and 1M phosphoric acid to stop development. Plates were read at 450nm on a Biotek Synergy HT detector. Absolute concentrations of serum antibodies were determined by interpolation from standard curve, with attention paid to keeping within standard and sample linear ranges. All samples were done in duplicate over 4-step dilution series, and each plate with own standard curve. For NP-specific assays, plates were coated with NP(<8)-BSA (#N-

5050L-10; Biosearch Technologies) or NP(>20)-BSA (#N-5050H-10; Biosearch Technologies). Relative titers were determined by interpolation on plate reference curve generated for each plate using a constant sample across all plates, with attention paid to keeping within plate reference and sample linear ranges. All samples were done in duplicate over 4-step (*Mir182*$^{-/-}$ expts) or 8-step (183c$^{GT/GT}$ expts) dilution series.

Purification and stimulation of T cells. Naïve CD4 and CD8 T cells from peripheral lymphoid organs were sorted in a flow cytometer based on CD25^{-} CD62L^{+} CD44^{-} cell surface expression. Cells were labeled with CellTrace Violet dye (#C34557; Invitrogen) according to manufacturer's protocol and activated *in vitro* using plate bound anti-CD3, soluble anti-CD28 and soluble IL-2 for 4 days.

***Listeria monocytogenes* infection and analysis.** Mice were intravenously infected with 5x10^{3} CFU of *Listeria monocytogenes* expressing chicken ovalbumin (LM-OVA). Fluorescent-dye-labeled antibodies against cell surface markers TCRβ, CD4, CD8, and CD44 were purchased from eBiosciences. PE-conjugated K^{b}/ova-tetramer was obtained from the Tetramer Core Facility at MSKCC. Cells were incubated with specific antibodies for 30 min on ice in the presence of 2.4G2 mAb to block FcγR binding. To determine IFNγ and TNFα expression, lymphocytes were stimulated with 5 mg/ml of $LLO_{190\text{-}201}$ for CD4^{+} T cells or 10nM SIINFEKL peptide for CD8^{+} T cells in the presence of GolgiStop (BD Biosciences) for 5 hrs at 37 °C. After stimulation, cells were incubated with cell surface antibodies, fixed and permeabilized, and stained with anti-IFNγ and anti-TNFα (eBiosciences).

Flow cytometry. All samples were acquired with an LSRII flow cytometer (Becton Dickinson) and data was analyzed with FlowJo software (TreeStar).

Intracellular flow cytometry staining. To stain for Blimp1 and Bcl6, cells were fixed and permeabilized using BioLegend True-Nuclear Transcription Factor Buffer Set (#424401). To stain for intracellular Ig, cells were fixed and permeabilized using BD Biosciences CytoFix/Cytoperm Fixation/Permeabilization Solution Kit (#554715) without GolgiStop.

SRBC immunization. Packed 100% sheep red blood cells were purchased from Innovative Research (#IC100-0210). Mice were immunized intraperitoneally with $1x10^9$ SRBCs in sterile PBS per 200μL dose on day 0, boosted day 10, and sacrificed day 14.

LPS immunization. "TLR-grade" LPS from *Salmonella minnesota* R595 (#ALX-581-008-L002) was purchased from Enzo Life Sciences. Mice were immunized intraperitoneally with 50μg in sterile PBS per 200μL dose on day 0 and sacrificed day 3.

NP-Ficoll immunization. NP(30)-AECM-Ficoll (#F-1420-10) was purchased from Biosearch Technologies. Mice were immunized intraperitoneally with 100μg in sterile PBS per 200μL dose on day 0 and sacrificed day 5.

ELISpot. Assays were done in Millipore Multi-Screen HA filtration 96-well plates (#MSIPN4W). IgM, IgG1, and IgG3 coating antibodies same as for ELISA. Secondary antibodies were purchased from VectorLabs for detecting IgM (#BA-2020) and IgG (#BA-9200), followed by HRP-Avidin D (#A-2004; VectorLabs). For NP-specific assays, plates were coated with NP(>20)-BSA (#N-5050H-10; Biosearch Technologies). PBS+2% BSA was used as blocking buffer, ELISpot AEC substrate (#551951; BD

Biosciences) to develop. Plates were scanned on a CTL ImmunoSpot S6 Entry instrument and analyzed using CTL ImmunoSpot software, version 7.0.9.5. All samples were done over 12-step dilution series. Plotted "spots per 10^6 cells" determined by averaging spots per 10^6 cells over a minimum of 3 different dilutions, with attention paid to using wells within linear range. Counting parameters were held constant across all plates of the same assay type. Quality control of automated counting was performed on every plate by visual inspection.

Statistical analysis. P values were determined by ratio paired t test or two-tailed unpaired t test, as indicated. Ratio paired t test was preferred in most cases to manage difficulties in obtaining homogeneous experimental cohorts. $\alpha = 0.05$ was used in all experiments. All error bars represent standard deviation (s.d.).

CHAPTER 3

miR-182 is strongly induced in B cells undergoing CSR

To identify miRs that are involved in tempering DNA repair to allow for the long range synapsis and incongruent ligation necessary for productive CSR, we isolated mature, naïve B cells from spleens of wild-type (WT) and AID-deficient (*Aicda*$^{-/-}$) mice and generated miR expression profiles for their resting and activated states. *Ex vivo* activation of splenic B cells was achieved with a combination of anti-CD40 + IL-4. This approach was designed to identify miRs that are not just strongly induced upon activation, but whose induction is also AID-dependent. In doing so, we aimed to narrow our search to miRs that respond specifically to DNA damage caused by AID activity. We utilized a simple measure, which we called the fold-change ratio (FCR), to rank the disparity in fold-change induction upon activation between WT and *Aicda*$^{-/-}$ B cells. We thereby generated a list of 30 abundant miR candidates which exhibited FCR>1.5 or <0.667 (Fig. 9). miR-182 was identified as the most strongly induced miR upon B cell activation (Fig. 10A). There was an ~90-fold induction of miR-182 expression in WT B cells activated to undergo CSR. This induction was significantly dampened (to ~30-fold) in *Aicda*$^{-/-}$ B cells, suggesting that the enhanced induction could be dependent on AID-induced DNA breaks (Fig. 10A, inset). miR-182 is abundantly expressed, as it easily falls in the top 10% of expressed miRs in activated B cells and is readily quantifiable in activated lymphocytes (Fig. 10B, C). Additionally, normalized sequencing counts showed that miR-182 clusters with, and in most cases outnumbers, other miRs reported to play a role in B cell biology (87) (Fig. 9, 10B). The induction of miR-182 expression upon activation of B cells was also observed in independent qPCR analysis of *ex vivo*

miRNA name	Avg FCR	log2(Avg FCR)	p-value	Avg WT FC	Avg Aicda-/- FC
mmu-miR-182	2.32	1.21	4.11E-05	90.97	39.28
mmu-miR-467a	2.22	1.15	1.65E-04	19.99	9.00
mmu-miR-98*	2.40	1.26	4.00E-02	12.96	5.41
mmu-miR-155	1.62	0.69	2.44E-02	12.42	7.68
mmu-miR-92b	1.50	0.59	4.11E-05	11.47	7.64
mmu-miR-219-5p	2.28	1.19	4.11E-05	10.35	4.55
mmu-miR-130b	1.64	0.71	4.11E-05	5.72	3.49
mmu-miR-374	3.93	1.97	7.77E-03	3.74	0.95
mmu-miR-148a	2.09	1.07	4.11E-05	3.71	1.77
mmu-miR-17*	1.81	0.85	1.23E-03	2.95	1.64
mmu-miR-15b	1.79	0.84	4.11E-05	2.23	1.24
mmu-miR-221	1.81	0.85	1.88E-02	2.20	1.21
mmu-miR-21	2.14	1.10	4.11E-05	2.01	0.94
mmu-miR-15a	1.57	0.65	4.11E-05	1.25	0.79
mmu-miR-152	1.82	0.86	1.42E-02	1.17	0.65
mmu-miR-195	2.89	1.53	4.11E-05	1.14	0.39
mmu-miR-16	1.66	0.73	4.11E-05	1.13	0.68
mmu-miR-7a	2.03	1.02	1.42E-02	1.05	0.52
mmu-miR-23a	1.84	0.88	8.23E-05	0.76	0.41
mmu-miR-328	0.66	-0.59	4.11E-05	0.67	1.01
mmu-miR-200c	1.61	0.69	7.82E-04	0.58	0.36
mmu-miR-340-3p	1.53	0.61	1.06E-02	0.43	0.28
mmu-miR-1981*	0.64	-0.63	7.77E-03	0.43	0.67
mmu-miR-146a*	0.63	-0.67	7.82E-04	0.41	0.65
mmu-miR-200b	2.38	1.25	1.65E-04	0.38	0.16
mmu-miR-330	0.52	-0.95	8.23E-05	0.37	0.72
mmu-miR-141	1.78	0.83	4.00E-02	0.27	0.15
mmu-miR-26b	1.56	0.64	7.82E-04	0.22	0.14
mmu-miR--3107;486	1.76	0.82	1.88E-02	0.11	0.06

FC = Activated/Resting
FCR = (WT FC)/(Aicda-/- FC)

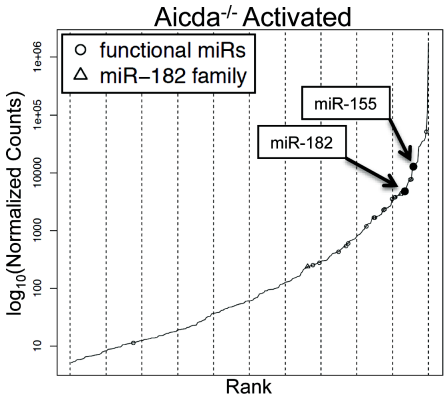

Functional miRs

mmu-miR-16	mmu-miR-17
mmu-miR-181a	mmu-miR-210
mmu-miR-92a	mmu-miR-19a
mmu-miR-93	mmu-miR-15a
mmu-miR-92b	mmu-miR-181b
mmu-miR-150	mmu-miR-18a
mmu-miR-19b	mmu-miR-29b
mmu-miR-29a	mmu-miR-125b-5p
mmu-miR-20a	

Figure 9. Small RNA sequencing top candidates, activated *Aicda*$^{-/-}$ B cell waterfall plot, and list of "functional miRs."
Supplementary information related to Figure 10. Listed “functional miRs” refer to miRs in which there is published evidence citing a role in B cell development and/or function (86).

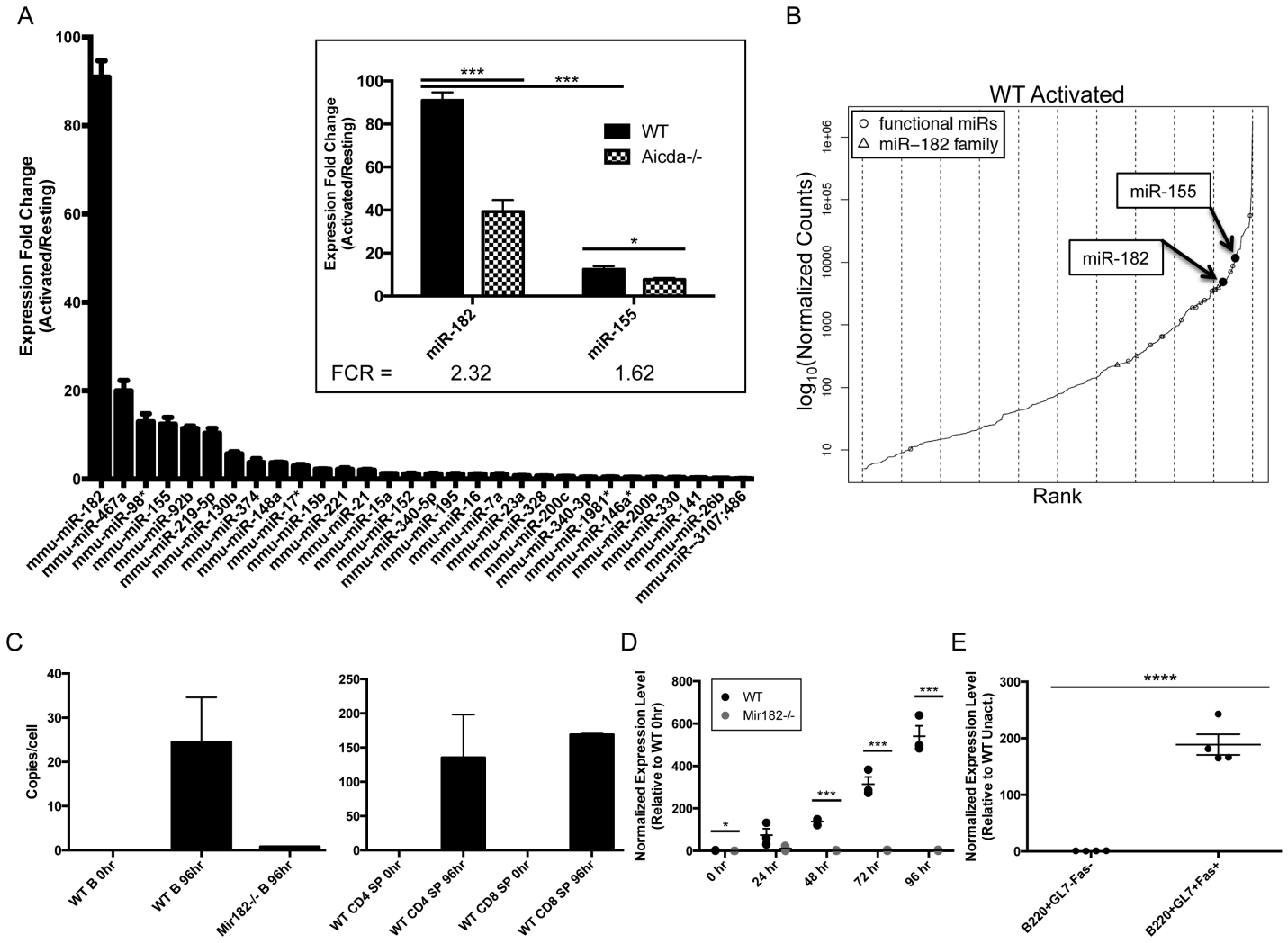

Figure 10. miR-182 is strongly induced upon B cell activation in an AID-dependent manner.

Figure 10 (cont.). (**A**) Expression fold-change of top 30 miR candidates in WT B cells (activated/resting) identified by miR expression profiling. n=3 (**Inset**) Expression fold-change of miR-182 and miR-155 (activated/resting). Fold-change ratio (FCR) = Fold-change WT/Fold-change *Aicda*$^{-/-}$. (**B**) Normalized sequencing counts of all expressed miRs were ranked and plotted. Marked "functional miRs" refer to miRs in which there is published evidence citing a role in B cell development and/or function (86). (**C-E**) TaqMan qPCR was used to monitor expression of miR-182. (**C**) Approximate miR-182 absolute copy number was determined by interpolation on a standard curve generated using synthesized miR-182 RNA spiked into *Mir182*$^{-/-}$ RNA sample over a dilution series. n=3 for WT 96 hr samples, n=1 for other samples. (**D**) Mature splenic B cells were isolated and stimulated with anti-CD40 (0.5μg/mL) and IL-4 (12.5 ng/mL). n=3. (**E**) WT C57BL/6 mice immunized with NP(20-29)-CGG were sacrificed day 10 and indicated cell populations were FACS-sorted from splenocytes. *p<0.1, ***p<0.001, ****p<0.001 (t-test).

stimulated (Fig. 10D) and *in vivo* activated B cells (Fig. 10E).

miR-182 deficiency has minimal impact on B cell development, CSR and affinity maturation

Since miR-182 has been strongly implicated in DNA repair, we extensively characterized B cells derived from mice with a targeted deletion of miR-182 (*Mir182*$^{-/-}$) (64). In the knockout *Mir182* allele, the only disruption is a neomycin cassette replacing the *Mir182* gene itself (Fig. 11A – B) Accordingly, miR-182 was not detected in B cells from *Mir182*$^{-/-}$ mice (Fig. 10D).

Initially we characterized B cell development in *Mir182*$^{-/-}$ mice. Cell numbers in the bone marrow and spleen were similar between WT and *Mir182*$^{-/-}$ mice (Fig. 12A). No significant difference in the frequency of pro-, pre-, and immature B cell populations in the bone marrow was observed (Fig. 12B). Thus, early B cell development appears unaffected by absence of miR-182 and strongly suggests that V(D)J recombination, another process heavily reliant on DNA repair (8), remains intact. There was a statistically significant, albeit modest, decrease in the frequency of mature B cells (B220^{+} CD43^{-}) in total splenocyte populations from *Mir182*$^{-/-}$ mice (Fig. 12C). This difference was not reflected in the frequency of total (B220^{+} IgM^{+}) and mature (IgM^{lo} IgD^{hi}) B cells (Fig. 12C) suggesting that the slight reduction in percentage of B cells in spleen is due to a mild perturbation in the non-B cell population which could include T cells, macrophages, dendritic cells and other stromal cells. Furthermore, the frequencies of immature (IgM^{hi} IgD^{lo}), IgM^{hi} IgD^{hi}, T2-transitional (CD23^{+} IgM^{+} CD21^{hi}), follicular (CD23^{+} IgM^{+} CD21^{lo}), marginal zone (CD23^{-} IgM^{hi} CD21^{hi}) and bone marrow

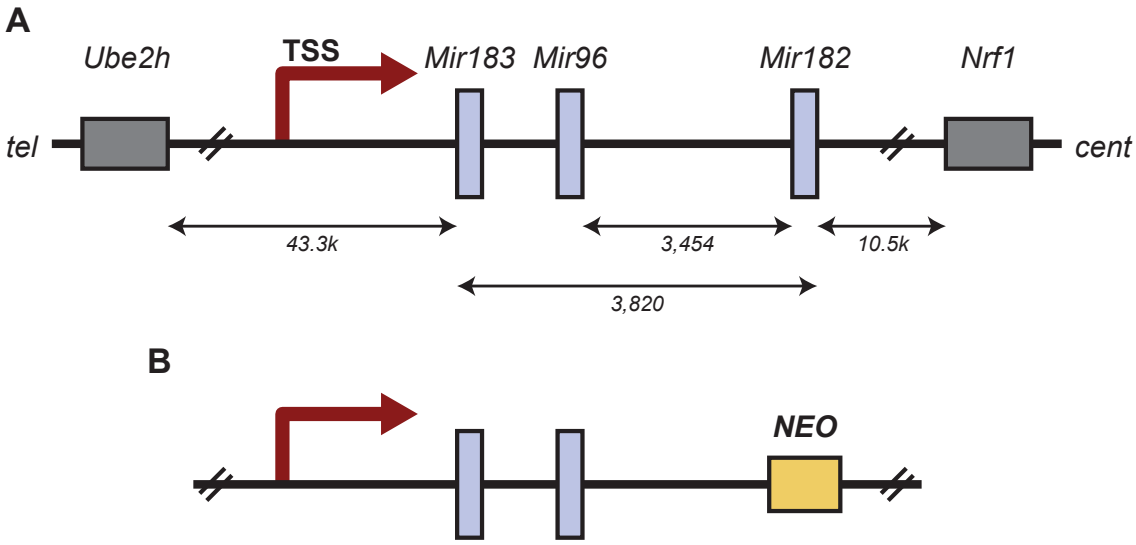

Figure 11. The *Mir182* genetic locus and knockout allele.
(**A**) The *Mir182* genetic locus on *Mus musculus* chromosome 6qA3. Numbers under arrows indicate base pair distances.
(**B**) The *Mir182* knockout allele, in which a neomycin resistance gene (*NEO*) cassette replaces the *Mir182* gene.

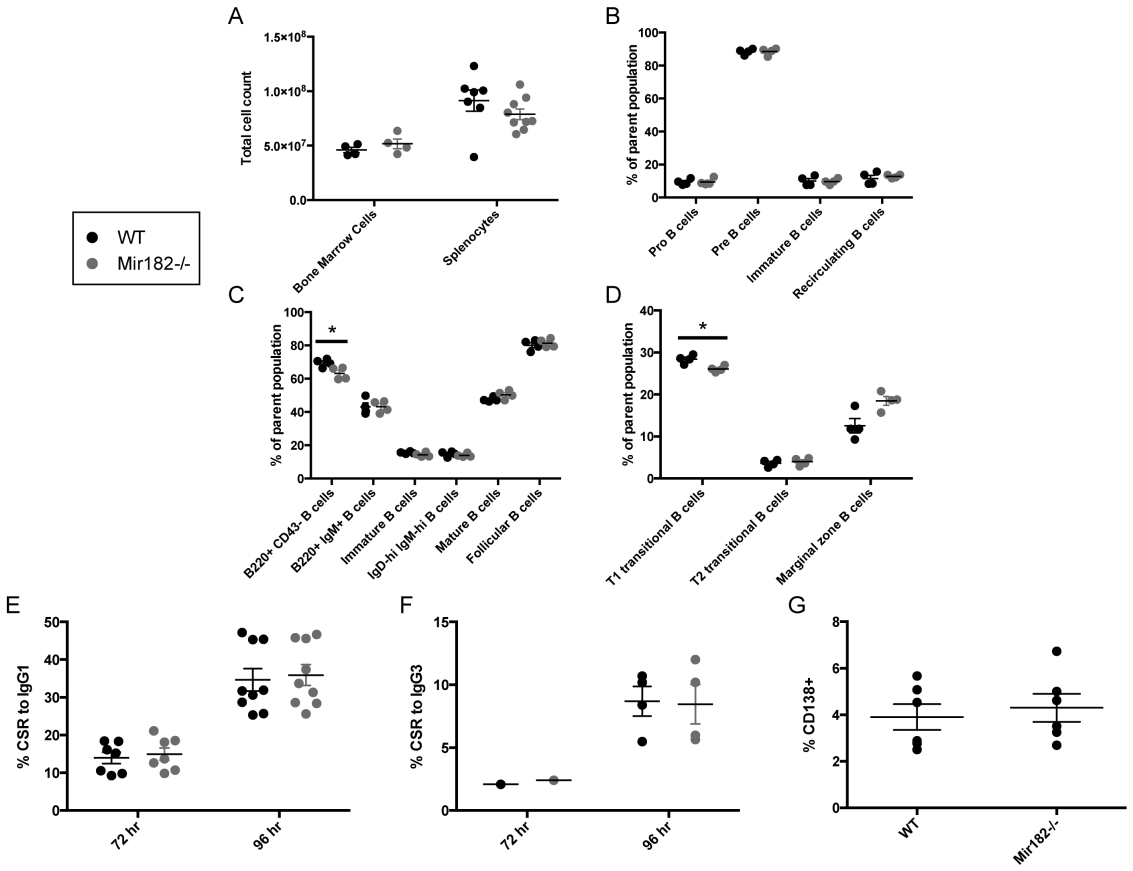

Figure 12. B cell development and CSR are unperturbed by miR-182 deficiency. (**A**) Cellularity of bone marrow and spleen. (**B**) Bone marrow was analyzed for immature ($B220^{lo}$ IgM^{+}) and recirculating ($B220^{hi}$ IgM^{+}) B cells as a percentage of live singlets. $B220^{lo}$ IgM^{-} B cells were gated and examined for Pro ($CD43^{+}$) and Pre ($CD43^{-}$) B cells. (**C, D**) Splenocytes were analyzed for relevant B cell populations. Parent population for $B220^{+}$ $CD43^{-}$ and $B220^{+}$ IgM^{+} B cells is live singlets. Parent population for Immature (IgM^{hi} IgD^{lo}), IgM^{hi} IgD^{hi}, and Mature (IgM^{lo} IgD^{hi}) is $B220^{+}$ live singlets. Parent population for Follicular (IgM^{+} $CD21^{lo}$) and T2 transitional (IgM^{+} $CD21^{hi}$) B cells is $B220^{+}$ $CD23^{+}$ live singlets. Parent population for T1 transitional (IgM^{hi} $CD21^{lo}$) and Marginal zone (IgM^{hi} $CD21^{hi}$) B cells is $B220^{+}$ $CD23^{-}$ live singlets. (**E**) Primary mature splenic B cells were stimulated with anti-CD40 and IL-4 and assayed for surface IgG1 expression by flow cytometry. (**F**) Splenic B cells were stimulated with LPS and assayed for surface IgG3 expression by flow cytometry. (**G**) Splenic B cells were stimulated with anti-CD40, IL-4 and IL-5 and assayed for surface CD138 (Syndecan) expression by flow cytometry. *p<0.1 (t-test).

recirculating ($B220^{hi}$ IgM^{+}) B cell populations were all equivalent (Fig. 12C – D). There was a small but statistically significant decrease in the percentage of T1-transitional B cells ($CD23^{-}$ IgM^{hi} $CD21^{lo}$) in *Mir182*$^{-/-}$ mice (Fig. 12D). Overall, we conclude that B cell development is not impaired in *Mir182*$^{-/-}$ mice.

To determine the requirement of miR-182 in CSR, we stimulated splenic B cells *ex vivo* with anti-CD40 and IL-4 and assayed for CSR to IgG1. Despite the dramatic induction of miR-182 expression (Fig. 10), loss of miR-182 had no impact on the ability of B cells to undergo CSR to IgG1 (Fig. 12E). Likewise, splenic B cells from *Mir182*$^{-/-}$ mice cultured in LPS underwent CSR to IgG3 at WT levels (Fig. 12F). Thus, loss of miR-182 had no effect on the intrinsic ability of B cells to undergo CSR in culture. Additionally, miR-182 did not influence the differentiation of activated B cells into antibody-secreting plasma cells as measured by surface expression of CD138 (Syndecan) following stimulation of splenic B cells with anti-CD40, IL-4 and IL-5 (Fig. 12G).

To assess the participation of miR-182 in secondary diversification of B cells *in vivo*, we analyzed WT and *Mir182*$^{-/-}$ mice following immunization with the T cell-dependent antigen NP-CGG (Fig. 13A). The fraction of germinal center B cells ($GL7^{+}$ Fas^{+}) in spleens of immunized WT and *Mir182*$^{-/-}$ mice was similar, and as expected (85), markedly lower than that from *Aicda*$^{-/-}$ mice (Fig. 13B – C). Analysis of serum from immunized mice failed to show any significant difference in immunization-dependent secretion of various antibody isotypes (Fig. 13D), indicating that *in vivo* CSR in response to NP-CGG was normal and further bolstering the claim that plasma cell differentiation does not rely on miR-182. Finally, to assess antigen-specific affinity maturation, we probed for low- and high-affinity NP-specific serum antibodies via the binding of

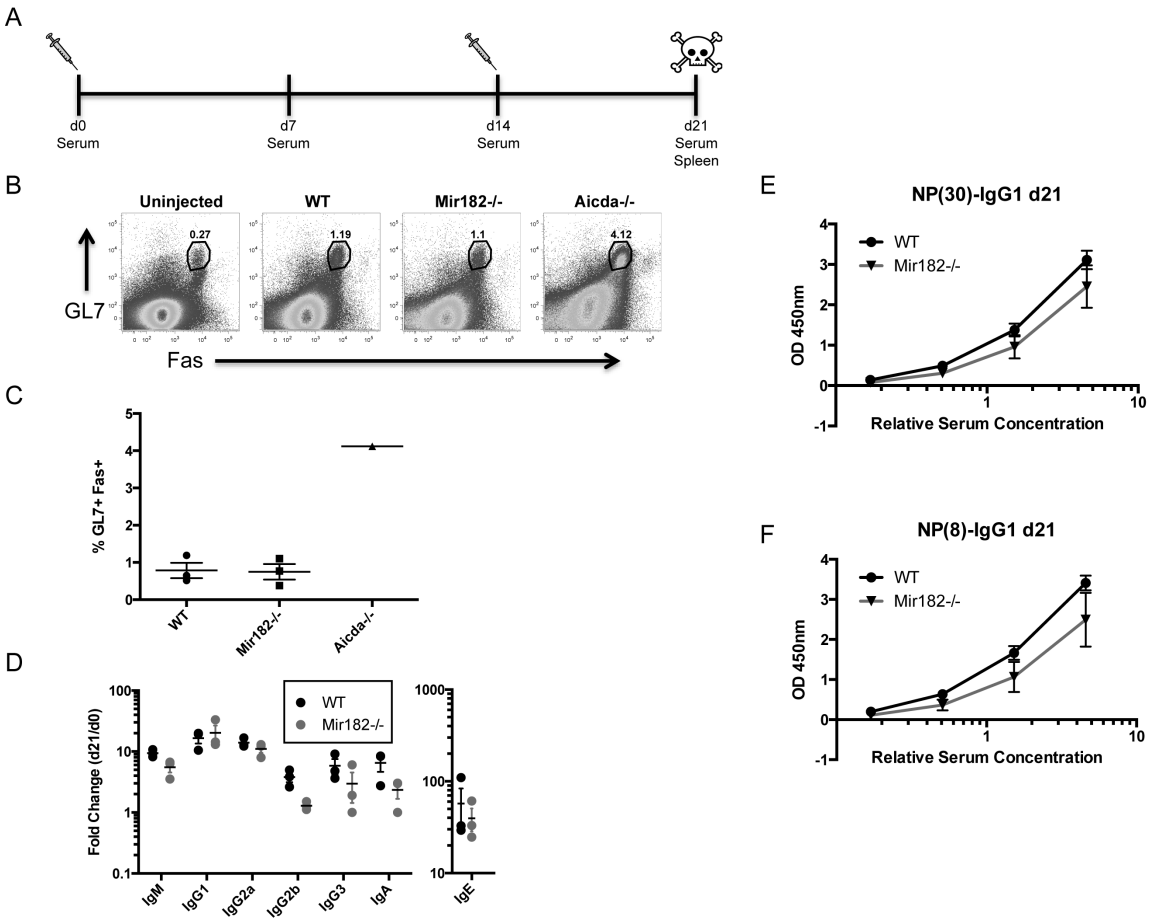

Figure 13. Antigen-dependent primary B cell response is normal in *Mir182*$^{-/-}$ mice. (**A**) Schematic of NP-CGG immunization protocol with. (**B**) Abundance of germinal center B cells ($GL7^{+}Fas^{+}$) following NP-CGG immunization was assessed by flow cytometry. *Aicda*$^{-/-}$ mice, which have significantly higher germinal center B cells (24), were used as controls. (**C**) Quantification of germinal center B cells in immunized mice. (**D**) Fold-change in serum isotype concentrations upon NP-CGG immunization, determined by ELISA. (**E-F**) Detection of low-affinity (**E**) and high-affinity (**F**) NP-specific IgG_1 serum antibodies by ELISA.

NP(30)- and NP(8)-BSA, respectively. Both low-affinity (Fig. 13E) and high-affinity (Fig. 13F) NP-specific antibodies were generated at normal levels in *Mir182*$^{-/-}$ mice.

Overall, the B cell-dependent immune response in *Mir182*$^{-/-}$ mice was typical, displaying no statistically significant differences with WT mice. While there may be a trend for slightly lowered production of some isotypes, the magnitude of the difference is unlikely to be biologically relevant. Importantly, the primary isotype induced by NP exposure, IgG1, is clearly produced at rates similar to WT counterparts. We conclude that miR-182 plays a minimal role, if any, in B cell development and B cell function during a primary response to a T cell-dependent antigen.

miR-182 is dispensable for T cell development and activation

A significant body of work has evaluated the role of miR-182 in T cell function. Transient knockdown of miR-182 using antagomiR technology suggested it was critical in CD4$^+$ helper T cell activation, clonal expansion, and *in vivo* function (72, 73). A detailed examination of *Mir182*$^{-/-}$ mice revealed no significant differences in thymic and peripheral T cell populations. The proportions of developing double negative CD4$^-$ CD8$^-$ (DN), double positive CD4$^+$ CD8$^+$ (DP), single positive CD4$^+$/CD8$^+$ (SP) and mature CD4$^+$/CD8$^+$ SP cells in the thymus (Fig 14A – B), as well as the fraction of mature CD4$^+$/CD8$^+$ SP and T regulatory cells (T_{reg}) in the periphery (Fig. 14C – D), was similar between WT and *Mir182*$^{-/-}$ mice, arguing against a role for miR-182 in T cell development.

To assess proliferation of T cells upon activation in culture, naïve splenic CD4 SP T cells from WT and *Mir182*$^{-/-}$ mice were stimulated *ex vivo* with anti-CD28, anti-CD3,

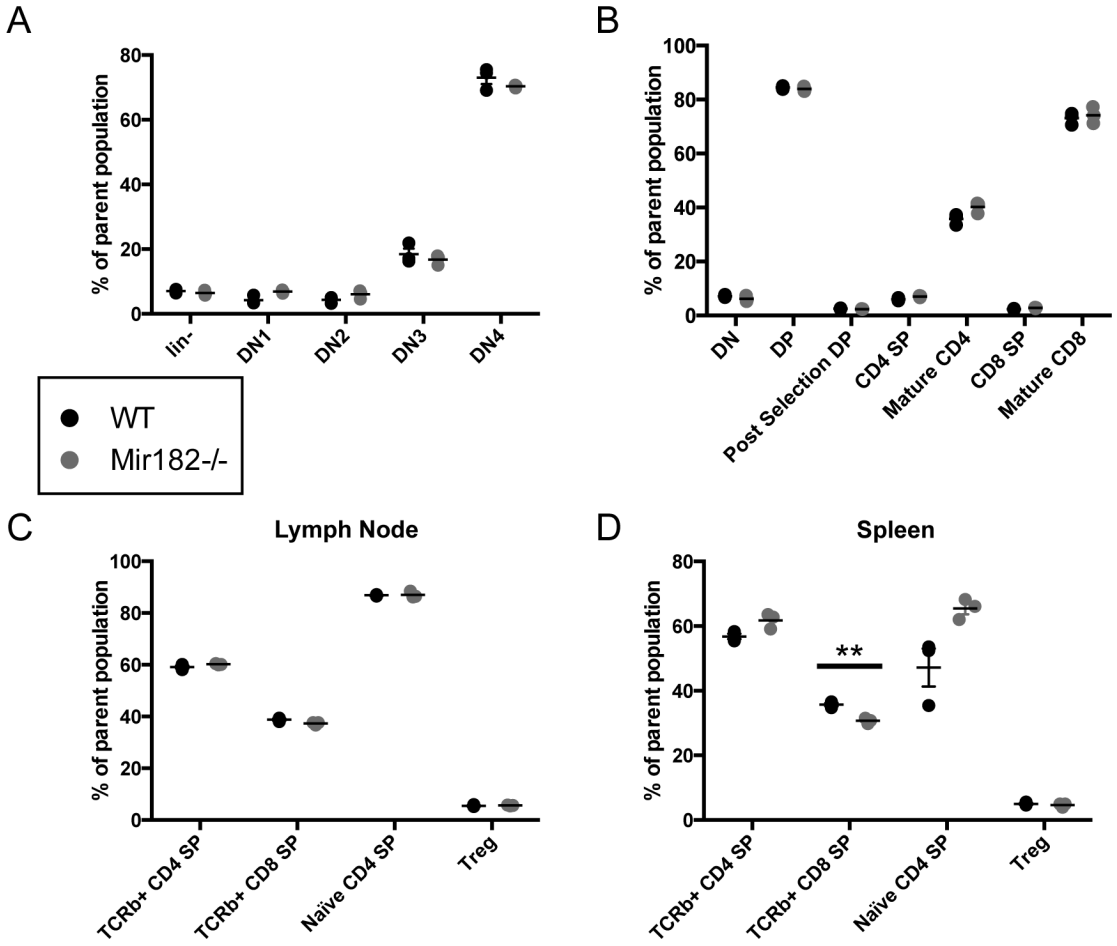

Figure 14. T cell development is unimpaired in *Mir182*$^{-/-}$ mice.
(**A-B**) Thymic T cell populations observed by flow cytometry. (**A**) Parent population for lin$^-$ is live singlets. Parent gate for DN1-4 is lin$^-$. Lin markers = CD19, CD4, CD8a, TCRβ, TCRγδ , CD11b, CD11c, Nk1.1, Ly6G(Gr1), Ter119. (**B**) Parent population for DN, DP, CD4 SP and CD8 SP is live singlets. Post-selection DP is % CD69$^+$ TCRβ$^+$ of CD4$^+$ CD8$^+$ live singlets. Mature CD4/CD8 SP is % CD69$^-$ CD62L$^+$ of CD4$^+$/CD8$^+$ SP live singlets. (**C-D**) Analysis of peripheral T cell populations from lymph nodes (**C**) or spleen (**D**). Parent population for CD4/CD8 SP is live singlets. TCRb+ DN/DP/CD4 SP/CD8 SP is % DN/DP/CD4$^+$ SP/CD8$^+$ SP of TCRβ$^+$ live singlets. Naïve CD4 SP is % CD62L$^+$ CD44$^-$ of CD4$^+$ SP live singlets. Treg is % CD25$^+$ CD44$^-$ of CD4$^+$ SP live singlets.

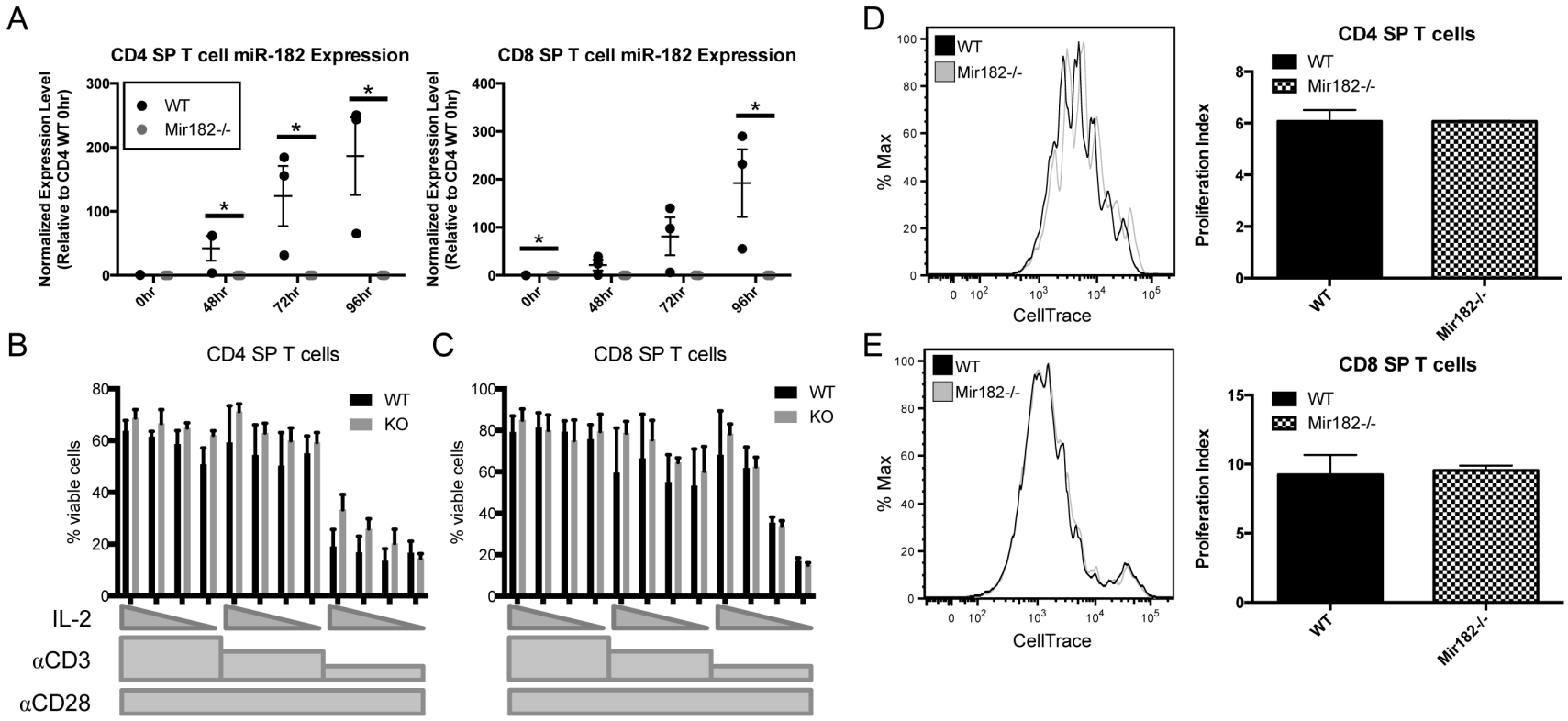

Figure 15. T cell activation is normal in *Mir182*$^{-/-}$ mice.

Figure 15 (cont.). (**A**) Sorted naïve splenic SP T cells were isolated from indicated mice and stimulated with plate-bound anti-CD3 (1μg/mL), soluble anti-CD28 (4μg/mL) and soluble IL-2 (1U/mL) and TaqMan qPCR was used to monitor expression of miR-182. (**B, C**) Sorted naïve splenic SP T cells were isolated from indicated mice and stimulated with plate-bound anti-CD3 (10, 1, or 0.2 μg/mL), soluble anti-CD28 (2 μg/mL) and soluble IL-2 (50, 25, 10, or 1 U/mL). Bar graphs depict % viability for $CD4^+$/$CD8^+$ SP T cells over stimulation conditions used. (**D**) Histogram overlay depicts representative CellTrace dilution profiles of $CD4^+$ SP T cells stimulated with anti-CD3 (1 μg/mL), anti-CD28 (2 μg/mL) and IL-2 (1 U/mL). Representative proliferation index for same stimulation conditions is shown. (**E**) Histogram overlay depicts representative CellTrace dilution profiles of $CD8^+$ SP T cells stimulated with anti-CD3 (10 μg/mL), anti-CD28 (2 μg/mL) and IL-2 (10 U/mL). Representative proliferation index for $CD8^+$ SP T cells stimulated with anti-CD3 (1 μg/mL), anti-CD28 (2 μg/mL) and IL-2 (25 U/mL) is shown. (**A-E**) n=3, *p<0.1 (t-test). (**B-E**) Data representative of 2 experiments.

and IL-2. Indeed, miR-182 was strongly induced upon activation of WT $CD4^+$ helper T cells, as well as $CD8^+$ cytotoxic T cells (Fig. 15A). However, there was no significant difference in viability (as assessed by live/dead staining) or proliferation (as measured by CellTrace dye dilution) of CD4 T cells upon activation (Fig. 15B, D), in direct contrast to results observed with transient knockdown (72). Likewise, no difference was found in viability and proliferation of cytotoxic T cells upon activation (Fig. 15C, E).

In vivo systemic immune response does not require miR-182

To functionally test *in vivo* immune response to a pathogen, we infected WT and *Mir182*$^{-/-}$ mice with *Listeria monocytogenes* expressing ovalbumin (OVA) Ag to induce a well-characterized systemic infection. $CD4^+$ and $CD8^+$ SP T cells were isolated from spleen and liver after 7 days (Fig. 16A). miR-182 was markedly induced upon *in vivo* activation of T cells infected with *L. monocytogenes* (Fig. 16B). It is noteworthy that although $CD44^+$ T cells can be detected in uninfected mice, robust induction of miR-182 in these cells occurs only upon infection (Fig. 16B). Sorted $CD4^+$ and $CD8^+$ SP T cells were restimulated *ex vivo* with listeriolysin O (LLO) or OVA-derived SIINFEKL peptide, respectively (Fig. 16A). No difference in effector cytokine production, as measured by the percentage of cells expressing intracellular IFNg and TNFa, was detected in both spleen and liver for $CD4^+$ SP (Fig. 16C) and $CD8^+$ SP (Fig. 16E) cells. Similarly, there was only minimal perturbation in the abundance and activation of OVA-specific cytotoxic T cells (Fig. 16D). Thus, *Mir182*$^{-/-}$ mice present no defect in the systemic immune response to *L. monocytogenes.* This contradicts previously published work that implicated miR-182 in promoting the *in vivo* function of helper T cells (72), though different approaches were used to test functional relevance.

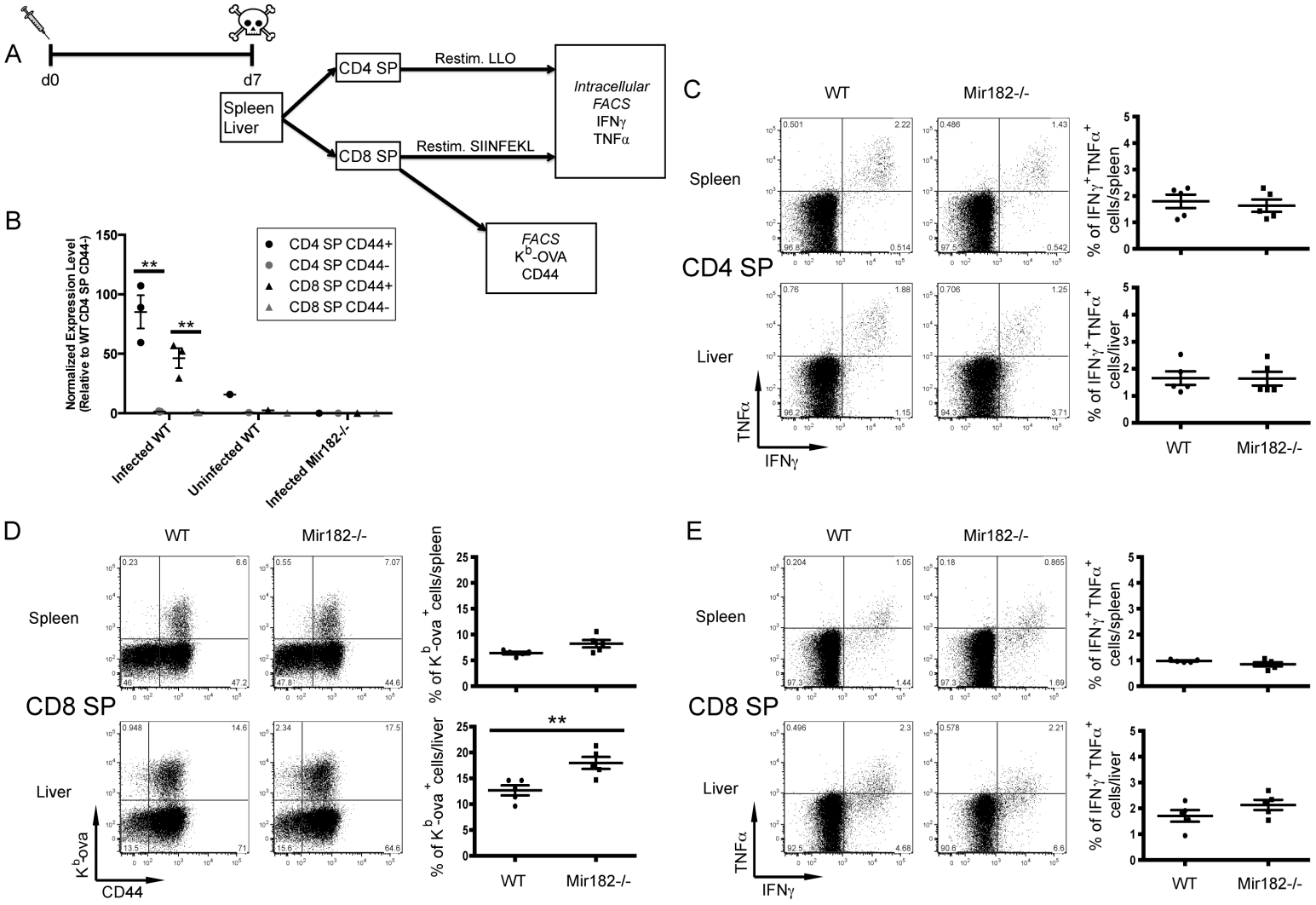

Figure 16. miR-182 deletion does not impair immune response to *Listeria monocytogenes*.

Figure 16 (cont.). (**A**) Schematic for intravenous infection with *Listeria monocytogenes*-OVA and subsequent analysis. (**B**) WT and *Mir182*$^{-/-}$ mice were infected with *L. monocytogenes* and sacrificed on day 7. Indicated cell populations were FACS-sorted from splenocytes and analyzed for miR-182 expression by TaqMan qPCR. $^{**}p<0.01$ (t-test) (**C**) Indicated cells were restimulated *ex vivo* with LLO peptide for 3 hours then analyzed by flow cytometry for intracellular effector cytokines. (**D**) Indicated cells were analyzed for surface expression of CD44 and OVA-specific TCRβ. (**E**) Indicated cells were restimulated *ex vivo* with SIINFEKL peptide for 3 hours then analyzed by flow cytometry for intracellular effector cytokines. (**C-E**) $^{**}p<0.01$ (Mann-Whitney test).

Discussion

Our results clearly demonstrate a striking lack of phenotype in a broad survey of the adaptive immune system in *Mir182*$^{-/-}$ mice. There is thus a remarkable lack of correlation between its expression pattern and role in B cells. This is contrary to the well-documented role of miR-155 in B cell development and CSR (88-90), even though induction of miR-155 is significantly less robust than that of miR-182 (Fig. 10). While miR-182 has been strongly implicated in DNA repair, it is evident that the repair modulatory activity is not relevant to either CSR or to suppression of lymphomagenesis as *Mir182*$^{-/-}$ mice are not tumor prone (data not shown). One explanation for the lack of a B cell defect is functional compensation by miR-183 and miR-96, both of which are expressed from a polycistronic transcript together with miR-182 and whose expression is not altered in either direction in *Mir182*$^{-/-}$ B cells (Fig. 17). Analysis of mice with deletion of this entire miR cluster could address the possibility of compensation.

The lack of phenotype in T cells is even more striking given that multiple reports have demonstrated a role of miR-182 in T cell function (72, 73). The failure to recapitulate observations derived from antagomiR-knockdown experiments could be due to off target effects of knockdown technology. But our results could also hint at an underappreciated malleability of miR networks upon long-term deprivation of one of its components. The potentially disparate biological consequences of acute and chronic miR deficiency beg careful reevaluation of published miR knockdown studies and consideration in future interpretations of miR modulation experiments.

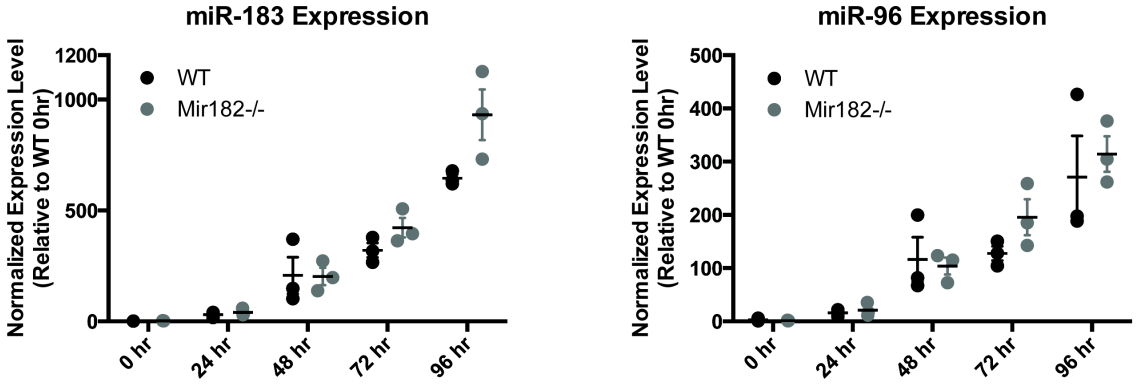

Figure 17. Expression of miR-182 family members miR-183 and miR-96.
Expression level of miR-183 and miR-96 in MACS-sorted murine splenic mature B cells *ex vivo* stimulated with LI for indicated time, measured by real-time qPCR and set relative to representative naïve WT sample.

CHAPTER 4

183c miRs are highly expressed in activated B cells, GC B cells, and plasmablasts

miR-182, -96, and -183 are clustered in an intronic locus on murine chromosome 6. This cluster (183c) may be synchronously expressed as part of a polycistronic transcript (61). Given that miR-182 is so strongly induced upon B cell activation, yet its absence is of debatable consequence (78, 91), we sought to carefully investigate the expression of the entire 183c family. As expected (78, 91), vigorous mature miR-182 induction was observed by qPCR in mature B cells stimulated *ex vivo* (Fig. 18A). Interestingly, the expression patterns of mature miR-183 (Fig. 18B) and miR-96 (Fig. 18C) in B cells activated by the same assortment of stimuli closely mirror that of miR-182, albeit with less pronounced induction. This suggests that, in B cells, transcription and processing of these genomically clustered miRs may be linked. Similarly, a parallel pattern was observed for 183c miR expression in GC B cells and plasmablasts induced upon immunization with SRBCs (Fig. 18E).

Due to their expression pattern, overwhelming sequence homology and predicted target overlap as determined using the TargetScan 7.1 algorithm (Fig. 18F) (92), we reasoned that miR-183 and miR-96 might provide sufficient redundancy to miR-182 to mask the individual loss of miR-182. To investigate the role of 183c miRs in B cell function, we employed the $183c^{GT/GT}$ mouse model. The 183c GT allele contains a promoterless gene trap construct inserted upstream of 183c. The gene trap consists of a splice acceptor and a β-galactosidase/neomycin cassette with its own polyA signal (Fig. 19). In forcing mis-splicing, the gene trap abrogates expression of all 183c miRs (61, 63). In the 183c We confirmed 183c miR expression was abolished in B cells and

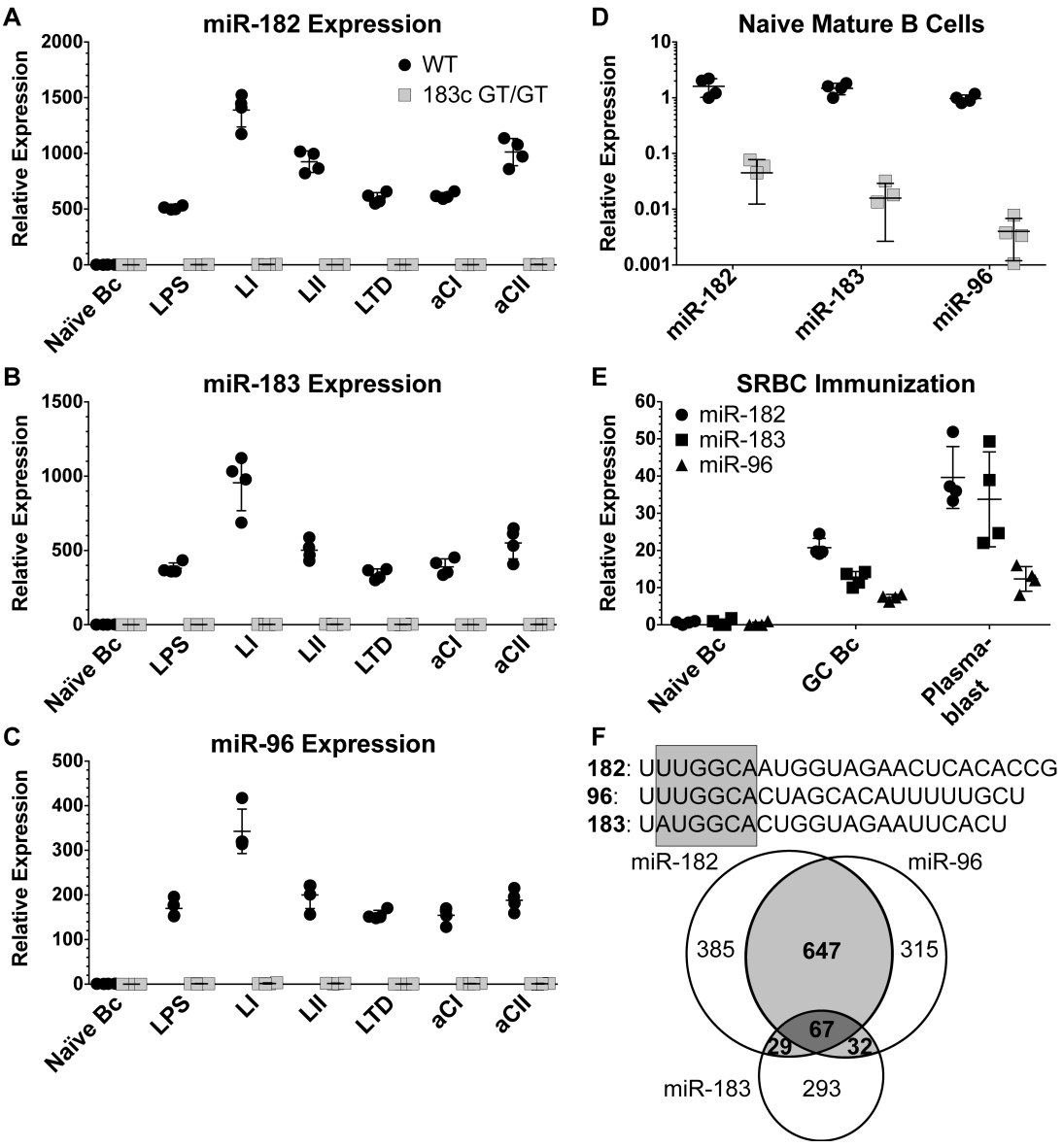

Figure 18. 183c expression is induced upon B cell activation.
(A - D) Expression level of miR-182 (A), miR-183 (B), and miR-96 (C) in MACS-sorted murine splenic mature B cells *ex vivo* stimulated for 96hrs, measured by real-time qPCR and set relative to representative naïve WT sample. LI = LPS + IL-4, LII = LPS + IL-2 + IL-5, LTD = LPS + TGFβ + αIgD-dextran, aCI = αCD40 + IL-4, aCII = αCD40 + IL-4 + IL-5. $n = 4$, 1 expt. (D) 183c expression in murine splenic naïve B cells. $n = 4$, 1 expt. **(E)** 183c expression level in splenic naïve B cells ($B220^+$ $CD38^+$ IgD^+ $CD138^-$ $GL7^-$ PNA^-), germinal center B cells ($B220^+$ $CD38^-$ IgD^- $CD138^-$ $GL7^+$ PNA^+), and plasmablasts ($B220^{lo}$ $CD138^+$ $GL7^-$ PNA^-) FACS-sorted from SRBC-immunized WT mice. $n = 4$, 1 expt. **(F)** Sequences of 183c miRs and diagram of TargetScan predicted target overlap. Grey box over sequence alignment indicates seed region. Circle area is to scale with predicted target number. See Table 2 for full list of predicted targets. Statistical significance determined by unpaired *t*-test. All WT vs. $183c^{GT/GT}$ and naïve vs. activated differences deemed highly significant, see Table 1 for p-values.

Table 1. Statistical tests related to Figure 18.

All comparisons by unpaired t test.

WT vs. 183c GT/GT ex vivo miR-182

	Significance	P value	Mean1	Mean2	Difference	SE of difference	t ratio	df
Naïve Bc	**	1.89E-03	1.61	0.04516	1.565	0.2972	5.266	6
96hr LPS	****	1.23E-09	511.2	2.178	509.1	8.265	61.59	6
96hr LI	****	1.69E-06	1390	3.549	1386	75.57	18.34	6
96hr LII	****	1.28E-06	925.2	1.885	923.3	48.02	19.23	6
96hr LTD	****	3.02E-07	600	1.511	598.5	24.4	24.52	6
96hr aCI	****	9.79E-09	619.9	1.471	618.5	14.19	43.57	6
96hr aCII	****	3.10E-06	1012	3.409	1009	60.94	16.55	6

WT vs. 183c GT/GT ex vivo miR-183

	Significance	P value	Mean1	Mean2	Difference	SE of difference	t ratio	df
Naïve Bc	***	1.53E-04	1.481	0.0159	1.465	0.1741	8.416	6
96hr LPS	****	7.85E-07	379.9	1.127	378.8	18.14	20.88	6
96hr LI	***	5.30E-05	955.5	2.144	953.3	93.87	10.16	6
96hr LII	****	5.92E-06	501.8	2.595	499.2	33.67	14.83	6
96hr LTD	****	1.47E-06	340	1.88	338.1	18.01	18.78	6
96hr aCI	****	7.39E-06	389.4	0.7669	388.7	27.22	14.28	6
96hr aCII	***	5.06E-05	550.5	2.086	548.4	53.56	10.24	6

WT vs. 183c GT/GT ex vivo miR-96

	Significance	P value	Mean1	Mean2	Difference	SE of difference	t ratio	df
Naïve Bc	****	2.05E-05	0.9679	0.004006	0.9639	0.08043	11.98	6
96hr LPS	****	3.45E-06	169.8	1.06	168.7	10.38	16.25	6
96hr LI	****	9.38E-06	342.7	1.634	341	24.89	13.7	6
96hr LII	****	1.27E-05	199.9	1.667	198.2	15.23	13.01	6
96hr LTD	****	9.32E-08	155.2	0.4408	154.7	5.179	29.88	6
96hr aCI	****	3.16E-06	154.4	1.138	153.3	9.292	16.5	6
96hr aCII	****	4.15E-06	188	1.066	186.9	11.87	15.75	6

Naive vs. LPS ex vivo 183c

	Significance	P value	Mean1	Mean2	Difference	SE of difference	t ratio	df
miR-182	****	1.00E-15	1.61	511.2	-509.6	12.97	39.28	18
miR-183	****	1.00E-15	1.481	379.9	-378.5	12.97	29.17	18
miR-96	****	1.35E-10	0.9679	169.8	-168.8	12.97	13.01	18

Naive vs. LI ex vivo 183c

	Significance	P value	Mean1	Mean2	Difference	SE of difference	t ratio	df
miR-182	****	1.44E-13	1.61	1390	-1388	71.04	19.54	18
miR-183	****	8.09E-11	1.481	955.5	-954	71.04	13.43	18
miR-96	***	1.40E-04	0.9679	342.7	-341.7	71.04	4.81	18

Naive vs. LII ex vivo 183c

	Significance	P value	Mean1	Mean2	Difference	SE of difference	t ratio	df
miR-182	****	1.00E-15	1.61	925.2	-923.5	34.98	26.4	18
miR-183	****	2.85E-11	1.481	501.8	-500.3	34.98	14.3	18
miR-96	****	2.15E-05	0.9679	199.9	-198.9	34.98	5.687	18

Naive vs. LTD ex vivo 183c

	Significance	P value	Mean1	Mean2	Difference	SE of difference	t ratio	df
miR-182	****	1.00E-15	1.61	600	-598.4	17.76	33.7	18
miR-183	****	2.20E-13	1.481	340	-338.5	17.76	19.06	18
miR-96	****	7.46E-08	0.9679	155.2	-154.2	17.76	8.685	18

Naive vs. aCI ex vivo 183c

	Significance	P value	Mean1	Mean2	Difference	SE of difference	t ratio	df
miR-182	****	1.00E-15	1.61	619.9	-618.3	18.52	33.39	18
miR-183	****	4.30E-14	1.481	389.4	-387.9	18.52	20.95	18
miR-96	****	1.48E-07	0.9679	154.4	-153.4	18.52	8.286	18

Naive vs. aCII ex vivo 183c

	Significance	P value	Mean1	Mean2	Difference	SE of difference	t ratio	df
miR-182	****	3.10E-14	1.61	1012	-1010	47.34	21.34	18
miR-183	****	8.71E-10	1.481	550.5	-549	47.34	11.6	18
miR-96	**	9.36E-04	0.9679	188	-187	47.34	3.951	18

Naive vs. GC in vivo 183c

	Significance	P value	Mean1	Mean2	Difference	SE of difference	t ratio	df
miR-182	****	8.50E-14	0.5923	20.76	-20.16	1.001	20.14	18
miR-183	****	8.40E-10	0.6956	12.33	-11.64	1.001	11.62	18
miR-96	****	1.27E-06	0.25	7.361	-7.111	1.001	7.104	18

Naive vs. PC in vivo 183c

	Significance	P value	Mean1	Mean2	Difference	SE of difference	t ratio	df
miR-182	****	8.05E-08	0.5923	39.62	-39.03	4.517	8.64	18
miR-183	****	8.50E-07	0.6956	33.75	-33.06	4.517	7.319	18
miR-96	*	1.54E-02	0.25	12.34	-12.09	4.517	2.677	18

WT vs. 183c GT/GT in vivo miR-182 Statistical tests not performed because miR undetected in 183c GT/GT.
WT vs. 183c GT/GT in vivo miR-183 Statistical tests not performed because miR undetected in 183c GT/GT.
WT vs. 183c GT/GT in vivo miR-96 Statistical tests not performed because miR undetected in 183c GT/GT.

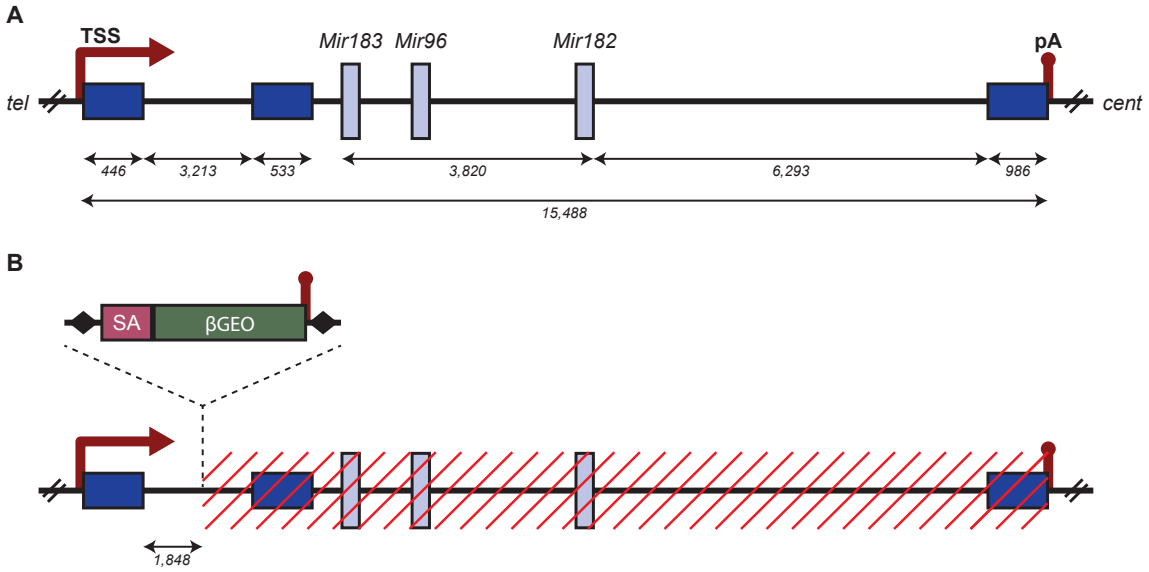

Figure 19. The 183c genetic locus and gene trap allele.
(**A**) The WT 183c allele, with dark blue boxes depicting exons of a putative transcriptional unit. Numbers under arrows indicate base pair distances.
(**B**) The 183c GT allele in which a gene trap has been inserted in intron 1 of the putative transcriptional unit. Black diamonds in the gene trap construct represent LTR sequences, SA refers to splice acceptor, and βGEO refers to the β-galactosidase/neomycin resistance gene fusion cassette.

plasmablasts derived from 183c$^{GT/GT}$ mice (Fig. 18). The 183c$^{GT/GT}$ mice thus provided a convenient model to assess the requirements of 183c miRs in B cell development and function.

183c$^{GT/GT}$ mice exhibit normal B cell development and peripheral B cell populations

Given that our work was the first, to our knowledge, to investigate humoral immunity in 183c$^{GT/GT}$ mice, we first characterized B cell development and homeostasis. In bone marrow, we observed frequencies of pro (CD43^{+} B220^{lo} IgM^{-}), pre (CD43^{-} B220^{lo} IgM^{-}), immature (B220^{lo} IgM^{+}), and mature recirculating (B220^{hi} IgM^{+}) B cells indistinguishable from WT (Fig. 20A). In the periphery, we observed similar spleen cellularity (Fig. 20B) and frequency of splenic follicular (IgM^{int} IgD^{+} CD21^{+} CD23^{+}) and marginal zone (IgM^{+} IgD^{-} CD21^{hi} CD23^{lo}) B cells (Fig. 20C). Judging by surface IgM and IgD expression, we ascertained peripheral staging of B cell maturity in the spleen to be normal (Fig. 20C). In total, B cell development appears to be unimpaired by ubiquitous loss of 183c miR expression.

Class switch recombination is unperturbed by 183c miR ablation

We first identified miR-182 as a promising candidate for regulating CSR in activated B cells in part due to robust induction upon activation by CSR-stimulating conditions and a significant dependency on AID sufficiency for this induction. Ultimately, we reported no CSR defect in *Mir182*$^{-/-}$ B cells (91). In continuation of this work, and to investigate possible compensation within the 183c cluster, we first sought to test if purified B cells from *183c*$^{GT/GT}$ mice could efficiently undergo CSR in *ex vivo*

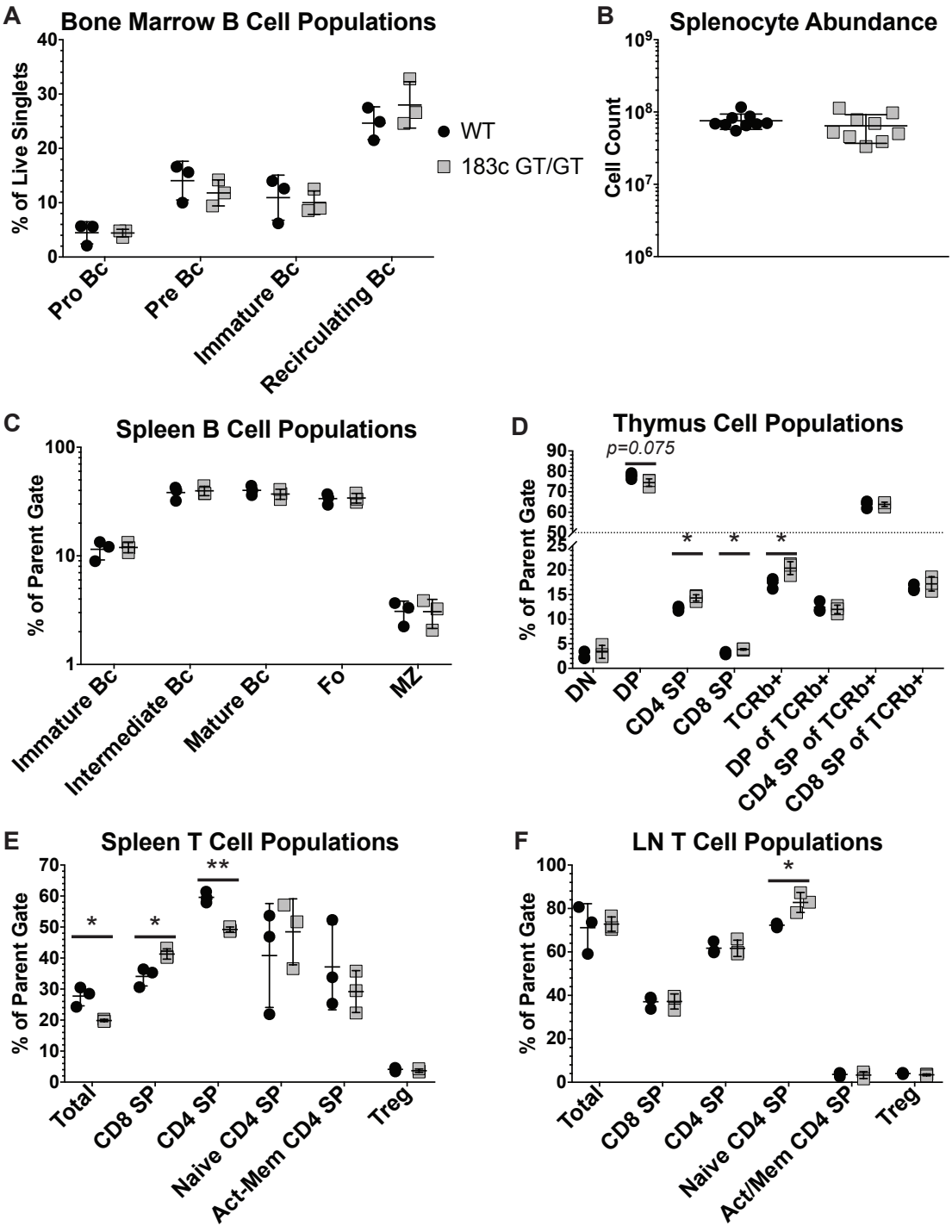

Figure 20. B cell development and peripheral T cell frequency in 183c$^{GT/GT}$ mice.

Figure 20 (cont.). 183c$^{GT/GT}$ and WT littermates were sacrificed, and bone marrow, spleen and pooled inguinal/brachial/axillary/cervical lymph node cells were analyzed by flow cytometry. **(A)** Quantification of bone marrow pro (CD43^{+} B220^{lo} IgM^{-}), pre (CD43^{-} B220^{lo} IgM^{-}), immature (B220^{lo} IgM^{+}) and mature recirculating (B220^{hi} IgM^{+}) B cell frequency. **(B)** Spleen cellularity. **(C)** Quantification of splenic immature (IgM^{hi} IgD^{lo} of B220^{+}), intermediate (IgM^{hi} IgD^{hi} of B220^{+}), mature (IgM^{lo} IgD^{hi} of B220^{+}), follicular (Fo: IgM^{int} IgD^{+} CD21^{+} CD23^{+}) and marginal zone (MZ: IgM^{+} IgD^{-} CD21^{hi} CD23^{lo}) B cell frequency. **(D)** Quantification of DN (CD8^{-} CD4^{-}), DP (CD8^{+} CD4^{+}), CD4 SP (CD8^{-} CD4^{+}), CD8 SP (CD8^{+} CD4^{-}), TCRβ^{+}, DP of TCRβ^{+}, CD4 SP (of TCRβ^{+}), and CD8 SP (of TCRβ^{+}) T cell frequency in thymus. **(E)** Quantification of total (TCRβ^{+}), CD8 SP (CD8^{+} CD4^{-} of TCRβ^{+}), CD4 SP (CD8^{-} CD4^{+} of TCRβ^{+}), naïve CD4 SP (CD44^{lo} CD62L^{+} of CD8^{-} CD4^{+} TCRβ^{+}), activated/memory CD4 SP (CD44^{hi} CD62L^{-} of CD8^{-} CD4^{+} TCRβ^{+}), and regulatory (T_{reg}: CD25^{+} CD44^{lo} of CD8^{-} CD4^{+} TCRβ^{+}) T cell frequency in spleen. **(F)** Same as (E) for lymph node. $n = 3$, 1 expt. Statistical significance determined by ratio paired *t*-test, * $p<0.05$, ** $p<0.005$.

culture. To our surprise, we found no difference in the ability of $183c^{GT/GT}$ to undergo CSR compared to WT, regardless of stimulation protocol (Fig. 21A – F). We conclude that expression of 183c miRs is not cell-intrinsically necessary for CSR, and that the lack of a CSR phenotype in *Mir182*$^{-/-}$ B cells was not due to compensation by miR-183 or miR-96.

During a humoral response, B cells are potentially exposed to complex arrays of stimuli including Ag, TLR ligands, secreted cytokines (e.g. IL-4, IL-21, BAFF) and membrane-bound CD154, the ligand for B cell-expressed CD40 canonically provided by Tfh cells (3, 93-95). *Ex vivo* stimulatory conditions mimic physiology in principle, but supraphysiological delivery of signaling molecules neglects intricate nuances of signaling crosstalk and cellular interactions known to occur *in vivo*. To overcome these caveats, we turned to TD and TI Ag *in vivo* immunization model systems.

Germinal centers in 183c$^{GT/GT}$ mice are light zone-skewed, though otherwise normal

SRBC immunization is a complex polyepitope TD Ag model system that induces robust GC reactions, whereby CSR and affinity maturation occur (21, 96). In response to SRBC immunization, we observed strong induction of $GL7^+$ Fas^+ GC B cells. There was a slight trend for reduced GC B cell frequency in $183c^{GT/GT}$, but the disparity was not statistically significant (Fig. 22A – B).

In spleens from unimmunized mice, we found a substantial reduction in total T cell frequency, accompanied by a propensity for increased frequency of $CD8^+$ T cells at the expense of $CD4^+$ T cells (Fig. 20D). This was surprising since it was not upheld in LN samples, and thymic $TCR\beta^+$ cells were actually somewhat elevated in $183c^{GT/GT}$ mice

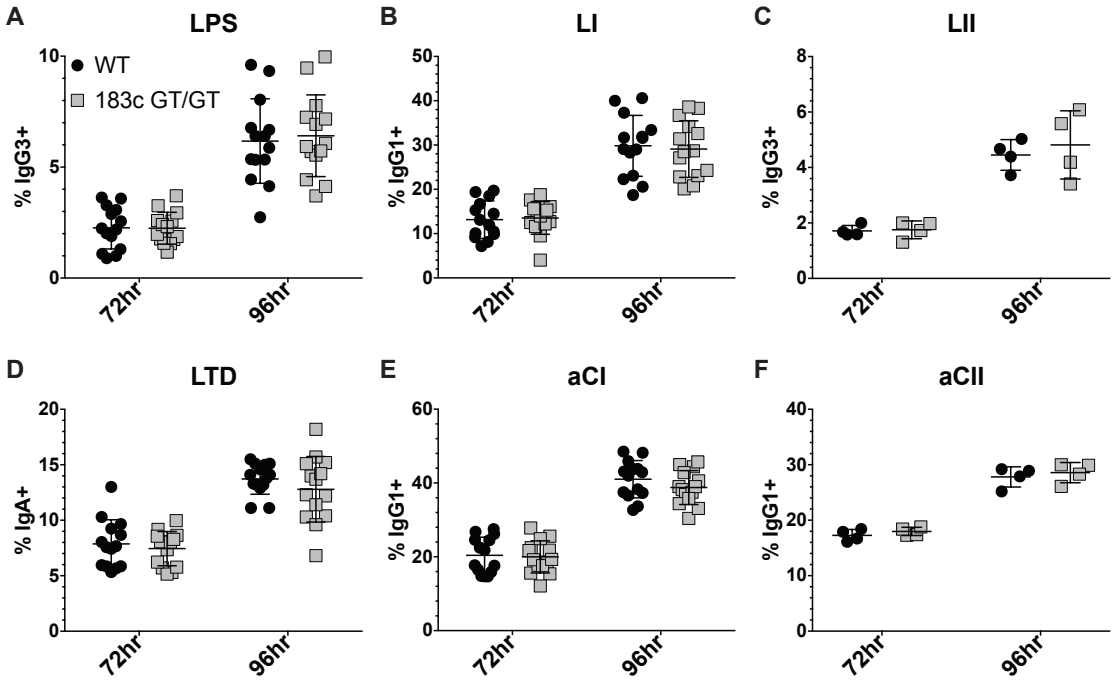

Figure 21. 183c is dispensable for CSR in B cells stimulated *ex vivo*.
(A – F) MACS-sorted murine splenic mature B cells were cultured and monitored by flow cytometry at 72 and 96 hrs for frequency of surface $IgG3^+$ cells upon LPS (A) and LII (C) stimulation, $IgG1^+$ upon LI (B), aCI (E), and aCII (F) stimulation, and IgA^+ upon LTD stimulation (D). LI = LPS + IL-4, LII = LPS + IL-2 + IL-5, LTD = LPS + TGFβ + αIgD-dextran, aCI = αCD40 + IL-4, aCII = αCD40 + IL-4 + IL-5. $n = 14$ for LPS, LI, LTD, and aCI, 5 expts; $n = 4$ for LII and aCII, 1 expt. Statistical significance determined by ratio paired *t*-test. All WT vs. $183c^{GT/GT}$ comparisons failed to meet statistical significance ($\alpha = 0.05$).

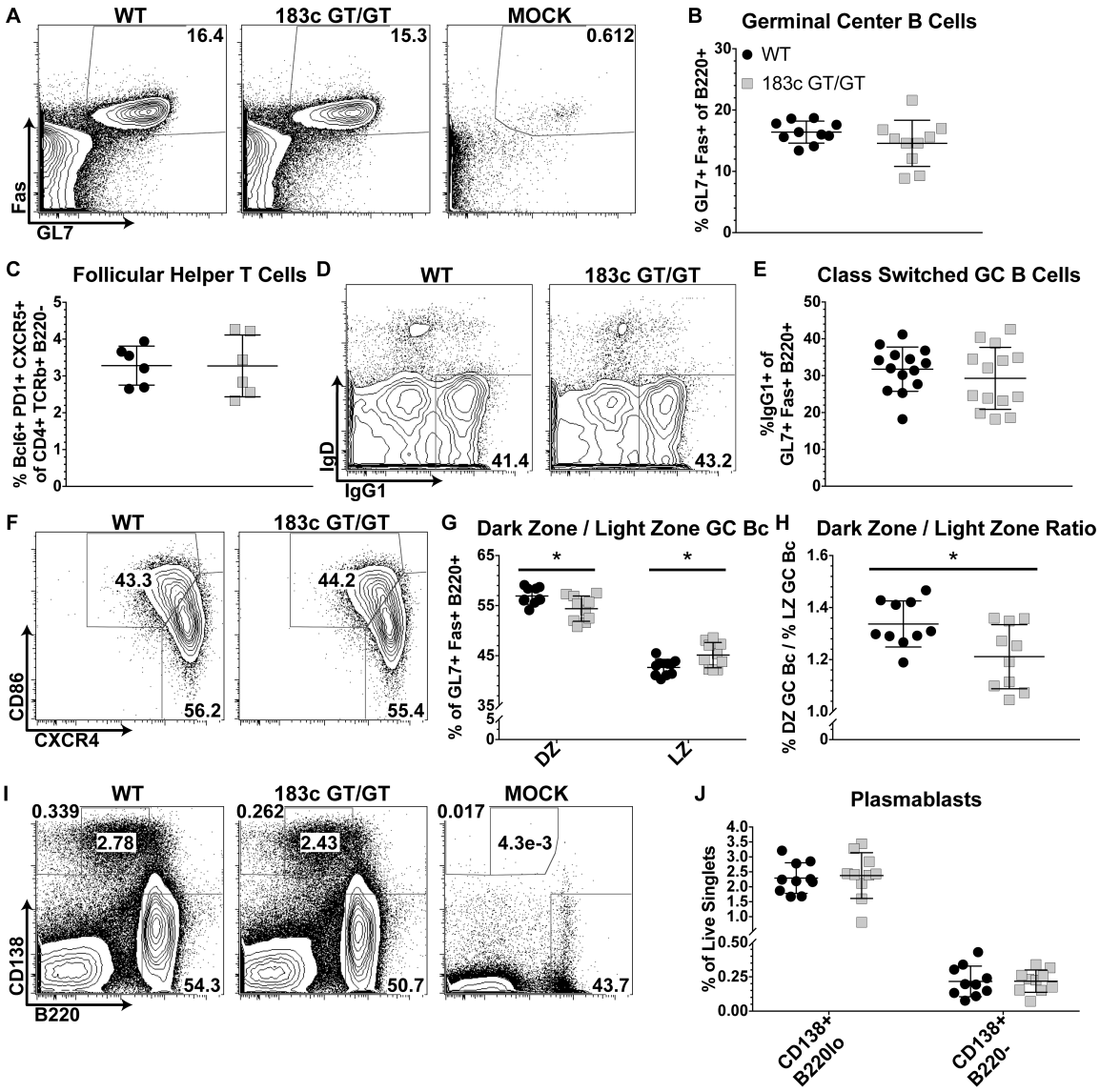

Figure 22. 183c$^{GT/GT}$ mice immunized with complex TD antigen, SRBC, exhibit normal, though light zone-skewed, germinal centers.

183c$^{GT/GT}$ and WT littermates were immunized intraperitoneally with 1x10^{9} SRBCs, boosted on day 10, and sacrificed on day 14. Total splenocytes were analyzed by flow cytometry. **(A – B)** Representative flow cytometry plots (A) and quantification (B) of GC B cell frequency (GL7^{+} Fas^{+} of B220^{+}). **(C)** Quantification of follicular helper T cell frequency (Tfh: Bcl6^{+} PD1^{+} CXCR5^{+} of CD4^{+} TCRb^{+} B220^{-}). *n* = 4, 1 expt. **(D – E)** Representative flow cytometry plots (D) and quantification (E) of isotype-switched IgG1^{+} GC B cell frequency (IgG1^{+} of GL7^{+} Fas^{+} B220^{+}). **(F – H)** Representative flow cytometry plots (F), quantification of dark zone (DZ: CXCR4^{hi} CD86^{lo}) and light zone (LZ: CXCR4^{lo} CD86^{hi}) germinal center B cell frequency (of GL7^{+} Fas^{+} B220^{+}) (G), and DZ/LZ ratio (H). **(I – J)** Representative flow cytometry plots (I) and quantification (J) of plasmablast (CD138^{+} B220^{lo}) and plasmacyte (CD138^{+} B220^{-}) frequency. All *n* = 10, 2 expts, except (H). Statistical significance determined by ratio paired *t*-test, * p<0.05.

(Fig. 20D) suggesting there is no block in early T cell development. Since $CD4^+$ Tfh cells are necessary for initiating and sustaining GC reactions (97), we were concerned by the observed reduction in homeostatic splenic $CD4^+$ T cells because this is the population from which Tfh cells derive. Thus, we quantified the frequency Tfh cells upon SRBC immunization as the percent $Bcl6^+$ $PD1^+$ $CXCR5^+$ of $CD4^+$ $TCRb^+$ $B220^-$ cells. We observed normal Tfh frequency in $183c^{GT/GT}$ mice (Fig. 22C), suggesting that GC reactions also appear normal from the T cell perspective.

B cells activated during SRBC immunization undergo CSR predominantly to IgG1 (96). Thus, we interrogated the frequency of surface $IgG1^+$ B cells within GCs as readout of capacity to undergo CSR *in vivo*. As expected we observed prolific CSR, with roughly 30% of WT GC B cells being $IgG1^+$. The mean of $183c^{GT/GT}$ samples was minimally decreased relative to WT, but the difference was not statistically significant (Fig. 22D – E).

The GC is a microanatomical structure that can be spatially divided into the DZ and LZ, through which GC B cells cycle. The DZ, constituted chiefly by GC B cells marked by high CXCR4 and low CD86 surface expression, is characterized by intense B cell proliferation and AID-mediated somatic hypermutation of Ig heavy and light chain loci. Instead, the LZ is comprised of $CD86^{hi}$ $CXCR4^{lo}$ GC B cells, FDCs, and Tfh cells that dictate selection of B cells with enhanced binding to Ag, thus driving affinity maturation (3). Accordingly, we assessed the balance of DZ to LZ GC B cells as an indicator of GC condition. Startlingly, we found that $183c^{GT/GT}$ GCs were significantly LZ-skewed (Fig. 22F – H). In sum, we conclude that $183c^{GT/GT}$ GCs appear essentially normal, though exhibiting a mild LZ skew.

183c$^{GT/GT}$ mice manifest a trend for reduced induction of serum antibodies, though affinity maturation remains intact

To further characterize the GC response in 183c$^{GT/GT}$ mice we utilized NP-CGG immunization, a well-characterized hapten TD Ag model system that facilitates identification of Ag (NP)-specific GC B cells and secreted antibodies. In agreement with the SRBC immunization results, the frequency of GC B cells was similar between WT and 183c$^{GT/GT}$ mice upon NP-CGG immunization (Fig. 23A). Frequency of NP specificity was also unchanged among GC B cells (Fig. 23A). To delve deeper, we harvested serum from NP-CGG-immunized mice and quantified serum antibodies by ELISA. We found no statistically significant differences at days 0, 7, 21 and 28 post-immunization in the serum concentration of total IgM (Fig. 23B) and IgG1 (Fig. 23D). We did observe a consistent trend across all timepoints observed for reduced induction of serum IgM and IgG1 relative to day 0, however the differences were not statistically significant (Fig. 23C, E). Next we evaluated serum titer of NP-specific IgM and IgG1 antibodies. Here we witnessed an analogous pattern to the total isotype assays: Few differences at individual timepoints (only NP-specific IgG1 at day 28 was significantly different) (Fig. 23F, I), but simultaneously a consistent downward trend in fold change induction rates (Fig. 23G, J). It should be noted that the consistent trend for reduced serum antibody induction in 183c$^{GT/GT}$ mice might be driven by the trend for slightly elevated serum antibody in 183c$^{GT/GT}$ at day 0, seen in all assays. In line with this interpretation, no apparent defect in 183c$^{GT/GT}$ plasmablast differentiation after SRBC immunization was noted (Fig. 22I – J).

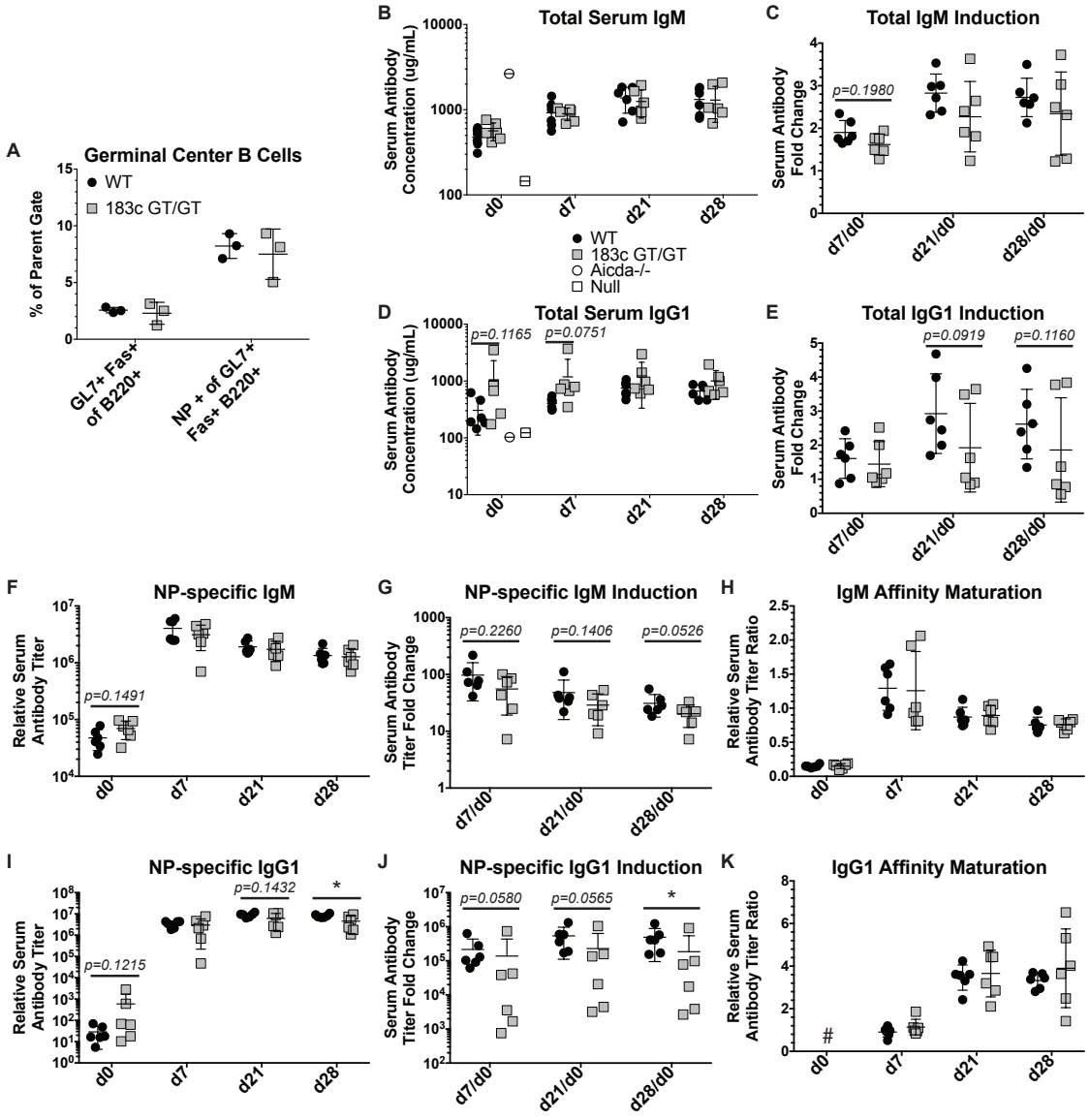

Figure 23. 183c$^{GT/GT}$ mice immunized with TD Ag NP-CGG trend for reduced serum antibody induction, though affinity maturation remains intact.
183c$^{GT/GT}$ mice immunized with TD Ag NP-CGG trend for reduced serum antibody induction, though affinity maturation remains intact. **(A)** 183c$^{GT/GT}$ and WT littermates were intraperitoneally immunized with 50μg NP(31)-CGG in alum, boosted on day 10, and sacrificed on day 14. Total splenocytes were analyzed by flow cytometry. Quantification of GC B cell (GL7$^+$ Fas$^+$ of B220$^+$) and NP-specific GC B cell (NP$^+$ of GL7$^+$ Fas$^+$ B220$^+$) frequency. n = 3, 1 expt. **(B – K)** 183c$^{GT/GT}$ and WT littermates were immunized with 100μg NP(31)-CGG in alum and serum was collected on days 0, 7, 14, 21 and 28. ELISA-based quantification of serum total IgM concentration (B) and induction (C), total IgG1 concentration (D) and induction (E), NP-specific IgM titer (F) and induction (G), and NP-specific IgG1 titer (I) and induction (J). *Aicda*$^{-/-}$ and null

Figure 23 (cont.). (empty well) are shown to demonstrate isotype specificity and assay limit of quantification, respectively (B & D). Affinity maturation assessed by ratio of high affinity (NP4) to broad (NP20) antigen binding for IgM (H) and IgG1 (K). # Indeterminate, as NP4-BSA-binding IgG1 levels were below level of quantification (K). $n = 6$, 1 expt. Statistical significance determined by ratio paired *t*-test, * $p<0.05$.

Importantly, though there may be a minor effect on induction of serum antibody, affinity maturation is distinctly unperturbed by the loss of 183c miRs, as evidenced by equivalent ratios of high affinity (NP4) to broad affinity (NP20) binding between WT and $183c^{GT/GT}$ IgM (Fig. 23H) and IgG1 (Fig. 23K) serum antibodies.

In conclusion, these results hint at a potential role for 183c miRs in promoting plasmablast differentiation, or perhaps in plasmablast function (e.g. the secretion of antibodies *per se*). Interestingly, a defective extrafollicular response in *Mir182*$^{-/-}$ mice immunized with NP-CGG, and separately NP-Ficoll, was recently demonstrated using ELISA and ELISpot. The significant reduction observed in the frequency of NP-specific IgG1-secreting plasmablasts suggests miR-182 plays a prominent role in promoting plasmablast differentiation (78). The role of 183c miRs in plasmablasts evidently requires further elucidation to resolve these inconsistencies. On a separate note, the lack of perceived impact on affinity maturation, assessed by NP-specific ELISA, bolsters the claim that GC reactions appear to be functional overall in $183c^{GT/GT}$ mice.

Induction of plasmablast markers and soluble antibody in culture does not require 183c expression

In light of the discordance among our results and published data (78), we initially turned back to our *ex vivo* culture system to interrogate the role of 183c miRs in the plasma fate decision. One benefit of this approach is that the arsenal of conditions at our disposal can be employed to fuel varying degrees of antibody secretion and induction of characteristic plasmablast markers such as CD138 and Blimp1, the master transcriptional regulator of the plasma lineage (4). Likewise, simultaneous use of protocols impinging different signaling pathways offer a broad perspective of the plasmablast fate decision.

We again utilized six different protocols to stimulate purified naïve mature splenic B cells, as described for Figure 17 and 19. Strikingly, we found no significant defect in expression of plasmablast markers CD138 (Fig. 24A – G) and intracellular Blimp1 (Fig. 24H – N), in $183c^{GT/GT}$ cultured B cells across all stimulation protocols. In fact, we uncovered a statistically significant increase in $CD138^{+}$ cells upon LTD stimulation at both 72hr and 96hr. Though not statistically significant, it is noteworthy that $Blimp1^{+}$ cell frequency upon LTD stimulation trends in the same way. Overall, it is unmistakable that these *ex vivo* B cell culture results reveal no defect in the efficiency of $183c^{GT/GT}$ B cells to induce expression of plasmablast markers.

From the same cultures, we harvested supernatant samples to measure soluble antibody concentration by ELISA. We found a trend for reduced IgM levels from $183c^{GT/GT}$ B cells cultured with LPS, LI, and LII stimulation (Fig. 25A), though the trend did not achieve statistical significance and was not echoed in LTD, aCI, and aCII stimulated cultures (Fig. 25A). Notably, we also did not see this trend when measuring other isotypes, instead finding statistically significant increases in supernatant IgG1 levels from $183c^{GT/GT}$ B cell cultures upon aCI and aCII (Fig. 25B), no difference in IgG3 levels irrespective of stimulation method (Fig. 25C), and trends for increases in both IgG2b (Fig. 25D) and IgA (Fig. 25E) levels upon LTD stimulation. On the whole, our data is not consistent with a defect in antibody secretion *per se*. The trend for context-dependent reduced soluble IgM, yet not of other isotypes, may warrant further investigation.

Humoral responses to both TI-1 and TI-2 antigens do not depend on 183c miR expression

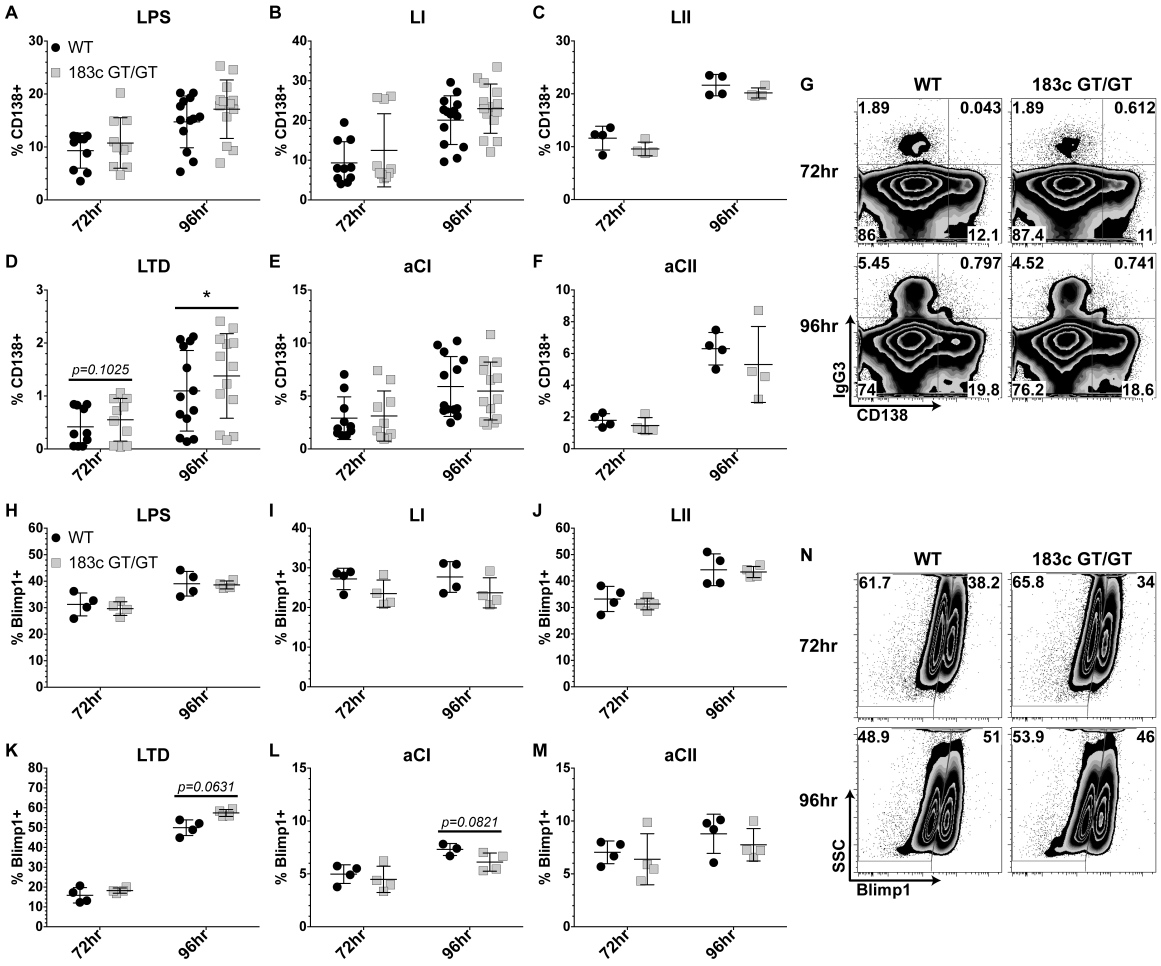

Figure 24. *Ex vivo* plasmablast marker induction is normal in absence of 183c expression.

MACS-sorted murine splenic mature B cells were cultured and monitored by flow cytometry at 72 and 96 hrs. **(A – F)** Frequency of $CD138^+$ cells upon LPS (A), LI (B), LII (C), LTD (D), aCI (E), and aCII (F) stimulation. $n = 14$ for 96hr LI, 5 expts; $n = 13$ for 96hr LPS, LTD, and aCI, 4 expts; $n = 10$ for 72hr LPS, LI, LTD and aCI, 3 expts; $n = 4$ for LII and aCII, 1 expt. **(G)** Representative flow cytometry plots of LPS-stimulated B cells. **(H - M)** Frequency of intracellular $Blimp1^+$ cells upon LPS (H), LI (I), LII (J), LTD (K), aCI (L), and aCII (M) stimulation. $n = 4$, 1 expt. **(N)** Representative flow cytometry plots of LII-stimulated B cells. LI = LPS + IL-4, LII = LPS + IL-2 + IL-5, LTD = LPS + TGFβ + αIgD-dextran, aCI = αCD40 + IL-4, aCII = αCD40 + IL-4 + IL-5. Statistical significance determined by ratio paired *t*-test, * $p<0.05$.

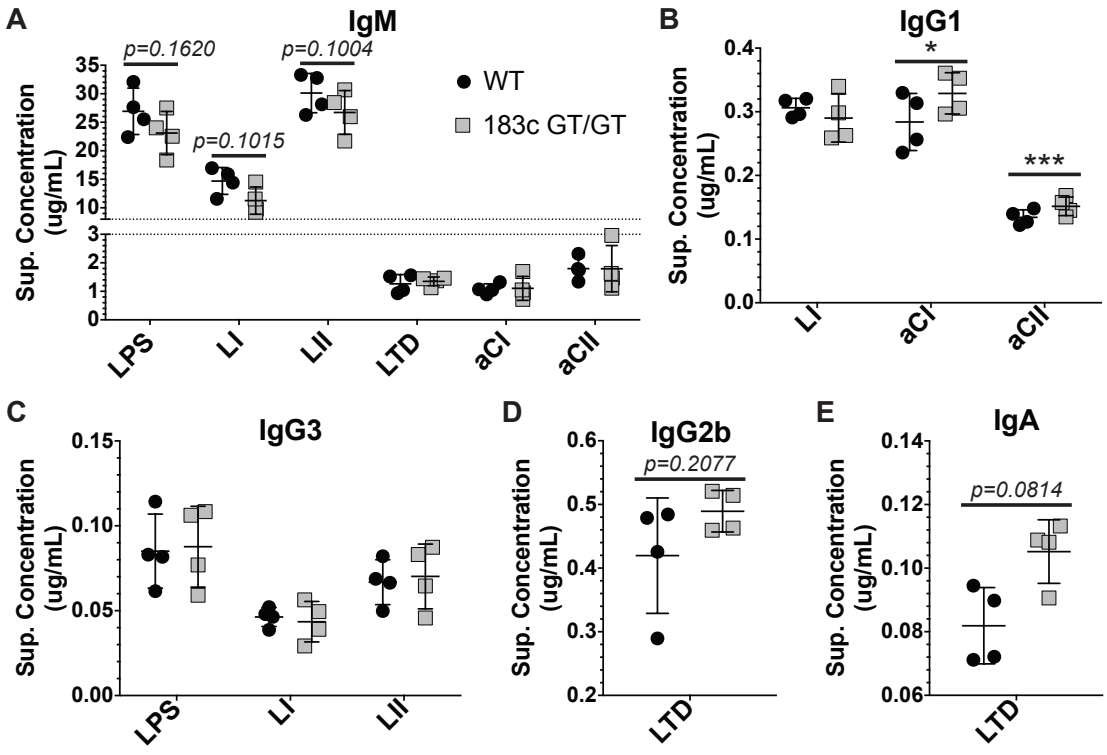

Figure 25. Antibody secretion in cultured B cells is not significantly impaired by 183c miR ablation.

MACS-sorted murine splenic mature B cells were cultured and supernatant was harvested at 96 hrs for ELISA. **(A – E)** Concentration of IgM (A), IgG1 (B), IgG3 (C), IgG2b (D) and IgA (E) in culture supernatant upon indicated stimulation protocol. LI = LPS + IL-4, LII = LPS + IL-2 + IL-5, LTD = LPS + TGFβ + αIgD-dextran, aCI = αCD40 + IL-4, aCII = αCD40 + IL-4 + IL-5. *n* =4, 1 expt. Statistical significance determined by ratio paired *t*-test, * $p<0.05$, *** $p<0.0005$.

To extend our findings beyond *ex vivo* stimulation we once again employed *in vivo* immunization models, this time with TI Ags that are dominated by the extrafollicular humoral response and hone in on plasmablast differentiation (98). When immunizing with these TI Ags, GC B cells were undetectable above background, as expected (data not shown).

First, we measured the extrafollicular response to intravenous immunization with TI-1 Ag LPS by quantifying $CD138^{+}$ $B220^{lo}$ plasmablasts using flow cytometry. We observed an equivalent proportion in WT and $183c^{GT/GT}$ mice (Fig. 26A – B). Similarly, we found no difference in the appearance of $Blimp1^{+}$ cells, or any disparity in the frequency of Blimp1 positivity in various $CD138^{+}$ subsets (Fig. 26C – D). As expected in a TI-1 extrafollicular response, an overwhelming majority of $CD138^{+}$ plasmablasts have not undergone CSR, and exhibit readily detectable high levels of intracellular IgM, indicating they likely secrete antibody (Fig. 26E – F). No difference was noted between WT and $183c^{GT/GT}$, except a slight decrease in the frequency of intra-IgM^{+} among $CD138^{+}$ $B220^{-}$ plasmacytes (Fig. 26F). Overall we conclude that, upon systemic LPS administration, 183c miRs are not necessary to mount an extrafollicular response composed of rapid and robust plasmablast differentiation.

Lastly, we immunized mice with the TI-2 Ag NP-Ficoll and performed ELISpot to measure the frequency of total and Ag-specific plasmablasts in the spleen. Similarly to TI-1 Ag, we did not detect a significant difference between WT and $183c^{GT/GT}$ samples in the frequency of IgM (Fig. 27A), IgG1 (Fig. 27B), IgG3 (Fig. 27C), NP-specific IgM (Fig. 27D – E), and NP-specific IgG (Fig. 27F – G) antibody-secreting cells. We also tested *Mir182*$^{-/-}$ mice to contextualize what we observe in $183c^{GT/GT}$ mice, but quite

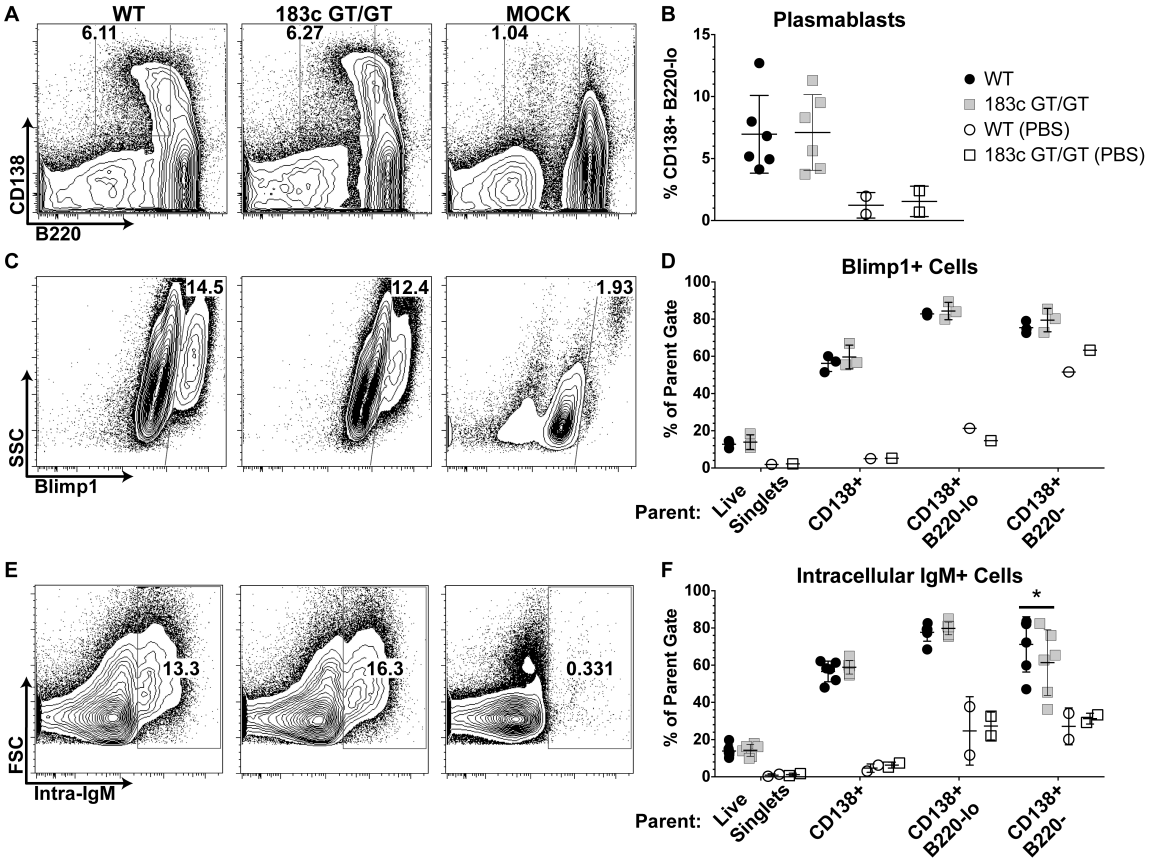

Figure 26. 183c is not required for humoral response to TI-1 antigen, LPS. $183c^{GT/GT}$ and WT littermates were intravenously immunized with 50μg LPS in sterile PBS and sacrificed on day 3. Total splenocytes were analyzed by flow cytometry. Representative flow cytometry plots **(A)** and quantification **(B)** of plasmablast ($CD138^{+}$ $B220^{lo}$) frequency. All $n = 6$ except $n = 2$ for mock immunization (PBS) controls, 2 expts. Representative flow cytometry plots **(C)** and quantification **(D)** of intracellular Blimp1+ cell frequency. All $n = 3$ except $n = 1$ for mock PBS controls, 1 expt. Representative flow cytometry plots **(E)** and quantification **(F)** of intracellular IgM^{+} frequency. All $n = 6$ except $n = 2$ for mock immunization (PBS) controls, 2 expts. Statistical significance determined by ratio paired *t*-test, * $p<0.05$.

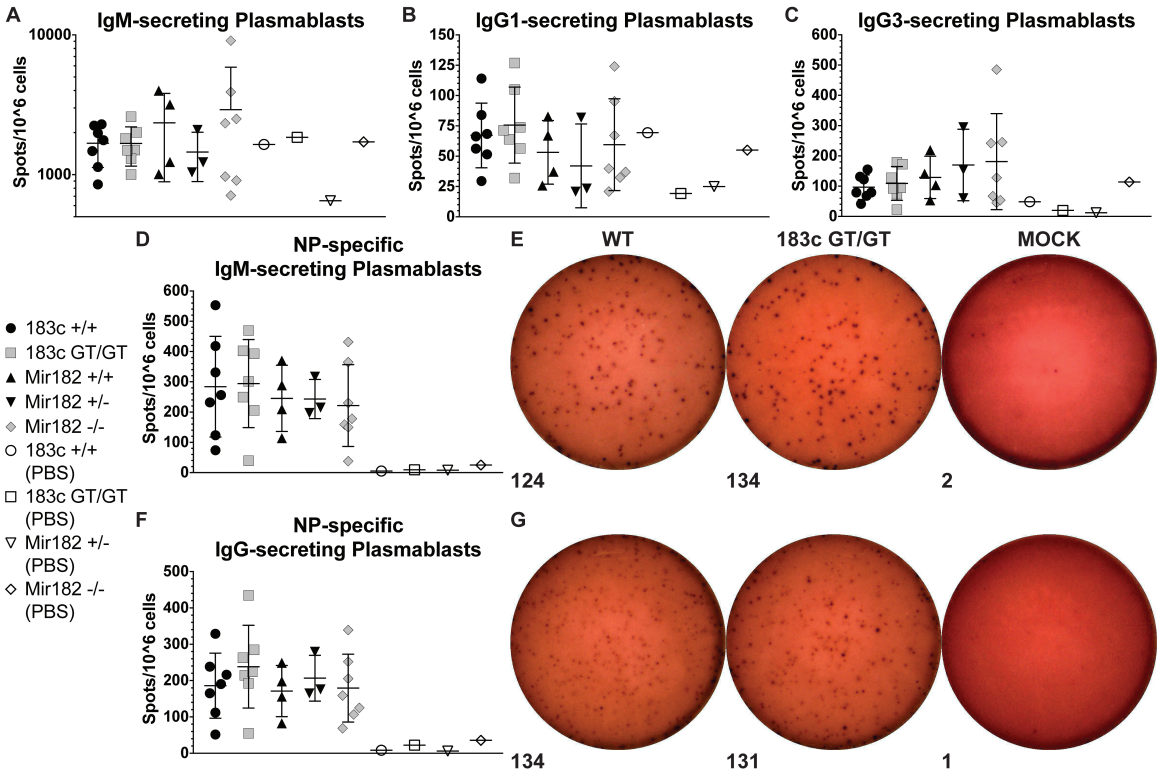

Figure 27. 183c is not required for humoral response to TI-2 antigen, NP-Ficoll. 183c$^{GT/GT}$, 183c$^{+/+}$, *Mir182*$^{-/-}$, *Mir182*$^{+/-}$, and *Mir182*$^{+/+}$ mice were intraperitoneally immunized with 100µg NP(30)-AECM-Ficoll in sterile PBS and sacrificed on day 5. Total splenocytes were analyzed by ELISpot. Quantification of IgM **(A)**, IgG1 **(B)**, and IgG3 **(C)** -secreting plasmablasts per 10^6 cells. **(D – E)** NP-specific IgM-secreting plasmablast quantification per 10^6 cells (D) and representative membrane images of wells seeded with $0.5x10^6$ cells (E). **(F – G)** NP-specific IgG-secreting plasmablast quantification per 10^6 cells (F) and representative membrane images of wells seeded with $0.5x10^6$ cells (G). Numbers below images represent spot counts done in CTL ImmunoSpot software (E & G). $n = 7$ for 183c$^{GT/GT}$, 183c$^{+/+}$ and *Mir182*$^{-/-}$; $n = 4$ for *Mir182*$^{+/+}$; $n = 3$ for *Mir182*$^{+/-}$; $n = 1$ for mock immunization (PBS) controls; 1 expt. Statistical significance determined by ratio paired *t*-test. All 183c$^{GT/GT}$ vs. 183c$^{+/+}$, *Mir182*$^{-/-}$ vs. *Mir182*$^{+/-}$, *Mir182*$^{-/-}$ vs. *Mir182*$^{+/+}$, and *Mir182*$^{-/-}$ vs. pooled *Mir182*$^{+/-}$ /*Mir182*$^{+/+}$ comparisons failed to meet statistical significance ($\alpha = 0.05$).

unexpectedly, we also detected no defect in *Mir182*$^{-/-}$ mice (Fig. 27A – D, F). Of note, we detected very little difference between mock- and NP-Ficoll-immunized animals in frequency of total IgM, IgG1, and IgG3 antibody-secreting cells (Fig. 27A –C), whereas the difference was stark for NP-specific assays (Fig. 27D – G). This highlights the subtlety and specificity of this immunization protocol in producing Ag-specific plasmablasts. In summary, we are led to conclude that expression of 183c miRs is nonessential for TI Ag-driven plasmablast differentiation. Further experimentation will be required to delineate if 183c miRs fulfill a particular role during humoral responses that is uniquely accessed during experimental immunization with the simple hapten TD Ag NP-CGG, yet not with the more complex, polyepitope TD Ag SRBC, nor with TI-1 Ag LPS and TI-2 Ag NP-Ficoll.

Discussion

In this work, we have provided compelling evidence that 183c miRs, though dramatically induced, play a minor role in mature B cell functions including CSR, the GC reaction and extrafollicular plasmablast response. In doing so, we have laid out a comprehensive framework for interrogating proximal events occurring during canonical humoral responses.

miR-182 was an attractive candidate for regulating subversion of the DNA damage response to enact efficient CSR, due to the robustness of expression during B cell activation, and its dependence on AID activity (91). Though we found no CSR defect in *Mir182*$^{-/-}$ mice, we considered the possibility of compensation by highly-related miR-183 and miR-96. This question pushed us to survey CSR in 183c$^{GT/GT}$ *ex vivo* B cell cultures.

The complete absence of a deviation from WT CSR efficiency, across a wide assortment of stimulation protocols (Fig. 21), indicates elimination of potential redundancy of miR-182 activity by other 183c miRs is not sufficient to impinge CSR efficiency.

Our results convincingly argue against a role for 183c miRs in the emergent phenomena of the GC reaction and affinity maturation during the response to TD Ags. Successful affinity maturation relies on the coordination of activities amongst GC B cells, Tfh cells, stromal populations (e.g. follicular dendritic cells), and myeloid cells (e.g. tingible-body macrophages). The lack of an effect on GCs in $183c^{GT/GT}$ mice suggests little to no impact of 183c miRs on AID-mediated SHM and the ability of GC B cells to process and present Ag, though we have not directly tested these parameters. Due to the ubiquitous lack of 183c expression in these mice, our results also suggest the dispensability of 183c miRs for the capacity of Tfh to bestow selection-guiding survival signals to GC B cells upon MHCII-mediated antigen presentation, and of FDCs to support B cell maintenance and distribute Ag to GC B cells, because the GC response inevitably collapses without these B cell-extrinsic functions (3).

Unexpectedly, $183c^{GT/GT}$ GCs display significantly altered DZ to LZ GC B cell balance. One possible explanation is that $183c^{GT/GT}$ GC B cells have reduced proliferative capacity while in the DZ state, however one would predict a DZ proliferation defect would likewise be reflected in overall GC size considering the bulk of GC B cell proliferation occurs in the DZ (3, 99). There was minimal overt difference in total GC B cell frequency (Fig. 22A – B). Similarly, no palpable proliferation defect was observed in any culture condition (data not shown). Furthermore, CSR efficiency is inexorably dependent on proliferation and can serve as a sensitive indicator (100-102). Since CSR

levels were normal in both *ex vivo* (Fig. 21) and *in vivo* (Fig. 22E) settings, proliferative capacity *per se* does not appear to be fundamentally obstructed by 183c loss.

Another explanation for the LZ tilt of $183c^{GT/GT}$ GCs is that 183c miR-mediated target repression governs the passage of GC B cells through LZ/DZ transient cell states, reinforcing DZ and/or promoting departure from LZ phenotypes. Recent work has implicated FoxO1 in programming the DZ state (103, 104). Akin to FoxO1 ablation, we also observed normal GC cellularity in conjunction with LZ skew, though the effect of disrupting FoxO1 was more severe. Intriguingly, there have also been reports of FoxO1 being repressed by miR-182 in several different cell types (72, 75, 76), yet perplexingly, if miR-182 represses FoxO1 one would expect $183c^{GT/GT}$ GCs to have DZ skew instead of LZ skew. In addition, FoxO1 disruption in GC B cells caused a drastic deficiency in CSR, and reduced SHM (103, 104). Contrary to this and arguing against FoxO1 as a target of 183c miRs, $183c^{GT/GT}$ mice had WT frequency of $IgG1^+$ GC B cells (Fig. 22E), as well as intact affinity maturation (Fig. 23H, K). Further studies will be needed to resolve whether 183c miRs target FoxO1 in the GC, and the mechanism by which 183c miR loss sways DZ/LZ balance.

Substantial discrepancies have surfaced regarding the role of $183c^{GT/GT}$ antibody-secreting plasmablasts. We first demonstrated no significant difference in serum antibody induction over 21 days by *Mir182*$^{-/-}$ mice immunized with NP-CGG (91). Shortly thereafter, a study was released proposing *Mir182*$^{-/-}$ mice did in fact suffer from a defect in plasmablast generation, as evidenced by ELISA-based measurement of serum antibodies and ELISpot-based assessment of plasmablast frequency. The defect was most severe upon NP-Ficoll immunization, or at an early timepoint (day 7) after NP-CGG

immunization (78). With the 183c$^{GT/GT}$ model, we sought to elucidate the role of these miRs in plasmablast generation. Firstly, we found that there was a trend for reduced serum antibody induction upon NP-CGG (Fig. 23B, D, G, J), though only statistically significant for NP-specific IgG1 induction at d28 (Fig. 23J). However, there was also a consistent trend for elevated serum IgM (Fig. 23B), IgG1 (Fig. 23D), NP-specific IgM (Fig. 23F) and NP-specific IgG1 (Fig. 23I) in 183c$^{GT/GT}$ mice prior to immunization, which may confound the interpretation that 183c$^{GT/GT}$ mice are unable to effectively incite plasmablast formation upon immunization. We also found a trend for diminished soluble IgM in 183c$^{GT/GT}$ B cell cultures (Fig. 25A), though it was not consistent among all stimulation protocols tested (Fig. 25A) and was not seen for any other isotype (Fig. 25B – E). Taken together, these results hint there may be a slight effect of 183c miR loss in plasmablast differentiation or antibody secretion *per se*, but ultimately the observed inconsistencies warrant substantial skepticism.

The conclusion that 183c miRs promote plasmablast generation is severely undermined by our subsequent work regarding plasmablast differentiation in a variety of settings. For one, we observed no differences in plasmablast marker expression and soluble antibody levels in response to an assortment of stimuli *ex vivo* (Fig. 24). Secondly, we were unable to detect any difference in plasmablast frequency upon SRBC (TD) immunization (Fig. 22I – J). Subsequently, LPS (TI-1) immunization revealed no effect on plasmablast generation (Fig. 26). Lastly, plasmablast generation was comparable to WT upon NP-Ficoll (TI-2) immunization in not just 183c$^{GT/GT}$ mice but, remarkably, also in *Mir182*$^{-/-}$ mice (Fig. 27). We present numerous results that are in direct conflict with the most suggestive previously published results supporting a

plasmablast differentiation defect in *Mir182*$^{-/-}$ mice upon NP-Ficoll immunization (78). A potential explanation for this inconsistency is alluded to by the discordance of our report and the work of Li et al. in the frequency of NP-specific IgG1-secreting plasmablasts in WT mice. Whereas we quantified a mean of nearly 200 secreting cells per million splenocytes, Li et al. only enumerate about 20 per million. The disagreement of our results with even WT samples may hint at disparate immunization potency or assay sensitivity, potentially enlightening why our results diverge.

Nonetheless, the multitude of approaches we have employed, both *ex vivo* and *in vivo,* gives us confidence in the assertion that 183c miRs play at best a minor role in primary humoral responses, specifically in CSR, GC and extrafollicular plasmablast programs. Moreover, we present persuasive evidence that the absence of a phenotype in *Mir182*$^{-/-}$ B cells is not due to masking by clustered paralogs miR-183 and miR-96.

CHAPTER 5

PERSPECTIVES

The simplest interpretation of my data is that 183c miR activity is unimportant for proximal humoral response processes. Perhaps, the intense observed induction of 183c miR expression serves a different purpose that has not been studied such as priming for memory B cell differentiation. It is possible the importance of 183c miRs only becomes apparent under conditions of distinct or more severe stress, such as chronic infection. An alternative is that 183c miR expression is purely vestigial in mammalian B cells.

Another possibility is that there are other yet to be described 183c miR paralogs in the mouse genome that compensate for 183c miR absence. Mining the TargetScan miR family database (92), we found evidence for just this scenario. For example, there is annotation for a miR-96 paralog, miR-1271, in the *Homo sapiens*, *Pan troglodytes* (chimpanzee), *Macaca mulatta* (rhesus macaque), *Bos taurus* (bovine), and *Canis familiaris* (canine) genomes (105), as well as a miR-183 paralog, miR-891b-3p, in the *Macaca mulatta* genome.

A final possibility is neatly illustrated by published reports in *C. elegans*. Systematic knockout of individual miRs, expected to unveil a bounty of developmental phenotypes, revealed startlingly few phenotypes (106, 107). In a fascinating follow-up, these individual mutants were reappraised in the context of a sensitized background. For example, miR activity was slashed by eliminating *alg-1*, one of two Argonaute-like proteins in *Caenorhabditis elegans*. Strikingly, a wealth of phenotypes were now uncovered (108). This suggests that the miR:target interaction network was robust

enough to cope with individual perturbations, perhaps by rewiring in such a way to fulfill the repressive activity that was lost. Speculatively, compensatory rewiring might entail miRs dissociating from weaker, perhaps less consequential, interactions to participate in stronger associations with functional binding sites that have become available upon loss of another miR (Fig. 28). This is possible of course within the confines of our current understanding of miR:target interaction, e.g. seed complementarity, conceivably by coopting *bona fide* unidentified paralogs and/or more distantly-related miRs that retain sufficient similarity to overlap activity. Overlapping miR binding sites that are offset would necessitate even less homology among competing miRs to achieve layered repression. Decreasing overall miR levels nonspecifically would be expected to stifle this robustness, and this is precisely what was observed on the *alg-1* sensitized background. Intriguingly, *Ago2* (encoding Argonaute2) is a common predicted target of all three 183c miRs (Table 2), tantalizing the notion of a protective feedback loop that enhances miR:target interaction network robustness upon the loss of 183c miR expression. It will be of great interest to determine if *Ago2* and other genes involved in miR biogenesis and activity may be regulated in such a way to modulate network features, perhaps serving as a protective buffer against loss of critical miR activity.

Accordingly, greater emphasis on overall network activity in miR studies is an imperative implication of our work. Our results may be the latest example in a growing body of evidence intimating an underappreciated miR:target interaction network robustness that compromises the utility of traditional genetic approaches in studying miRs, and advocates an approach that considers the perspective of the entire network rather than only individual nodes.

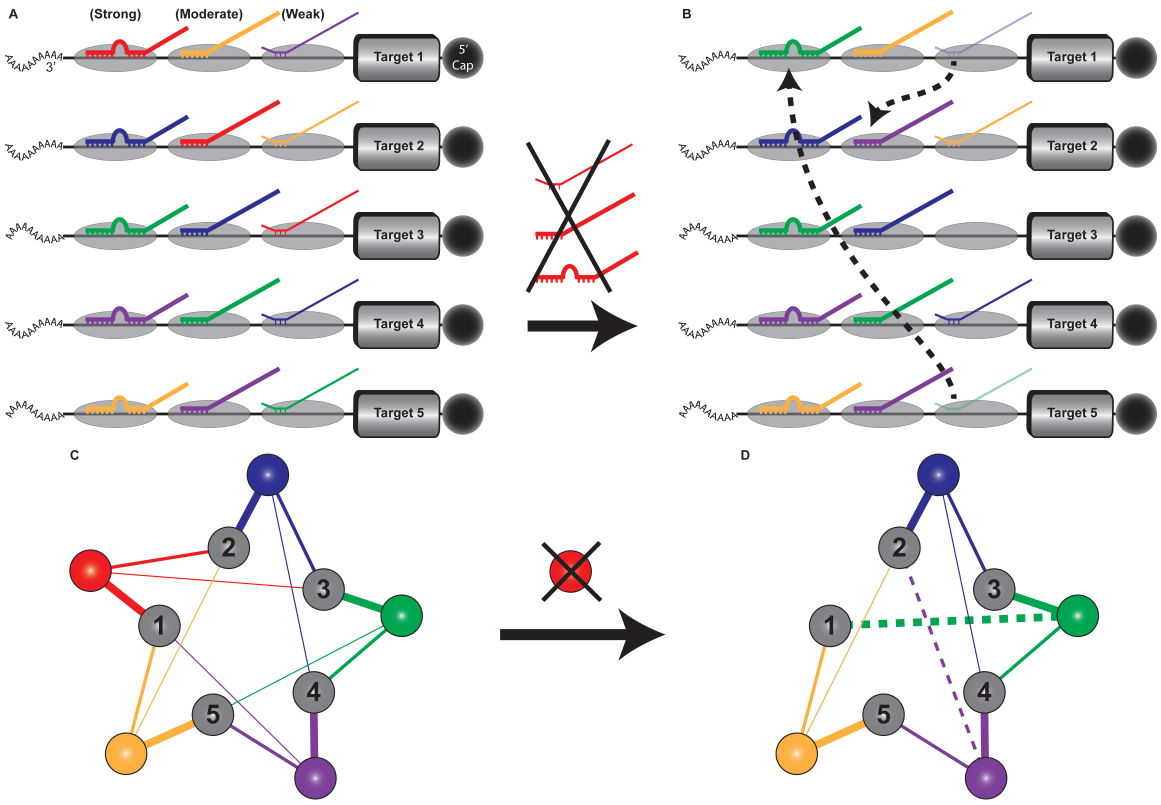

Figure 28. Schematic diagram of miRNA:target interaction network rewiring. **(A - B)** Depicted are 5 mRNA transcripts targeted in 3' UTR miR binding sites (grey ellipses) by 5 different miR species distinguished by color. Grey boxes represent transcript ORFs. Three levels of miR:target interaction strength, determined by extent of sequence complementarity, are shown as "Strong," "Moderate," and "Weak." In this simple model, target repression correlates with strength of interaction and weak interactions confer little to no functional consequence. Each transcript participates in one miR interaction of each level. Upon ablation of the red miR species, green and purple miR weak interactions are abandoned in favor of stronger interactions that were previously outcompeted by red miR (B). The result is that weak interactions are sacrificed but each target is still repressed by a strong and moderate interaction. **(C - D)** The same scenario is depicted using network diagrams. Numbered nodes represent targets 1 - 5, colored nodes represent the 5 miR species and the thickness of edges signifies the strength of the interaction. Upon ablation of the red miR species, green and purple miR weak interactions are again abandoned in favor of stronger interactions that were previously outcompeted by red miR (D). New interactions are indicated by dotted lines.

Table 2. List of *in silico* target overlap predictions for 183c miRs.
Target predictions done using TargetScan 7.1 Mouse web interface with default settings. http://www.targetscan.org/mmu_71/

TOTAL:	1128	421	1061
	182 Target gene	**183 Target gene**	**96 Target gene**

67
Common to all 183c
Bach2
Gm16039
Cpeb1
Adcy6
Celf6
Sox6
Ezr
Snx30
Tcf7l2
Pdcd6
Fam118a
Gria1
Foxo1
Paip2
Celf2
Cep170b
Dmxl1
Med1
Qk
Slc35a1
Nckap1
Brms1l
Cnot6l
Tiam1
Dgkh
Bmp2k
Fgf9
Col25a1
Celf1
Gm28048
Lphn1
B3gnt2
Dock4
Sppl2a
Kcnj14
Mfap3
Slc22a23
Map3k2
Mecom
Kcnk10
Ccnd2
Ptpn4
Zic3
Myo1b
Daam1
Nr4a3
Bnc2
Fem1c
Fndc3b
Rsf1
Ago2
Eea1
Mdm4
Phf6
Med12l
Rab21
Smim14
Jade2
Scn3a
Scn2a1
Dcx
Gpr85
Dgcr2
Mkl2
Aff4
Slc30a9
Nufip2

REFERENCES

1. Murphy, K., and C. Weaver. 2017. *Janeway's Immunobiology*. Garland Science, New York.
2. Crotty, S. 2015. A brief history of T cell help to B cells. *Nature Publishing Group* 15:185-189.
3. Victora, G. D., and M. C. Nussenzweig. 2012. Germinal centers. *Annual review of immunology* 30:429-457.
4. Nutt, S. L., P. D. Hodgkin, D. M. Tarlinton, and L. M. Corcoran. 2015. The generation of antibody-secreting plasma cells. *Nature Publishing Group* 15:160-171.
5. Vaidyanathan, B., W.-F. Yen, J. N. Pucella, and J. Chaudhuri. 2014. AIDing Chromatin and Transcription-Coupled Orchestration of Immunoglobulin Class-Switch Recombination. *Frontiers in immunology* 5:120.
6. Sawai, C. M., S. Babovic, S. Upadhaya, D. J. H. F. Knapp, Y. Lavin, C. M. Lau, A. Goloborodko, J. Feng, J. Fujisaki, L. Ding, L. A. Mirny, M. Merad, C. J. Eaves, and B. Reizis. 2016. Hematopoietic Stem Cells Are the Major Source of Multilineage Hematopoiesis in Adult Animals. *Immunity* 45:597-609.
7. Busch, K., K. Klapproth, M. Barile, M. Flossdorf, T. Holland-Letz, S. M. Schlenner, M. Reth, T. Höfer, and H.-R. Rodewald. 2015. Fundamental properties of unperturbed haematopoiesis from stem cells in vivo. *Nature* 518:542-546.
8. Fugmann, S. D., A. I. Lee, P. E. Shockett, I. J. Villey, and D. G. Schatz. 2000. The RAG proteins and V(D)J recombination: complexes, ends, and transposition. *Annual review of immunology* 18:495-527.
9. Lane, P. J., D. Gray, S. Oldfield, and I. C. MacLennan. 1986. Differences in the recruitment of virgin B cells into antibody responses to thymus-dependent and thymus-independent type-2 antigens. *European journal of immunology* 16:1569-1575.
10. Stavnezer, J. 2011. Complex regulation and function of activation-induced cytidine deaminase. *Trends Immunol* 32:194-201.
11. Liu, M., J. L. Duke, D. J. Richter, C. G. Vinuesa, C. C. Goodnow, S. H. Kleinstein, and D. G. Schatz. 2008. Two levels of protection for the B cell genome during somatic hypermutation. *Nature* 451:841-845.
12. Matthews, A. J., S. Zheng, L. J. DiMenna, and J. Chaudhuri. 2014. Regulation of immunoglobulin class-switch recombination: choreography of noncoding transcription, targeted DNA deamination, and long-range DNA repair. *Advances in immunology* 122:1-57.
13. Pasqualucci, L., G. Bhagat, M. Jankovic, M. Compagno, P. Smith, M. Muramatsu, T. Honjo, H. C. Morse, 3rd, M. C. Nussenzweig, and R. Dalla-Favera. 2008. AID is required for germinal center-derived lymphomagenesis. *Nature genetics* 40:108-112.
14. Nussenzweig, A., and M. C. Nussenzweig. 2010. Origin of chromosomal translocations in lymphoid cancer. *Cell* 141:27-38.

15. Keim, C., D. Kazadi, G. Rothschild, and U. Basu. 2013. Regulation of AID, the B-cell genome mutator. *Genes Dev* 27:1-17.
16. Vinuesa, C. G., and P. P. Chang. 2013. Innate B cell helpers reveal novel types of antibody responses. *Nature immunology* 14:119-126.
17. Schwickert, T. A., G. D. Victora, D. R. Fooksman, A. O. Kamphorst, M. R. Mugnier, A. D. Gitlin, M. L. Dustin, and M. C. Nussenzweig. 2011. A dynamic T cell-limited checkpoint regulates affinity-dependent B cell entry into the germinal center. *The Journal of experimental medicine* 208:1243-1252.
18. García de Vinuesa C, O. L., and S. D. P, Toellner KM, MacLennan IC. 1999. T-independent type 2 antigens induce B cell proliferation in multiple splenic sites, but exponential growth is confined to extrafollicular foci. *Eur. J. Immunol.* 29:1314-1327.
19. Quintana, F. J., A. Solomon, I. R. Cohen, and G. Nussbaum. 2008. Induction of IgG3 to LPS via toll-like receptor 4 co-stimulation. *PloS one* 3.
20. Reboldi, A., and J. G. Cyster. 2016. Peyer's patches: organizing B-cell responses at the intestinal frontier. *Immunological reviews* 271:230-245.
21. Paus, D., T. G. Phan, T. D. Chan, S. Gardam, A. Basten, and R. Brink. 2006. Antigen recognition strength regulates the choice between extrafollicular plasma cell and germinal center B cell differentiation. *The Journal of experimental medicine* 203:1081-1091.
22. Zhang, T.-t., D. G. Gonzalez, C. M. Cote, S. M. Kerfoot, S. Deng, Y. Cheng, M. Magari, and A. M. Haberman. 2017. Germinal center B cell development has distinctly regulated stages completed by disengagement from T cell help. *eLife* 6:1-20.
23. Barwick, B. G., C. D. Scharer, A. P. R. Bally, and J. M. Boss. 2016. Plasma cell differentiation is coupled to division-dependent DNA hypomethylation and gene regulation. *Nature immunology*:1-13.
24. Sze, D. M., K. M. Toellner, C. García de Vinuesa, D. R. Taylor, and I. C. MacLennan. 2000. Intrinsic constraint on plasmablast growth and extrinsic limits of plasma cell survival. *The Journal of experimental medicine* 192:813-821.
25. Shih, T. A., M. Roederer, and M. C. Nussenzweig. 2002. Role of antigen receptor affinity in T cell-independent antibody responses in vivo. *Nature immunology* 3:399-406.
26. Hsu, M.-C., K.-M. Toellner, C. G. Vinuesa, and I. C. M. Maclennan. 2006. B cell clones that sustain long-term plasmablast growth in T-independent extrafollicular antibody responses. *Proceedings of the National Academy of Sciences of the United States of America* 103:5905-5910.
27. Weisel, F., and M. Shlomchik. 2017. Memory B Cells of Mice and Humans. *Annual review of immunology*:255-284.
28. Nurieva, R. I., Y. Chung, G. J. Martinez, X. O. Yang, S. Tanaka, T. D. Matskevitch, Y.-H. Wang, and C. Dong. 2009. Bcl6 mediates the development of T follicular helper cells. *Science (New York, N.Y.)* 325:1001-1005.
29. Yu, D., S. Rao, L. M. Tsai, S. K. Lee, Y. He, E. L. Sutcliffe, M. Srivastava, M. Linterman, L. Zheng, N. Simpson, J. I. Ellyard, I. A. Parish, C. S. Ma, Q.-J. Li, C. R. Parish, C. R. Mackay, and C. G. Vinuesa. 2009. The transcriptional repressor

Bcl-6 directs T follicular helper cell lineage commitment. *Immunity* 31:457-468.
30. Johnston, R. J., A. C. Poholek, D. DiToro, I. Yusuf, D. Eto, B. Barnett, A. L. Dent, J. Craft, and S. Crotty. 2009. Bcl6 and Blimp-1 are reciprocal and antagonistic regulators of T follicular helper cell differentiation. *Science (New York, N.Y.)* 325:1006-1010.
31. Kroenke, M. A., D. Eto, M. Locci, M. Cho, T. Davidson, E. K. Haddad, and S. Crotty. 2012. Bcl6 and Maf Cooperate To Instruct Human Follicular Helper CD4 T Cell Differentiation. *The Journal of Immunology* 188:3734-3744.
32. Choi, Y. S., and S. Crotty. 2015. T follicular Helper Cells. *Methods in molecular biology (Clifton, N.J.)* 1291:49-61.
33. Calame, K. L., K. I. Lin, and C. Tunyaplin. 2003. Regulatory mechanisms that determine the development and function of plasma cells. *Annual review of immunology* 21:205-230.
34. Cimmino, L., G. A. Martins, J. Liao, E. Magnusdottir, G. Grunig, R. K. Perez, and K. L. Calame. 2008. Blimp-1 Attenuates Th1 Differentiation by Repression of ifng, tbx21, and bcl6 Gene Expression. *The Journal of Immunology* 181:2338-2347.
35. Shapiro-Shelef, M., K.-I. Lin, L. J. McHeyzer-Williams, J. Liao, M. G. McHeyzer-Williams, and K. Calame. 2003. Blimp-1 is required for the formation of immunoglobulin secreting plasma cells and pre-plasma memory B cells. *Immunity* 19:607-620.
36. Mayer, C. T., A. Gazumyan, E. E. Kara, A. D. Gitlin, J. Golijanin, C. Viant, J. Pai, T. Y. Oliveira, Q. Wang, A. Escolano, M. Medina-Ramirez, R. W. Sanders, and M. C. Nussenzweig. 2017. The microanatomic segregation of selection by apoptosis in the germinal center. *Science* 358:eaao2602.
37. Gitlin, A. D., Z. Shulman, and M. C. Nussenzweig. 2014. Clonal selection in the germinal centre by regulated proliferation and hypermutation. *Nature* 509:637-640.
38. Gitlin, A. D., C. T. Mayer, T. Y. Oliveira, Z. Shulman, M. J. K. Jones, A. Koren, and M. C. Nussenzweig. 2015. T cell help controls the speed of the cell cycle in germinal center B cells. *Science (New York, NY)* 349:1-8.
39. Weisel, F. J., G. V. Zuccarino-Catania, M. Chikina, and M. J. Shlomchik. 2016. A Temporal Switch in the Germinal Center Determines Differential Output of Memory B and Plasma Cells. *Immunity* 44:116-130.
40. Suan, D., C. Sundling, and R. Brink. 2017. Plasma cell and memory B cell differentiation from the germinal center. *Current opinion in immunology* 45:97-102.
41. Gitlin, A. D., L. V. Boehmer, A. Gazumyan, Z. Shulman, T. Y. Oliveira, M. C. Nussenzweig, A. D. Gitlin, L. V. Boehmer, A. Gazumyan, Z. Shulman, and T. Y. Oliveira. 2016. Independent Roles of Switching and Hypermutation in the Development and Persistence of B Lymphocyte Memory Article Independent Roles of Switching and Hypermutation in the Development and Persistence of B Lymphocyte Memory. *Immunity*:1-13.
42. Dominguez-Sola, D., G. D. Victora, C. Y. Ying, R. T. Phan, M. Saito, M. C. Nussenzweig, and R. Dalla-Favera. 2012. The proto-oncogene MYC is

required for selection in the germinal center and cyclic reentry. *Nature immunology* 13:1083-1091.
43. Suurmond, J. D., Betty. 2015. Autoantibodies in Systemic Autoimmune Diseases. *The Journal of clinical investigation* 2:1-9.
44. Lech, M., and H.-J. Anders. 2013. The Pathogenesis of Lupus Nephritis. *Journal of the American Society of Nephrology* 24:1357-1366.
45. Mesin, L., J. Ersching, and Gabriel D. Victora. 2016. Germinal Center B Cell Dynamics. *Immunity* 45:471-482.
46. Thorley-Lawson, D., K. W. Deitsch, K. A. Duca, and C. Torgbor. 2016. The Link between Plasmodium falciparum Malaria and Endemic Burkitt's Lymphoma - New Insight into a 50-Year-Old Enigma. *PLoS pathogens* 12:12-16.
47. Shalapour, S., and M. Karin. 2015. Immunity, inflammation, and cancer: An eternal fight between good and evil. *Journal of Clinical Investigation* 125:3347-3355.
48. Rana, T. M. 2007. Illuminating the silence: understanding the structure and function of small RNAs. *Nature reviews. Molecular cell biology* 8:23-36.
49. Bartel, D. P. 2009. MicroRNAs: target recognition and regulatory functions. *Cell* 136:215-233.
50. Wienholds, E., and R. H. A. Plasterk. 2005. MicroRNA function in animal development. *FEBS Letters* 579:5911-5922.
51. Alvarez-Garcia, I. 2005. MicroRNA functions in animal development and human disease. *Development* 132:4653-4662.
52. Sun, K., and E. C. Lai. 2013. Adult-specific functions of animal microRNAs. *Nature Reviews Genetics* 14:535-548.
53. Xiao, C., and K. Rajewsky. 2009. MicroRNA control in the immune system: basic principles. *Cell* 136:26-36.
54. Lawrie, C. H. 2013. MicroRNAs in hematological malignancies. *Blood Rev* 27:143-154.
55. Lin, S., and R. I. Gregory. 2015. MicroRNA biogenesis pathways in cancer. *Nature Reviews Cancer* 15:321-333.
56. Newman, M. A., and S. M. Hammond. 2010. Emerging paradigms of regulated microRNA processing. *Genes Dev* 24:1086-1092.
57. Flynt, A. S., and E. C. Lai. 2008. Biological principles of microRNA-mediated regulation: shared themes amid diversity. *Nature reviews. Genetics* 9:831-842.
58. Ebert, M. S., and P. A. Sharp. 2012. Roles for microRNAs in conferring robustness to biological processes. *Cell* 149:515-524.
59. Loeb, G. B., A. A. Khan, D. Canner, J. B. Hiatt, J. Shendure, R. B. Darnell, C. S. Leslie, and A. Y. Rudensky. 2012. Transcriptome-wide miR-155 binding map reveals widespread noncanonical microRNA targeting. *Molecular cell* 48:760-770.
60. Dambal, S., M. Shah, B. Mihelich, and L. Nonn. 2015. The microRNA-183 cluster: the family that plays together stays together. *Nucleic acids research*:gkv703-716.
61. Lumayag, S., C. E. Haldin, N. J. Corbett, K. J. Wahlin, C. Cowan, S. Turturro, P. E. Larsen, B. Kovacs, P. D. Witmer, D. Valle, D. J. Zack, D. A. Nicholson, and S. Xu.

2013. Inactivation of the microRNA-183/96/182 cluster results in syndromic retinal degeneration. *Proceedings of the National Academy of Sciences of the United States of America* 110:E507-516.

62. Lagos-Quintana, M., R. Rauhut, J. Meyer, A. Borkhardt, and T. Tuschl. 2003. New microRNAs from mouse and human. *RNA (New York, N.Y.)* 9:175-179.
63. Xu, S., P. D. Witmer, S. Lumayag, B. Kovacs, and D. Valle. 2007. MicroRNA (miRNA) transcriptome of mouse retina and identification of a sensory organ-specific miRNA cluster. *The Journal of biological chemistry* 282:25053-25066.
64. Jin, Z. B., G. Hirokawa, L. Gui, R. Takahashi, F. Osakada, Y. Hiura, M. Takahashi, O. Yasuhara, and N. Iwai. 2009. Targeted deletion of miR-182, an abundant retinal microRNA. *Molecular vision* 15:523-533.
65. Lewis, M. A., E. Quint, A. M. Glazier, H. Fuchs, M. H. De Angelis, C. Langford, S. Van Dongen, C. Abreu-Goodger, M. Piipari, N. Redshaw, T. Dalmay, M. Á. Moreno-Pelayo, A. J. Enright, and K. P. Steel. 2009. An ENU-induced mutation of miR-96 associated with progressive hearing loss in mice. *Nature Publishing Group* 41:614-618.
66. Kuhn, S., S. L. Johnson, D. N. Furness, J. Chen, N. Ingham, J. M. Hilton, G. Steffes, M. A. Lewis, V. Zampini, C. M. Hackney, S. Masetto, M. C. Holley, K. P. Steel, and W. Marcotti. 2011. miR-96 regulates the progression of differentiation in mammalian cochlear inner and outer hair cells. *Proceedings of the National Academy of Sciences* 108:2355-2360.
67. Wang, L., M. J. Zhu, A. M. Ren, H. F. Wu, W. M. Han, R. Y. Tan, and R. Q. Tu. 2014. A ten-microRNA signature identified from a genome-wide microRNA expression profiling in human epithelial ovarian cancer. *PloS one* 9:e96472.
68. Wang, S., M.-H. Yang, X.-Y. Wang, J. Lin, and Y.-Q. Ding. 2014. Increased expression of miRNA-182 in colorectal carcinoma: an independent and tissue-specific prognostic factor. *International journal of clinical and experimental pathology* 7:3498-3503.
69. Lei, R., J. Tang, X. Zhuang, R. Deng, G. Li, J. Yu, Y. Liang, J. Xiao, H.-Y. Wang, Q. Yang, and G. Hu. 2014. Suppression of MIM by microRNA-182 activates RhoA and promotes breast cancer metastasis. *Oncogene* 33:1287-1296.
70. Segura, M. F., D. Hanniford, S. Menendez, L. Reavie, X. Zou, S. Alvarez-Diaz, J. Zakrzewski, E. Blochin, A. Rose, D. Bogunovic, D. Polsky, J. Wei, P. Lee, I. Belitskaya-Levy, N. Bhardwaj, I. Osman, and E. Hernando. 2009. Aberrant miR-182 expression promotes melanoma metastasis by repressing FOXO3 and microphthalmia-associated transcription factor. *Proceedings of the National Academy of Sciences of the United States of America* 106:1814-1819.
71. Sachdeva, M., J. K. Mito, C. L. Lee, M. Zhang, Z. Li, R. D. Dodd, D. Cason, L. Luo, Y. Ma, D. Van Mater, R. Gladdy, D. C. Lev, D. M. Cardona, and D. G. Kirsch. 2014. MicroRNA-182 drives metastasis of primary sarcomas by targeting multiple genes. *The Journal of clinical investigation* 124:4305-4319.
72. Stittrich, A. B., C. Haftmann, E. Sgouroudis, A. A. Kuhl, A. N. Hegazy, I. Panse, R. Riedel, M. Flossdorf, J. Dong, F. Fuhrmann, G. A. Heinz, Z. Fang, N. Li, U. Bissels, F. Hatam, A. Jahn, B. Hammoud, M. Matz, F. M. Schulze, R. Baumgrass, A. Bosio, H. J. Mollenkopf, J. Grun, A. Thiel, W. Chen, T. Hofer, C.

Loddenkemper, M. Lohning, H. D. Chang, N. Rajewsky, A. Radbruch, and M. F. Mashreghi. 2010. The microRNA miR-182 is induced by IL-2 and promotes clonal expansion of activated helper T lymphocytes. *Nature immunology* 11:1057-1062.

73. Kelada, S., P. Sethupathy, I. S. Okoye, E. Kistasis, S. Czieso, S. D. White, D. Chou, C. Martens, S. M. Ricklefs, K. Virtaneva, D. E. Sturdevant, S. F. Porcella, Y. Belkaid, T. A. Wynn, and M. S. Wilson. 2013. miR-182 and miR-10a are key regulators of Treg specialisation and stability during Schistosome and Leishmania-associated inflammation. *PLoS pathogens* 9:e1003451.
74. Wan, C., C.-Y. Ping, X.-Y. Shang, J.-T. Tian, S.-H. Zhao, L. Li, S.-H. Fang, W. Sun, Y.-F. Zhao, Z.-Y. Li, Y.-W. Xu, L.-L. Mu, J.-H. Wang, Q.-F. Kong, G.-Y. Wang, H.-L. Li, and B. Sun. 2016. MicroRNA 182 inhibits CD4+CD25+Foxp3+ Treg differentiation in experimental autoimmune encephalomyelitis. *Clinical Immunology*:1-8.
75. Ichiyama, K., A. Gonzalez-Martin, B.-s. Kim, H. Y. Jin, W. Jin, W. Xu, M. Sabouri-Ghomi, S. Xu, P. Zheng, C. Xiao, and C. Dong. 2016. The MicroRNA-183-96-182 Cluster Promotes T Helper 17 Cell Pathogenicity by Negatively Regulating Transcription Factor Foxo1 Expression. *Immunity* 44:1284-1298.
76. Zhang, D., Y. Li, X. Yao, H. Wang, L. Zhao, H. Jiang, X. Yao, S. Zhang, C. Ye, W. Liu, H. Cao, S. Yu, Y.-c. Wang, Q. Li, J. Jiang, Y. Liu, L. Zhang, Y. Liu, N. Iwai, H. Wang, J. Li, J. Li, X. Li, Z.-B. Jin, and H. Ying. 2016. miR-182 Regulates Metabolic Homeostasis by Modulating Glucose Utilization in Muscle. *Cell reports*:1-12.
77. Muraleedharan, C. K., S. A. McClellan, R. P. Barrett, C. Li, D. Montenegro, T. Carion, E. Berger, L. D. Hazlett, and S. Xu. 2016. Inactivation of the miR-183/96/182 Cluster Decreases the Severity of Pseudomonas aeruginosa -Induced Keratitis. *Investigative Opthalmology & Visual Science* 57:1506.
78. Li, Y.-F., X. Ou, S. Xu, Z.-B. Jin, N. Iwai, and K.-P. Lam. 2016. Loss of miR-182 affects B-cell extrafollicular antibody response. *Immunology*:n/a-n/a.
79. Moskwa, P., F. M. Buffa, Y. Pan, R. Panchakshari, P. Gottipati, R. J. Muschel, J. Beech, R. Kulshrestha, K. Abdelmohsen, D. M. Weinstock, M. Gorospe, A. L. Harris, T. Helleday, and D. Chowdhury. 2011. miR-182-mediated downregulation of BRCA1 impacts DNA repair and sensitivity to PARP inhibitors. *Molecular cell* 41:210-220.
80. Krishnan, K., A. L. Steptoe, H. C. Martin, S. Wani, K. Nones, N. Waddell, M. Mariasegaram, P. T. Simpson, S. R. Lakhani, B. Gabrielli, A. Vlassov, N. Cloonan, and S. M. Grimmond. 2013. MicroRNA-182-5p targets a network of genes involved in DNA repair. *RNA* 19:230-242.
81. Bothmer, A., D. F. Robbiani, N. Feldhahn, A. Gazumyan, A. Nussenzweig, and M. C. Nussenzweig. 2010. 53BP1 regulates DNA resection and the choice between classical and alternative end joining during class switch recombination. *The Journal of experimental medicine* 207:855-865.
82. Jankovic, M., N. Feldhahn, T. Y. Oliveira, I. T. Silva, K. R. Kieffer-Kwon, A. Yamane, W. Resch, I. Klein, D. F. Robbiani, R. Casellas, and M. C. Nussenzweig.

2013. 53BP1 alters the landscape of DNA rearrangements and suppresses AID-induced B cell lymphoma. *Molecular cell* 49:623-631.
83. Manis, J. P., J. C. Morales, Z. Xia, J. L. Kutok, F. W. Alt, and P. B. Carpenter. 2004. 53BP1 links DNA damage-response pathways to immunoglobulin heavy chain class-switch recombination. *Nature immunology* 5:481-487.
84. Ward, I. M., B. Reina-San-Martin, A. Olaru, K. Minn, K. Tamada, J. S. Lau, M. Cascalho, L. Chen, A. Nussenzweig, F. Livak, M. C. Nussenzweig, and J. Chen. 2004. 53BP1 is required for class switch recombination. *The Journal of cell biology* 165:459-464.
85. Muramatsu, M., K. Kinoshita, S. Fagarasan, S. Yamada, Y. Shinkai, and T. Honjo. 2000. Class switch recombination and hypermutation require activation-induced cytidine deaminase (AID), a potential RNA editing enzyme. *Cell* 102:553-563.
86. Schmittgen, T. D., and K. J. Livak. 2008. Analyzing real-time PCR data by the comparative CT method. *Nature protocols* 3:1101-1108.
87. Li, J., Y. Wan, Q. Ji, Y. Fang, and Y. Wu. 2013. The role of microRNAs in B-cell development and function. *Cellular & molecular immunology* 10:107-112.
88. Dorsett, Y., K. M. McBride, M. Jankovic, A. Gazumyan, T. H. Thai, D. F. Robbiani, M. Di Virgilio, B. Reina San-Martin, G. Heidkamp, T. A. Schwickert, T. Eisenreich, K. Rajewsky, and M. C. Nussenzweig. 2008. MicroRNA-155 suppresses activation-induced cytidine deaminase-mediated Myc-Igh translocation. *Immunity* 28:630-638.
89. Teng, G., P. Hakimpour, P. Landgraf, A. Rice, T. Tuschl, R. Casellas, and F. N. Papavasiliou. 2008. MicroRNA-155 is a negative regulator of activation-induced cytidine deaminase. *Immunity* 28:621-629.
90. Vigorito, E., K. L. Perks, C. Abreu-Goodger, S. Bunting, Z. Xiang, S. Kohlhaas, P. P. Das, E. A. Miska, A. Rodriguez, A. Bradley, K. G. Smith, C. Rada, A. J. Enright, K. M. Toellner, I. C. Maclennan, and M. Turner. 2007. microRNA-155 regulates the generation of immunoglobulin class-switched plasma cells. *Immunity* 27:847-859.
91. Pucella, J. N., W. F. Yen, M. V. Kim, J. van der Veeken, N. D. Socci, Y. Naito, M. O. Li, N. Iwai, and J. Chaudhuri. 2015. miR-182 is largely dispensable for adaptive immunity: lack of correlation between expression and function. *J Immunol* 194:2635-2642.
92. Agarwal, V., G. W. Bell, J.-W. Nam, and D. P. Bartel. 2015. Predicting effective microRNA target sites in mammalian mRNAs. *eLife* 4:101.
93. Kawai, T., and S. Akira. 2006. TLR signaling. *Cell Death and Differentiation* 13:816-825.
94. Mackay, F., and P. Schneider. 2009. Cracking the BAFF code. *Nature Publishing Group* 9:491-502.
95. Elgueta, R., M. J. Benson, V. C. D. Vries, and R. J. Noelle. 2009. Molecular mechanism and function of CD40 / CD40L engagement in the immune system. *Immunological Reviews* 229:152-172.
96. Klein, U., S. Casola, G. Cattoretti, Q. Shen, M. Lia, T. Mo, T. Ludwig, K. Rajewsky, and R. Dalla-Favera. 2006. Transcription factor IRF4 controls plasma cell

differentiation and class-switch recombination. *Nature immunology* 7:773-782.
97. Crotty, S. 2014. T Follicular Helper Cell Differentiation, Function, and Roles in Disease. *Immunity* 41:529-542.
98. Mond, J. J., A. Lees, and C. M. Snapper. 1995. T Cell-Independent Antigens Type 2. *Annual review of immunology* 13:655-692.
99. Schwickert, T. A., R. L. Lindquist, G. Shakhar, G. Livshits, D. Skokos, M. H. Kosco-Vilbois, M. L. Dustin, and M. C. Nussenzweig. 2007. In vivo imaging of germinal centres reveals a dynamic open structure. *Nature* 446:83-87.
100. Hodgkin, P. D., J. H. Lee, and A. B. Lyons. 1996. B cell differentiation and isotype switching is related to division cycle number. *The Journal of experimental medicine* 184:277-281.
101. Hasbold, J., A. B. Lyons, M. R. Kehry, and P. D. Hodgkin. 1998. Cell division number regulates IgG1 and IgE switching of B cells following stimulation by CD40 ligand and IL-4. *European Journal of Immunology* 28:1040-1051.
102. He, M., E. M. Cortizas, R. E. Verdun, and E. Severinson. 2015. Cyclin-Dependent Kinases Regulate Ig Class Switching by Controlling Access of AID to the Switch Region. *The Journal of Immunology*:1402146.
103. Dominguez-Sola, D., J. Kung, A. B. Holmes, V. A. Wells, T. Mo, K. Basso, and R. Dalla-Favera. 2015. The FOXO1 Transcription Factor Instructs the Germinal Center Dark Zone Program. *Immunity*:1-11.
104. Sander, S., V. T. Chu, T. Yasuda, A. Franklin, R. Graf, D. P. Calado, S. Li, K. Imami, M. Selbach, M. Di Virgilio, L. Bullinger, and K. Rajewsky. 2015. PI3 Kinase and FOXO1 Transcription Factor Activity Differentially Control B Cells in the Germinal Center Light and Dark Zones. *Immunity*:1-12.
105. Jensen, K. P., and J. Covault. 2011. Human miR-1271 is a miR-96 paralog with distinct non-conserved brain expression pattern. *Nucleic acids research* 39:701-711.
106. Miska, E. A., E. Alvarez-Saavedra, A. L. Abbott, N. C. Lau, A. B. Hellman, S. M. McGonagle, D. P. Bartel, V. R. Ambros, and H. R. Horvitz. 2007. Most Caenorhabditis elegans microRNAs are individually not essential for development or viability. *PLoS genetics* 3:e215.
107. Alvarez-Saavedra, E., and H. R. Horvitz. 2010. Many families of C. elegans microRNAs are not essential for development or viability. *Current biology : CB* 20:367-373.
108. Brenner, J. L., K. L. Jasiewicz, A. F. Fahley, B. J. Kemp, and A. L. Abbott. 2010. Loss of individual microRNAs causes mutant phenotypes in sensitized genetic backgrounds in C. elegans. *Current biology : CB* 20:1321-1325.